Measurement and Modelling of L-band Forest Emission for Future Soil Moisture Retrieval from SMOS Signatures

Grant, J.P.

2009

Measurement and Modelling of L-band Forest Emission for Future Soil Moisture Retrieval from SMOS Signatures

Jennifer P. Grant

Cover: Photography of Bray forest by K. Saleh Contell (overview) and J.P. Grant (close-up); Artist's impression of SMOS by AOES Medialab, © ESA.

Measurement and Modelling of L-band Forest Emission for Future Soil Moisture Retrieval from SMOS Signatures.
(PhD thesis, Vrije Universiteit Amsterdam)
In Dutch: Microgolfstraling van Bossen bij 1.4 GHz: Experimenteel onderzoek en modelontwikkeling ten behoeve van bodemvochtmetingen vanuit de ruimte.
(Academisch proefschrift, Vrije Universiteit Amsterdam)

This study was funded by the Netherlands Institute for Space Research of the Netherlands Organisation for Scientific Research (NWO-SRON), and the French National Institute for Agricultural Research (INRA).

ISBN 978 90 8659 321 7
NUR-code: 934
Subject headings:
passive microwaves / remote sensing / forest / litter / soil moisture

VRIJE UNIVERSITEIT

Measurement and Modelling of L-band Forest Emission for Future Soil Moisture Retrieval from SMOS Signatures

ACADEMISCH PROEFSCHRIFT

ter verkrijging van de graad Doctor aan
de Vrije Universiteit Amsterdam,
op gezag van de rector magnificus
prof.dr. L.M. Bouter,
in het openbaar te verdedigen
ten overstaan van de promotiecommissie
van de faculteit der Aard- en Levenswetenschappen
op vrijdag 19 juni 2009 om 10.45 uur
in de aula van de universiteit,
De Boelelaan 1105

door

Jennifer Phillippa Grant

geboren te Nocton, Verenigd Koninkrijk

promotor:	prof.dr. A.J. Dolman
copromotoren:	dr. A.A. van de Griend
	dr. J.P. Wigneron

thesis committee: dr. R.A.M. de Jeu
dr. Y.H. Kerr
dr. P. de Rosnay
dr. K. Saleh Contell
dr. M. Schwank
prof.dr. Z. Su

Acknowledgements

Despite the hard work involved at times, doing a PhD was an unforgettable experience. I am extremely grateful for being offered the opportunity to do so. This particular project was conducted as a collaboration between the Vrije Universiteit Amsterdam (VUA) in the Netherlands, and the Institut National de la Recherche Agronomique (INRA) Bordeaux in France. During the past four years, I spent a total of nine months in Bordeaux. Consequently, besides learning about microwave remote sensing, I also learnt more about the French culture and language. To me, this was a definite bonus. As it turned out though, my travels were not just limited to France. I was lucky enough to meet, and work with, colleagues from different parts of the world. I hereby thank everyone who contributed to this thesis.

First and foremost, I am deeply indebted to my co-promotors Adriaan van de Griend and Jean-Pierre Wigneron, who were my main supervisors. I must thank Adriaan especially for continuing even after retirement. My supervision may sometimes have seemed a bit unusual, with one supervisor being retired, and the other generally some distance away. Fortunately, everyone involved assumed a flexible attitude and the slightly unconventional situation was never a problem. I was actually very lucky with my supervisors, as their knowledge and methods complemented each other very nicely. This meant that I always had someone to help me with a particular issue, and also that I obtained a broader outlook on both my own project and on research in general. I am infinitely grateful to both of you!

Next, I would like to thank my promotor Han Dolman for his help on the project management side. I think the main question Han heard from me during these four years was: “Please could you sign for my travel expenses?” He always agreed readily to this, which I very much appreciated. In fact, he effectively left me in charge of overall budget management, which I think suited both of us just fine.

For a crucial part of this thesis, the field experiments, I received skilled assistance from both VUA and INRA staff. I thank the staff of the VUA workplace, especially Michel Groen, for helping with the preparations, and the INRA technicians, above all Alain Kruszewski, for their help in the field. Alain’s dedicated assistance at the Bray site on numerous occasions was truly indispensable.

Furthermore, I sincerely thank my colleagues in Amsterdam for their help with all the numerous questions and programming issues which came up through the years. Also, a big ‘merci beaucoup!’ to everyone in the EPHYSE research unit at INRA. They welcomed me warmly at every visit and helped me with any kind of practical, cultural or language issue I happened to come across. As a result of this, my time spent in France was always very enjoyable and sociable.

Because of the international aspect of this research, additional contributions have been made by a number of foreign colleagues. First of all, I must thank Niels Skou, Sten Schmidl Søbjærg and Jan Balling of DTU Copenhagen in Denmark for the use of the EMIRAD radiometer and the technical support to go with it, and also for hosting me during a study trip in 2005. Further inspiring and enjoyable collaboration, often coupled with study trips and/or field work abroad, took place with (in order of becoming involved): Yann Kerr of CNES/CESBIO Toulouse, France; Kauzar Saleh Contell of the University of Cambridge, UK; Paolo Ferrazzoli and Andrea Della

Vecchia of Tor Vergata University in Rome, Italy; Mike Schwank of WSL Birmensdorf and Massimo Guglielmetti of ETH Zurich, both in Switzerland; François Demontoux, Gilles Ruffié, Bénédicte Le Crom and Heather Lawrence of the IMS Laboratory, University of Bordeaux I, France; Jeff Walker, Christoph Rüdiger and Rocco Panciera of the University of Melbourne, Australia; and Ernesto López-Baeza, Aurelio Cano and Cristina Millán-Scheiding of the University of Valencia, Spain. Of this list, Mike Schwank and Kauzar Saleh Contell deserve special thanks as they contributed significantly throughout the whole thesis.
The FOSMEX data set, on which part of chapter 3 is based, was kindly made available by Swiss colleagues through Mike Schwank. I am also grateful to all the NAFE '05 participants for their contributions towards the 'Roscommon' data set, on which chapter 5 is based.
Finally, I would like to thank my thesis committee for giving their time to review this work.

Besides the extensive professional support, I was also very lucky to have a truly interested and supportive group of extended family, in-laws and friends rally round on the home front. I thank everyone wholeheartedly even though their contributions may have been less tangible than those of professional colleagues.
My parents and sister were unfailingly encouraging and supportive. To have this kind of permanent background was both comfortable and stimulating. I am also very grateful to have my sister and my best friend Lisa as my ushers or 'paranimfen' at the defence ceremony. Lisa and I started our respective PhDs almost simultaneously, and it was helpful in many different ways to exchange experiences and advice as frequently (and often rather lengthily) as we did.
Last but not least, I take my hat off to PJ. I am convinced he does not quite realize exactly how significant his contribution was. My deepest thanks to him for all the love and support I received throughout this project.

Contents

List of acronyms

AI	Angular Index
CESBIO	Centre d'Etudes Spatiales de la Biosphère (Centre for the Study of the Biosphere from Space)
CF	Cost Function
CNES	Centre National d'Etudes Spatiales (French Space Agency)
DTU	Danmarks Tekniske Universitet (Technical University of Denmark)
ELBARA	L-band Radiometer of ETH Zürich
EMIRAD	Radiometer of DTU Copenhagen
EPHYSE	Ecologie Fonctionelle et Physique de l'Environnement (Functional Ecology and Environmental Physics research unit)
ESA	European Space Agency
ETH	Eidgenössische Technische Hochschule (Swiss Federal Institute of Technology)
FLIR	Forward Looking Infrared
FOSMEX	Forest Soil Moisture Experiment
IMS	Laboratoire de l'Intégration du Matériau au Système (Laboratory of Integration from Materials to System)
INRA	Institut National de la Recherche Agronomique (French National Institute for Agricultural Research)
IR	Infrared
JD	Julian Day
LAI	Leaf Area Index
LB	Leaf Biomass
L-MEB	L-band Microwave Emission of the Biosphere
MIRAS	Microwave Imaging Radiometer using Aperture Synthesis
MODIS	Moderate Resolution Imaging Spectroradiometer
MORA	Monofrequency Radiometer of ETH Zürich
NAFE	National Airborne Field Experiment
NDVI	Normalized Difference Vegetation Index
PLMR	Polarimetric L-band Multibeam Radiometer
RMSE	Root Mean Square Error
RMS	Root Mean Square
SLA	Specific Leaf Area
SMOS	Soil Moisture and Ocean Salinity
SS	Skill Score
SVAT	Soil-Vegetation-Atmosphere Transfer
TM	Thematic Mapper
VUA	Vrije Universiteit Amsterdam (VU University Amsterdam)
VWC	Vegetation Water Content
WSL	Eidgenössische Forschungsanstalt für Wald, Schnee und Landschaft (Swiss Federal Institute for Forest, Snow and Landscape Research)

List of symbols

A_t		Temperature weighting parameter
B_t		Canopy type dependent parameter
d		Difference
D_L	[m]	Litter layer thickness
e		Emissivity
f	[Hz]	Frequency
H		Horizontal polarisation
H_R		Surface roughness
LM	[$kgkg^{-1}$]	Litter moisture
N_R		Angular dependence of surface roughness
P		Polarisation
p		Parameter
Q_R		Polarisation mixing
R		Reflectivity
rtt		Ratio of canopy structure parameters
SM	[m^3m^{-3}]	Soil moisture
T	[K]	Thermodynamic Temperature
T_B	[K]	Brightness temperature
T_{IR}	[K]	Infrared temperature
tt^P		Canopy structure parameter
V		Vertical polarisation
z	[m]	Depth
α		Power attenuation coefficient (chapter 2) or forest fraction (chapter 5)
β		Correction parameter
Γ		Transmissivity
γ		Transmissivity
Δ		Difference
δ		Difference
δ_T	[m]	Thermal sampling depth
ε		Dielectric constant
ε'		Real part of the dielectric constant
ε''		Imaginary part of the dielectric constant
θ	[°]	Observation angle
λ	[m]	Wavelength
π		pi
σ		Standard deviation
τ		Vegetation optical depth
φ	[°]	Azimuth angle
ω		Single scattering albedo

Sub- and Superscripts

C	Canopy
coh	Coherent
corr	Corrected
eff	Effective
F	Forest floor (chapter 4) or forest (chapter 5)
G	Grass
gc	Ground-canopy
H	Horizontal polarisation
ini	Initial
L	Litter
lit	Litter
NAD	Nadir (theoretical)
obs	Observed
ret	Retrieved
S	Soil
sim	Simulated
V	Vertical polarisation
0	Nadir
*	Smooth

Chapter 1

Introduction

This PhD project was conducted as a collaboration between the Department of Hydrology and Geo-Environmental Sciences of the VU University Amsterdam (VUA), the Netherlands, and the Functional Ecology and Environmental Physics (EPHYSE) research unit of the National Institute for Agricultural Research (INRA) Bordeaux, France.
Further cooperation took place with CNES/CESBIO Toulouse, France; the Technical University of Denmark, Copenhagen, Denmark; the Tor Vergata University, Rome, Italy; the Swiss Federal Institute WSL; the IMS Laboratory, Bordeaux, France; the University of Melbourne, Australia; the University of Valencia, Spain and the University of Cambridge, UK.

1.1 Background

1.1.1 SMOS

The Soil Moisture and Ocean Salinity (SMOS) mission of the European Space Agency (ESA) is planned for launch in 2009. Over land, SMOS will attempt to retrieve soil moisture with a maximum error of 4% by volume and global soil moisture maps will be provided with a temporal resolution of 2-3 days. SMOS will carry a fully polarimetric L-band ($\lambda \approx 21$ cm, $f \approx 1.4$ GHz) Microwave Imaging Radiometer using Aperture Synthesis (MIRAS). The passive microwave observations will be done at multiple viewing angles between 0° and 55° angles, and with a spatial resolution ranging from 35 km at nadir up to 50 km (Kerr *et al*. 2001). The multiple-angle configuration allows for a significant improvement in retrieval accuracy compared to that of previous comparable missions. Furthermore, the all-weather capabilities of passive microwaves make it possible to provide measurements constantly and routinely.

Soil moisture is an important variable in the global water cycle and an essential input in meteorological, climatological and soil-vegetation-atmosphere transfer (SVAT) models. SMOS will provide estimates of the soil moisture content in the top soil layer. This layer can be seen as the interface between the vegetation and the hydrological system: surface soil moisture determines hydrological processes such as evaporation, infiltration and run-off, while vadose zone soil moisture controls the uptake of water by the vegetation, as this unsaturated zone includes the root zone of the vegetation layer. The amount of water available for uptake by plants partly determines the rates of photosynthesis and transpiration, and is by this also linked to CO_2 fixation and meteorological variables such as atmospheric vapour pressure and air temperature. Soil moisture is thus an essential variable in any of the Earth's natural environmental systems over land and as such deserves close attention.

Additionally to soil moisture, SMOS is expected to retrieve vegetation optical depth, which is linked to vegetation water content. The expected accuracy of vegetation

water content estimates is about 0.5 kgm^{-2} every six days (Kerr *et al*., 2001). Because the amount of water available in the vegetation controls plant transpiration, photosynthesis and CO_2 sequestration, the vegetation optical depth will also be useful for monitoring vegetation dynamics and crop production. Furthermore, information on vegetation water status can be important for drought forecasting and monitoring of fire hazards.

1.1.2 (L-band) Passive microwaves, soil and vegetation

The dielectric constant or permittivity of a material is a measure of its polarity and thus of its response to the electric field resulting from electromagnetic radiation, e.g. microwaves. Below the resonance frequency (< 10 GHz), the dielectric constant of water is around 80, whereas that of a dry soil is about 3 and that of air is 1. The large difference between the permittivities of soil and water explains why microwaves are especially well-suited to monitoring soil moisture content. The more water present in a soil, the less the polar H_2O molecules will be bound to the soil particles and the more they will be free to move about, thus increasing the dielectric constant of the soil medium. The amount of free water in the soil also determines the moisture availability for plants and is thus an important factor in the processes of photosynthesis and transpiration. The L-band (1-2 GHz) frequency is especially well-suited to measuring the water content of materials as the radiation frequency of the neutral hydrogen atom lies around 1.4 GHz.

Observed passive microwave radiation is expressed as brightness temperature (T_B), which depends on both the emissivity (e) and physical temperature (T) of the observed material.
Soil and vegetation layers show different emission behaviour with increasing moisture, due to the different types of medium concerned in both cases.
Because a soil layer forms a rather dense medium, so-called ‘surface-effects’ become more important in the radiative transfer. The main influence of H_2O in soil is through an increase in dielectric constant, which reflects a change in the density of the soil medium relative to that of the air above, and thus an increase in reflection (R), which is related to emissivity by $e = 1\text{-}R$. If reflection at the soil-air interface becomes very high, upwelling soil emission will become quite low. Thus, dry soil emission is very high (~ 0.8), but wet soil emission is much lower (~ 0.5), with exact values also depending on soil type.
A vegetation layer forms a much less dense medium than soil, and can be seen as a cloud of air, vegetation and water particles. In this case, ‘volume effects’ play a greater role. An increase in water content of this layer will have much less effect on the dielectric properties of the medium as a whole. Instead, vegetation emission will increase directly through the increase of H_2O molecules within the layer.

Besides emitting its own radiation, a vegetation layer will also affect the upwelling radiation emitted by the soil layer. Part of the soil emission will be transmitted through the vegetation volume, while the other part will be lost by scattering and absorption within the vegetation canopy. With an increase of H_2O molecules in the vegetation layer when wet, the absorption of upwelling soil emission will also increase. In wet conditions, the total emission observed above the canopy will therefore contain less soil and more vegetation contribution. Transmission, scattering and absorption depend on vegetation structure and water content. It should therefore

be clear that wet conditions complicate signal interpretation and soil moisture retrievals to a certain extent: not only does soil emission decrease, while vegetation emission increases, but additionally, more of the soil emission will be absorbed by the canopy.
Therefore, it is especially important not only to understand the radiative transfer properties of each layer, but also to understand the change in emission behaviour with changing moisture conditions.

1.1.3 L-MEB

The L-band Microwave Emission of the Biosphere (L-MEB) model (Wigneron et al., 2007) is the main model used in this PhD research, as it is the forward model used in the SMOS Level 2 Soil Moisture Algorithm. This algorithm uses multi-angular data in order to simultaneously retrieve several parameters describing soil and vegetation characteristics. It uses an iterative approach, minimizing a cost function based on the differences between observed and simulated brightness temperature, for all observation angles. The strength of L-MEB lies in the fact that it is a relatively simple model, and therefore ideally suited to global-scale observations as in the case of SMOS. The model is presented in detail in chapters 2-5, therefore only a brief qualitative description will be given here.

L-MEB models the emission of a vegetation-covered soil, and takes into account the contributions of soil, vegetation and sky radiation.
In the soil module of L-MEB, soil moisture content and soil emission are linked through the use of the Dobson dielectric mixing model and the Fresnel equations, which relate soil moisture to the soil dielectric constant, and the dielectric constant to reflectivity, respectively. The smooth surface soil reflectivity resulting from the Fresnel equations is then corrected for soil roughness by a semi-empirical approach.
The vegetation module of L-MEB is based on a zero-order radiative transfer model (Kirdyashev *et al*., 1979). In the zero-order approach, the scattering source function in the radiative transfer equation is neglected. This model is also called the 'τ-ω' (tau-omega) model, in which the parameters τ and ω denote the vegetation optical depth and the single scattering albedo, respectively (Mo *et al*., 1982). As explained in §1.1.1, the vegetation optical depth is related to vegetation water content and it is a measure of the transmissivity of the vegetation layer. The optical depth and the single scattering albedo are interdependent and effective parameters resulting from the use of the Delta-Eddington approximation, which assumes that scattering is in the forward direction only. Multiple scattering in the vegetation and between the vegetation and the soil is neglected. By neglecting multiple scattering and the scattering source function, the zero-order approach will generally lead to a slight underestimation of emissivity in the case of forests (Mätzler *et al*, 2006). Especially for branches, the simple zero-order radiative transfer theory was found not to be directly applicable (Ferrazzoli *et al*., 2002). However, a solution to this problem was presented in the same study by defining the parameters τ and ω as best-fit equivalent (i.e. 'effective') parameters resulting from calibration with experimental data. In this case the zero-order approach can still be applied successfully to forests.
Finally, sky radiation is included in L-MEB through the use of a simplified approach depending mainly on surface altitude and air temperature. However, the contribution of sky radiation to the total emission is very small due to the low physical temperature of the sky and the absorption over the long distances involved. In the tower and

airborne experiments described in this thesis sky effects were not very significant, however, they will be more important in the case of space-borne sensors as the surface emission will travel a much longer distance through the atmosphere before reaching the sensor.

1.1.4 Forest studies

Just before starting this PhD research, a comprehensive review article (Pampaloni, 2004) was published, which outlined past and ongoing experimental and theoretical studies of the relationships between microwave emission and forest features at various scales. It was shown that microwave radiometry had proved useful for forest classification and monitoring of forest cover fraction, besides for estimating variables such as biomass, stand age, tree height and woody volume. At that time, the possibility of retrieving soil moisture underneath forests or in partially forested areas was mostly based on a few theoretical studies. Experimental observations were still very much lacking, especially long-term experimental data sets, which were virtually non-existent (Van de Griend and Wigneron, 2004a). These were necessary for validation of the then existing models and theoretical assumptions, and for calibration over forests in view of the upcoming SMOS mission. Long-term forest experiments at L-band were therefore started more or less simultaneously at sites in France and Germany, backed up by modelling work in Italy which provided a more physically-based calibration. Comparable and complementary experiments have since also been conducted in the USA.
With many land surface areas in temperate, boreal and tropical regions being at least partially covered by forest, microwave radiometry of forests is expected to remain a pertinent issue in view of upcoming global-scale satellite observations.

1.2 Research objectives

This PhD research was done as part of the background research for the SMOS mission. At the spatial resolution of SMOS, many pixels over land will contain a certain percentage of forest cover. Because forests usually consist of rather thick and dense vegetation layers, SMOS will not attempt to retrieve soil moisture in forested areas. However, modelling studies (Van de Griend *et al.*, 2003; Van de Griend *et al.*, 2004) have shown that it might be possible to retrieve soil moisture with the required accuracy in non-forested parts of the pixel if forest emission can be modelled accurately enough. At the beginning of this PhD project in 2004, not much was known of forest radiative transfer properties at L-band, and whether and/or how these varied with different moisture conditions.
These background aspects formed the motivation for this research and show the main goal of this work: to better understand and model forest emission properties at L-band in view of the SMOS mission soil moisture retrievals over mixed pixels. The focus hereby was on obtaining a greater knowledge of the angular and polarization dependence of the effective parameters τ and ω for a typical coniferous forest. As demonstrated by Van de Griend and Wigneron (2004a), this information was clearly lacking at the time. A second objective was to investigate the sensitivity of the L-band signal above forests to below-canopy and surface variables such as soil moisture, and litter and understory biomass and water content. This could aid in future studies on the ecology and hydrological state of the canopy and understory. Ultimately, this

knowledge could be used in drought and fire predictions, and could also contribute to ecological studies and SVAT modelling (cf. §1.1.1).
In order to accomplish the above objectives, a long-term field experiment was set up in France in order to capture the L-band emission for different moisture conditions of a Pine forest system. This experiment formed the starting point of this PhD research and was later followed up by additional field experiments to address more specific questions.

1.3 Thesis outline

The following four chapters present the results of this PhD project in answer to the research issues outlined in the previous paragraph. First, **chapter 2** presents the results of the long-term field experiment 'Bray 2004' done at the Bray research site in Les Landes forest, France, in 2004. In this experiment, L-band radiometric observations were done from a tower above the forest. This allowed for a first study of the changes in above-canopy L-band emission with varying soil and litter moisture conditions. **Chapter 3** concerns the calibration of the L-MEB model over a coniferous and a deciduous forest. Experimental data from a deciduous forest site in Jülich, Germany were kindly made available by Swiss colleagues. These were then combined with experimental data from the coniferous site at Bray in order to calibrate values of L-MEB vegetation and roughness parameters for the two forest types.
The previous two studies, as well as the literature, indicated that in order to fully understand the L-band emission of a forest system, more knowledge was required of the L-band radiative transfer properties of the litter layer and forest understory. Therefore, a study was done on this specific subject, the results of which are presented in **chapter 4**. Additional fieldwork was done at the Bray site, to observe the forest floor from underneath the canopy. Results show the contribution of each forest layer (soil, litter, grass understory and tree canopy) to above-canopy L-band emission. Furthermore, the relative contributions of the soil and litter layers to emission originating from the ground are shown for different moisture conditions.
Finally, **chapter 5** presents a study of the effect of fractional forest cover on soil moisture retrieval from mixed grassland/Eucalypt forest pixels. Data for this study were obtained as part of the National Airborne Field Experiment (NAFE) which was held in South-eastern Australia in 2005.
The four chapters presenting the results of this PhD research are followed by a short summary of the thesis and some concluding remarks.

Chapter 2

A Field Experiment on Microwave Forest Radiometry – L-band signal behaviour for varying conditions of surface wetness [*]

2.1 Introduction

The Bray 2004 experiment was conducted as part of the background research for ESA's Soil Moisture and Ocean Salinity (SMOS) mission planned for launch in 2009 (e.g. Kerr *et al*., 2001; Berger *et al*., 2003). The SMOS mission will carry a multi-angle, dual-polarization interferometric L-band (1.4 GHz) radiometer for monitoring soil moisture and ocean salinity at a global scale. Mission requirements include the retrieval of soil moisture with a precision of 4% by volume. Spatial resolution of the instrument is around 30 km at nadir view, which means that most pixels of the earth's surface will be inhomogeneous, consisting of a mixture of forest, lower vegetation and bare (agricultural) soil. A vegetation layer covering the soil will influence the radiometric signal, as it will attenuate the soil emission and add its own contribution, an effect which increases under wet conditions. Vegetation attenuation of the soil signal is related to vegetation water content (Jackson and O'Neill, 1990) and through this also to vegetation biomass.

In the tropical, temperate and boreal zones, forests make up a large area of the land surface and will therefore certainly influence the microwave emission at the spatial resolution of SMOS. In order to account for the contribution of forests to the microwave emission of heterogeneous pixels it is necessary to know the radiative transfer characteristics of different types of forest (Van de Griend *et al.*, 2003; 2004). At the moment, very little information exists on this subject, which was the main reason to conduct Bray 2004. Recent forest-related studies at L-band are based on modelling alone (e.g. Ferrazzoli *et al*., 2002) or a combination of modelling and the results of very short-term field experiments (e.g. Lang *et al*., 2001; Saleh *et al*., 2004a; Della Vecchia *et al*., 2006a). Because of the short-term character of these field experiments, little is known about L-band signal behaviour above forests for different wetness conditions, though a relatively small sensitivity to changes in soil moisture is predicted. Of course this depends on forest type, age and density (biomass).

Besides the water content of the soil and the vegetation layers, the microwave signal is also influenced by the geometrical structure of the vegetation. Several studies (e.g. Mätzler, 1990; Wigneron *et al*., 2004; Schwank *et al*., 2005) have shown that distinct changes in vegetation structure can be measured at L-band for low vegetation types such as crops and grass. However in the case of forests, a modelling study (Ferrazzoli *et al*., 2002) has shown that at L-band, the main contribution to emission comes from the branches. Therefore, on a yearly timescale, the change in signal caused by

[*] This chapter has been published as: Grant, J.P., Wigneron, J.-P., Van de Griend, A.A., Kruszewski, A., Schmidl Søbjærg, S. and Skou, N. (2007). A field experiment on microwave forest radiometry: L-band signal behaviour for varying conditions of surface wetness," *Remote Sensing of Environment, 109(1)*, 10-19.

temporal changes in vegetation structure will be small, especially in the case of evergreen forests.
Until recently, the small sensitivity to changes in soil moisture over forests was ascribed solely to the attenuating effect of the tree canopy and understory. However, there is growing evidence that the litter layer might also have an influence on above-canopy emission. This layer, consisting of plant debris, roots and organic matter, shows different radiometric characteristics at L-band than either soil or vegetation (Schmugge *et al*., 1988; Jackson and Schmugge, 1991; Saleh *et al*., 2006). For example, emissivity of the litter layer seems to be very high, especially when wet. As in many temperate and boreal forest systems, a substantial litter layer is also present at the Bray site.
During the Bray 2004 experiment L-band measurements were done over a coniferous forest in the Southwest of France. At the same time, ground measurements were taken of soil and litter moisture content and temperature, while precipitation data were already being permanently monitored at the site. The long-term character of the experiment allowed data to be obtained for a variety of moisture conditions.
This paper presents the Bray 2004 experiment and some radiometric characteristics of this pine forest at L-band and horizontal polarization. First, composite ground-canopy temperatures and resulting above-canopy emissivities are calculated. Second, a description of this forest system is given by showing the behaviour of various thermodynamic temperatures and soil and litter moisture patterns. Finally, the dependence of the above-canopy emission on incidence angle, precipitation and soil moisture content is shown.

2.2. Materials and Methods

2.2.1 Site description

The Bray site lies within the forest of Les Landes, at approximately 20 km southwest of Bordeaux, France (latitude 44°42′ N, longitude 0°46′ W, altitude 61 m). The Landes forest is a production forest consisting mainly of Maritime Pines (*Pinus pinaster* Ait). The trees at the Bray site were 34 years in age at the time of measurement, giving the stand an approximate height of 22 m. The trees are distributed in a grid of parallel rows along a northeast-southwest axis with an inter-row spacing of 4 m. Maximum (summer) values for canopy Leaf Area Index (LAI) and cover fraction were around 2.15 and 0.35 respectively (measurements by INRA-Bordeaux; pers. comm. D. Lousteau/D. Guyon). The understory consists mostly of grass (mainly *Molinia caerulea* L. Moench) and had maximum LAI and cover fraction values of around 2.48 and 0.65 respectively (measurements by INRA-Bordeaux). Total aboveground biomass of the trees was 11.28 kg m^{-2}, calculated from allometric relationships based on trunk diameter at breast height (Porté *et al*., 2000; 2002). This, together with the LAI values, indicates that the forest can be described as medium dense.
The soils are sandy and hydromorphic podzols, with dark organic matter in the first 60 cm. The percentage of sand in the soil surface layer generally exceeds 80%. Moisture contents at saturation and wilting point are 0.6 m^3m^{-3} and 0.12 m^3m^{-3} respectively (Ogée and Brunet, 2002), and the moisture content at field capacity for such a soil will then be around 0.25 m^3m^{-3}. On top of the soil lies a distinct litter layer, the upper part of which consists mainly of dead grass and the lower part of grass roots, pine needles

and other organic matter. In places the layer thickness exceeded 10 cm, and the large biomass was also indicated by measurements of water content resulting in values of over 10 kg m^{-2}.

2.2.2. Microwave and Infrared measurements

Microwave measurements were done with the dual-polarization L-band (1.41 GHz) radiometer EMIRAD of the Technical University of Denmark, of which technical details can be found in (Søbjærg, 2002). The radiometer has an integration time of 8 ms and gives an output measurement of brightness temperature (T_B) every second. The absolute accuracy and the sensitivity of the instrument are ±1 K and ±0.1 K, respectively (Søbjærg, 2002). EMIRAD was previously used successfully over a corn field near Avignon (Wigneron *et al.*, 2004). The antenna was a square shaped horn type with a base of 608 x 608 mm^2, a height of 850 mm, and a -3 dB (full) beamwidth of approximately 25°.

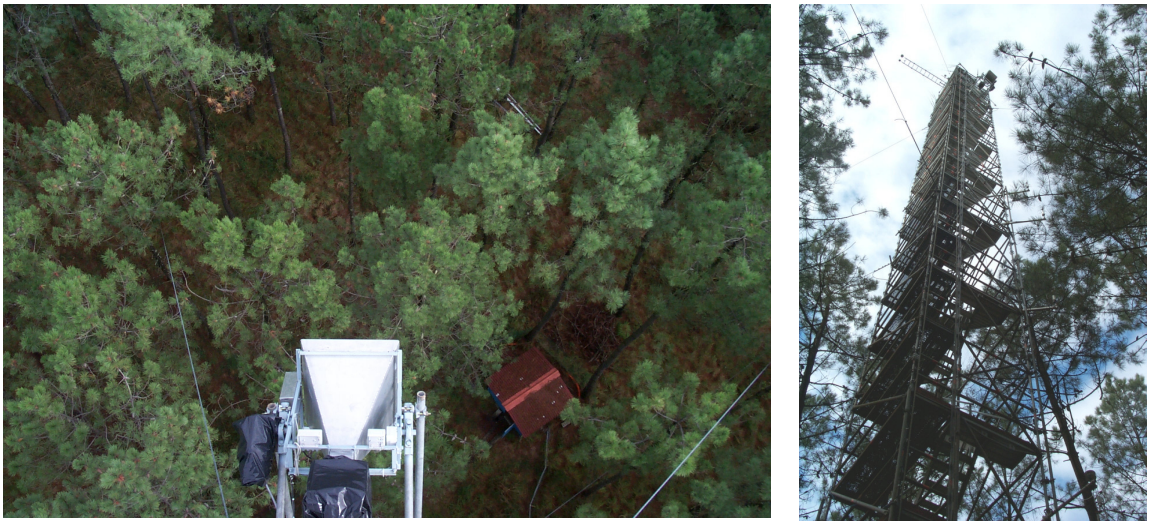

Figure 2-1: The EMIRAD L-band (1.4 GHz) radiometer at the Bray site, overlooking the forest from a 40 m mast.

At the Bray site, the radiometer was mounted on a 40 m mast over the forest (see fig. 2-1), giving it a -3 dB footprint of approximately 600 m^2 at an incidence angle of 45°. The look direction (azimuth) of the antenna was 020° from North. Measurements were done automatically at incidence angles of 25°, 30°, 35°, 40°, 45°, 50°, 55° and 60° from nadir. For each hour, the antenna was set to look at each angle for one minute, then at an angle of 45° for the remainder of that hour. Measurements were averaged to half-hourly values for the final data analysis.
A thermal IR radiometer (Heitronics KT 15.85D; 9.6 – 11.5 μm) was fixed next to the microwave instrument to give measurements of surface temperature (T_{IR}) over approximately the same footprint.

An internal calibration of the radiometer was done automatically for each measurement using an internal load (~ 320 K) and load + noise (~ 120 K) as described by Søbjærg (2002). External calibration corrects for losses in the antenna and cables and for noise generated by the physical temperature of the antenna and cables. During Bray 2004, an external calibration was carried out at intervals during the measurement campaign by directing the radiometer at the sky and correcting the measured

brightness temperatures to expected values (around 5.5 K) as calculated from Pellarin *et al*., (2003a). These sky measurements were done for angles between 125° and 160° from nadir, with 5° steps in between. Sky calibration was only done during the afternoon, when the solar incidence angle minimized the influence of the sun on the measurements. In total 15 days from throughout the whole experimental period were finally selected to use in the actual calibration, based on the quality of their results (criterion: no sudden steep increase in T_B during the measurements as this could result from external disturbance). Correction of measured to simulated brightness temperatures resulted in values for the antenna and cable losses. These were found to increase slightly over time, probably due to ageing of the cables. Using these loss values for data calibration resulted in a RMSE of 2.1 K between measured and simulated values of $T_{B,sky}$ for the horizontal polarization.
In general, the microwave measurements at vertical polarization were found to be influenced by some kind of disturbance, therefore only horizontally polarized measurements have been used for analysis so far. Some of the horizontally polarized T_B data were also affected by this disturbance, for which we have no conclusive explanation yet. It generally produced a steep increase in T_B. Therefore, the data were simply filtered by deleting any measurements for which $T_B > T_{IR}$. This resulted in 'gaps' in the data showing where the disturbance had been present. Measurements at the edges of these gaps were also deleted as an extra precaution. The remaining T_B data, used in this study, are considered to be relevant and correct.

2.2.3 Ground measurements

During the 6-month period, soil temperature was measured at four different locations at depths of 1, 2, 4, 8, 16, 32, 64 and 100 cm below the soil surface, using thermocouples made by INRA and a CR21X Campbell Scientific data logger. Temperature measurements were taken every 10 s and averaged to half-hourly values. The same method was used to record litter temperatures at 1, 3 and 5 cm above the mineral soil surface.

For the measurements of soil and litter moisture content, 3 ThetaProbes (Delta-T Devices Ltd., type ML2x) were placed in the soil layer and 3 in the litter layer, giving an integrated measurement for a depth of 0-5 cm. The ThetaProbes each consisted of 4 rods of 60 mm length, which were placed in the respective layer at an angle of approximately 20° relative to the vertical. This location and set-up were fixed during the whole experimental period. The probes were connected to a CS21X Campbell Scientific data logger, which averaged the measurements taken every 10 seconds to give half hourly values. Both *in situ* and laboratory measurements were used for calibration. The *in situ* measurements were done by periodically (~ 1-2 times per month) taking 12 samples each of soil and litter at regular intervals along a 48 m row, at a random location at the site. These samples were then dried at 105 °C for one day (soil) or at 65 °C for a minimum of three days (litter) whilst recording weights before and after. At the end of the experiment soil and litter samples were taken from the ThetaProbe measurement location and probe values and weight were recorded for each sample throughout a drying period in the laboratory. Calibration lines for each probe combined both the *in situ* and laboratory measurements. By including the *in situ* measurements in the calibration lines, the spatial heterogeneity in soil and litter moisture throughout the footprint was accounted for. Soil and litter moisture values used in this study can therefore be regarded as footprint representative values.

Dry bulk density of the Bray soil was already known to be 1.25 g cm^{-3} from previous experiments by INRA Bordeaux, thus making it possible to convert the soil moisture measurements into volumetric moisture contents.

A soil moisture profile was obtained from another ongoing monitoring experiment at the site. Volumetric soil moisture was recorded at depths of 5, 23, 34 and 80 cm below the soil surface using TDR Trase probes and a CR21X Campbell Scientific data logger. Moisture content was measured every four hours and afterwards interpolated to half-hour values using a standard spline interpolation technique.

Precipitation above the canopy was measured at 24 m height using a fixed ARG-100 rain gauge (UMS GmbH) and a CR10X Campbell Scientific datalogger. Measurements were totalled to half-hour values.

As the Bray site is included in several international programs aiming at monitoring CO_2 fluxes at regional and global scales (EUROFLUX, FLUXNET, CARBOEUROPE (e.g. Aubinet *et al.*, 2000)), additional meteorological and vegetation data were available for this site. For the results presented in this paper we made use of branch temperature data, measured using thermocouples made by INRA Bordeaux and averaged to give half-hour values.

2.3 Theoretical Background and Methodology

2.3.1 Relationship soil moisture-emissivity

According to the Rayleigh-Jeans approximation, emitted thermal radiation in the microwave region may be expressed as (Ulaby *et al.*, 1986):

$$T_{B(P)} = e_{(P)} * T \qquad (2\text{-}1)$$

where T_B is the observed brightness temperature, T is the thermodynamic temperature of the observed surface, e is the surface emissivity and P refers to the (vertical or horizontal) polarization. Soil emissivity is related to the complex soil dielectric constant ε as described in equations 2-2 and 2-3. The first of these equations shows the relationship between soil emissivity and soil reflectivity:

$$e_{S(P)} = 1 - R_S(\theta, P) \qquad (2\text{-}2)$$

where the subscript 'S' denotes 'soil' and $R_S(\theta, P)$ is the soil reflectivity as a function of incidence angle θ and polarization. Soil reflectivity is in turn linked to the soil dielectric constant ε through the Fresnel equations, which for the horizontal polarization (subscript 'H') is:

$$R_{S,H} = \left[\frac{\cos\theta - \sqrt{\varepsilon - \sin^2\theta}}{\cos\theta + \sqrt{\varepsilon - \sin^2\theta}} \right]^2 \qquad (2\text{-}3)$$

The dielectric constant is a measure of the soil response to an electromagnetic wave and may be estimated with a dielectric mixing model. It is frequency dependent and principally determined by the soil water content, but also dependent on factors such as soil texture, salinity and temperature. As an illustration, figure 2-2 shows the relationship between soil moisture content and emissivity for a smooth Bray type soil (sand 80%, clay 10%, bulk density = 1.25 g cm^{-3}), calculated with the Dobson dielectric mixing model (Dobson *et al*., 1985).

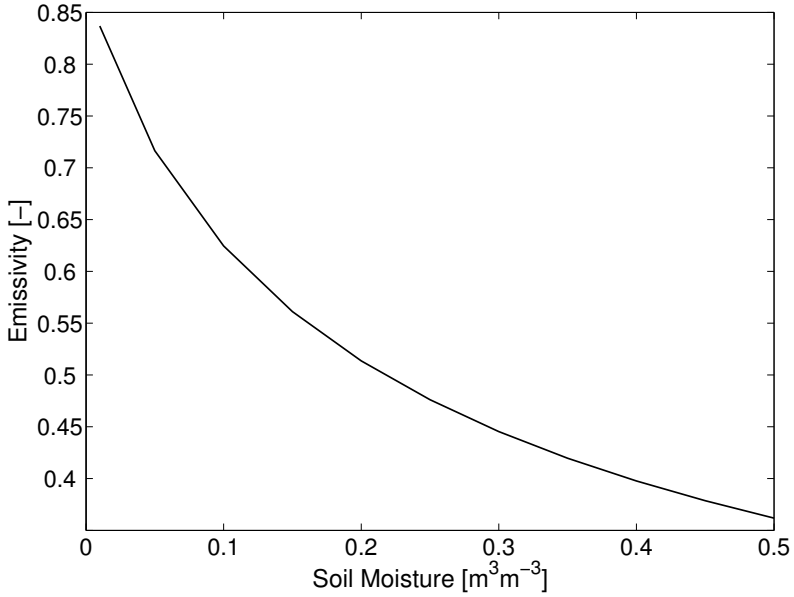

Figure 2-2: Modelling results using the method of Dobson *et al*. (1985): L-band (1.4 GHz) horizontally polarized soil emissivity at a 45º incidence angle *vs.* volumetric soil moisture. Soil parameters used in the model were representative of values found at the Bray site: sand 80%, clay 10%, bulk density 1.25 g cm^{-3} and an average top (0-5cm) soil temperature of 287.65 K.

2.3.2 Calculation of effective soil temperature

The contribution of the whole soil layer to the soil thermal emission from its surface is dependent on the soil temperature and dielectric (i.e. moisture) profiles and is expressed as the effective soil temperature. According to the theory of radiative transfer the effective soil temperature $T_{S,eff}$ at $\theta = 0°$ can be expressed as (Ulaby *et al*., 1986):

$$T_{S,eff} = \int_0^\infty T_S(z) \cdot W(z) \cdot dz \qquad (2\text{-}4)$$

where $T_S(z)$ is the soil temperature at depth z, and $W(z)$ is a temperature weighting function of the contribution of each soil layer to the effective temperature, expressed as ($\theta = 0°$):

$$W(z) = \alpha(z) \cdot \exp\left[-\int_0^z \alpha(z') \cdot dz' \right] \qquad (2\text{-}5)$$

where $\alpha(z)$ is the power attenuation coefficient related to the soil dielectric constant as:

$$\alpha(z) = (4\pi / \lambda) \cdot \varepsilon''(z) / 2(\varepsilon'(z))^{0.5} \quad (2\text{-}6)$$

where λ is the observation wavelength (in this case ≈ 21 cm) and ε' and ε'' are the real and imaginary part of the soil dielectric constant, respectively, calculated from a soil moisture profile using the previously mentioned Dobson model. Integration of the temperature profile over depth was done using a Gaussian weighting method.

2.3.3 Calculation of a composite ground-canopy temperature and emissivity

The forest is a complex system consisting of several different layers: soil, litter, understory and trees (trunks, branches, needles). It is therefore difficult to define an accurate formulation for the effective temperature T_{eff} that accounts for the contributions of all these different layers to the microwave surface emission measured above the forest. We chose to use an effective composite ground-canopy temperature (T_{gc}; gc for 'ground-canopy') as described in the forward model ('L-MEB') of the SMOS Level 2 algorithm (Kerr *et al*., 2006; Wigneron *et al*., 2007):

$$T_{\text{gc}} = A_t \cdot T_{\text{canopy}} + (1 - A_t) \cdot T_{\text{ground}} \quad (2\text{-}7)$$

where A_t ($0 \leq A_t \leq 1$) defines the contribution of each temperature component, based on the vegetation transmissivity:

$$A_t = B_t(1 - \Gamma(\theta, P)) \quad (2\text{-}8)$$

B_t is a canopy type dependent parameter, and $\Gamma(\theta,P)$ is the canopy transmissivity for viewing angle θ, which is related to the nadir vegetation optical depth τ_0 according to:

$$\Gamma(\theta, P) = e^{-\tau_0 / \cos\theta} \quad (2\text{-}9)$$

under the assumption of an isotropic canopy, i.e. there is no angular dependence of τ_0 (see Van de Griend and Wigneron, 2004a).

The infrared temperatures (T_{IR}) measured at Bray and averaged over all angles to half-hour values, were found to correspond reasonably closely to branch temperatures of the trees (R^2 = 0.84, RMSE = 3.9 K) and were therefore used as an estimate of canopy temperature T_{canopy} in eq. 2-7. For T_{ground} we used the effective soil temperature $T_{\text{S,eff}}$ calculated from equations 2-4 to 2-6.

Determination of the 'effective' thermodynamic temperature T_{gc} of the emitting forest system comes down to estimation of the parameters τ_0 and B_t in equations 2-7 to 2-9, because they describe the contributions of the canopy itself and the soil/litter surface. In order to estimate τ_0 and B_t, we selected five periods of 2-7 days during which it may be assumed that the forest conditions were basically constant, and thus microwave emission was constant. Selection criteria for the measurements used within each period were *1)* no rainfall during the past 24 hours, *2)* soil moisture

content below field capacity (< 0.25 m^3m^{-3}) and *3)* no sudden in-/decrease in soil moisture content during the period.
The assumption of constant emissivity was validated by calculating *i)* the angular index *AI* over short periods of time and *ii)* the emissivity for isothermal conditions. Both *AI* and isothermal emissivity rule out influences of temperature fluctuations, as will be explained below. In this case emission can be influenced by variations in moisture content only, if all other surface variables remain unchanged (eq. 2-1 to 2-3). Assuming constant emissivity therefore means assuming constant forest conditions, in order to give reliable values of τ_0 and B_t.
For the calculation of *i)*, the angular index *AI* was based on the general formulation of the polarization ratio, and is therefore expressed as:

$$AI = (T_B(\theta_1) - T_B(\theta_2))/(T_B(\theta_1) + T_B(\theta_2)) \qquad (2\text{-}10)$$

with, in this study: θ_1 = 50º and θ_2 = 25º. The use of a normalization such as this allows for the removal of temperature effects, and *AI* is therefore primarily dependent on moisture content (see e.g. Pellarin *et al*., 2003b).
Calculation of *ii)* was done by defining 'isothermal conditions' as times at which $T_{S,eff} - T_{IR} < 1$ K. At these times, the temperatures of soil and canopy being almost the same, there is only one representative temperature for the whole forest system. The resulting emissivity (from eq. 2-1) plotted in time is therefore also an expression of moisture content only.

The optimum values of τ_0 and B_t (eq. 2-7 to 2-9) for each of the five selected periods were then determined by minimizing the following error criterion:

$$\sum_0^N \left[T_B/T_{gc} - \frac{\sum_0^N (T_B/T_{gc})}{N} \right]^2 = \min. \qquad (2\text{-}11)$$

where N is the number of measurements in the given period and T_{gc} is defined as in eq. 2-7. The composite ground-canopy temperature T_{gc} was subsequently used to calculate the L-band emissivity from the above-forest T_B-observations using eq. 2-1, with the surface temperature T replaced by T_{gc}. This composite ground-canopy emissivity will be called e_{gc} (= T_B/T_{gc}). The criterion in eq. 2-11 is therefore based on minimization of the difference between measured and average values of emissivity e_{gc}. The results presented in this study were all calculated using an incidence angle of 45º.

2.4 Results

2.4.1 Parameter retrieval and validation

The minimization criterion (eq. 2-11) was applied to the T_B measurements for each of the five periods separately and resulting optimum values of τ_0 and B_t can be found in table 2-1. The standard deviation over the average values of τ_0 and B_t (table 2-1, last row) results in a 0.3 K uncertainty in T_{gc}.

Table 2-1: Optimum values (average ± standard deviation) found for parameters τ_0 and B_t after minimization of eq. 2-11, together with the resulting error of optimization and the number of observations (#) for the five selected periods.

Period (JD)	τ_0	B_t	*#*
251-252	0.66	0.55	40
261-263	0.51	0.31	71
272-276	0.65	0.53	46
303-307	0.72	0.62	85
321-327	0.58	0.43	103
All (average)	0.62 ± 0.08	0.65 ± 0.12	335

As an example of one of the five selected periods for validation, figure 2-3 shows (top-bottom) a time series of T_B, four temperatures of the forest system (T_{IR}, litter temperature T_{lit}, $T_{S,eff}$, T_{gc}), the angular index *AI*, emissivity e_{gc} (isothermal conditions marked by 'o'), soil moisture content and precipitation *P* for Julian Day (JD) 303-307 (29 Oct. – 2 Nov.). As can be seen in the figure, the T_B signal is mainly dominated by the behaviour of the thermodynamic temperatures. Both the isothermal emissivity values and the angular index *AI* are approximately constant over this short period of time, thus validating the assumption of constant emissivity on which the calculation of T_{gc} is based.

Following eq. 2-9, the average value found for τ_0 in table 2-1 ($\tau_0 = 0.62$) leads to $\Gamma_0 = 0.54$. Therefore, the approach described in the previous chapter first of all leads to a workable formulation of the optimum effective temperature of the complex emitting surface. Second, it demonstrates that the *nadir* canopy transmissivity $\Gamma_0(\theta = 45°)$ - this denotes that the vertical transmissivity has been derived from 45° observations - is of the order of 54%. Consequently, at an angle of 45°, 42% of the soil/litter surface contributes to the above-canopy emission for this specific forest (from eq. 2-9).

2.4.2 Behaviour of temperature and surface moisture

As an illustration, figure 2-4 shows soil temperatures measured at different depths (1, 8 and 64 cm below the soil surface) during the period Julian Day 302-307 (28 Oct.-2 Nov.), together with the calculated effective soil temperature (eq. 2-4). The diurnal range of the near-surface soil temperature is only around 2 degrees, which is not surprising for this kind of forest system in which the soil layer is sheltered from direct sunlight by mature trees, a grass understory and a substantial litter layer. In general, soil effective temperatures were found to lie very close to temperatures measured just under the soil surface.

Table 2-2: Correlation between 45° brightness temperature (T_B) measurements and infrared surface temperature (T_{IR}) measurements, litter temperature (T_{lit}) measurements, effective soil temperature from eq's 2-4 to 2-6 ($T_{S,eff}$) and effective ground-canopy temperature from eq's 2.7 to 2-9 (T_{gc}) at the Bray site between July and December 2004.

# = 1238	T_B	T_{IR}	T_{lit}	$T_{S,eff}$	T_{gc}
T_B	1.0000	0.8480	0.8450	0.8177	0.8686

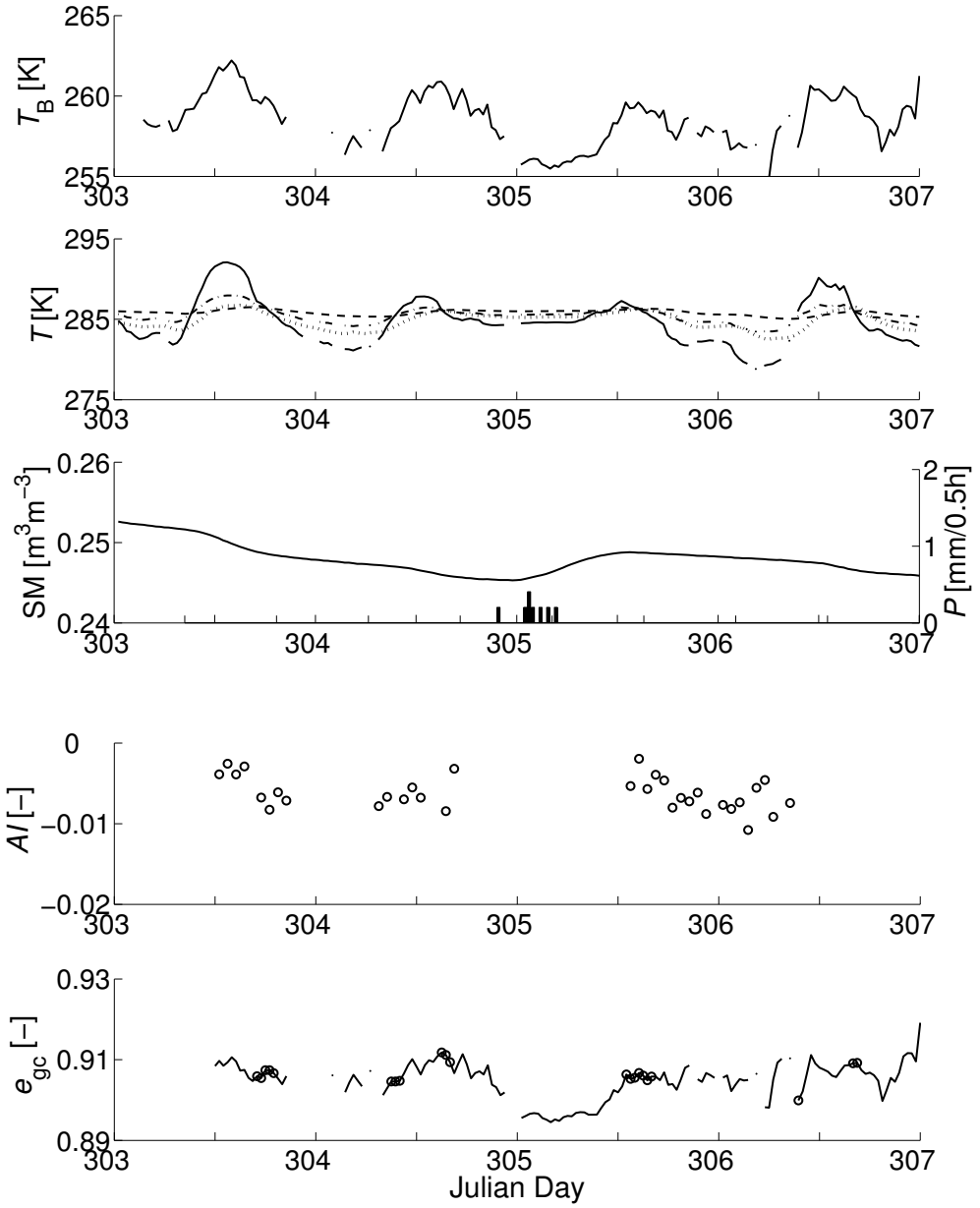

Figure 2-3: Results for Julian Day 303-307 (29 Oct. – 2 Nov.) using field measurements and modelling. Top-bottom: 1) measured brightness temperature (T_B) [K] at a 45º incidence angle; 2) measured surface (infrared) and litter temperatures (– T_{IR} and ··· T_{lit} respectively), effective soil temperature from eq's 2-4 to 2-6 (--- $T_{S,eff}$) and effective ground-canopy temperature from eq's 2-7 to 2-9 (– · – T_{gc}), all in [K]; 3) Measured volumetric soil moisture [m^{3}m^{-3}] and precipitation P [mm/half hour]; 4) Angular index AI [-] from eq. 2-10 with observations at 50º and 25º angles; 5) Ground-canopy emissivity e_{gc} [-] from eq. 2-1 and 45° observations, with isothermal conditions marked by 'o'.

In order to get an impression of their relative importance, four different thermodynamic temperatures were compared to the measured brightness temperature to see which was best correlated with T_B. Temperatures used were *i)* the infrared temperature T_{IR} measured from the tower, *ii)* the litter temperature T_{lit} measured within the litter layer, *iii)* the soil effective temperature $T_{S,eff}$ as described in eq. 2-4

and *iv)* the composite ground-canopy temperature T_{gc} from eq. 2-7. Table 2-2 shows the results of this correlation analysis for the whole experimental period.
As expected, the thermodynamic temperature T_{gc} has the highest correlation with T_B (87%), as this corresponds with the smallest variation in resulting emissivity, i.e the minimization criterion of eq. 2-11.

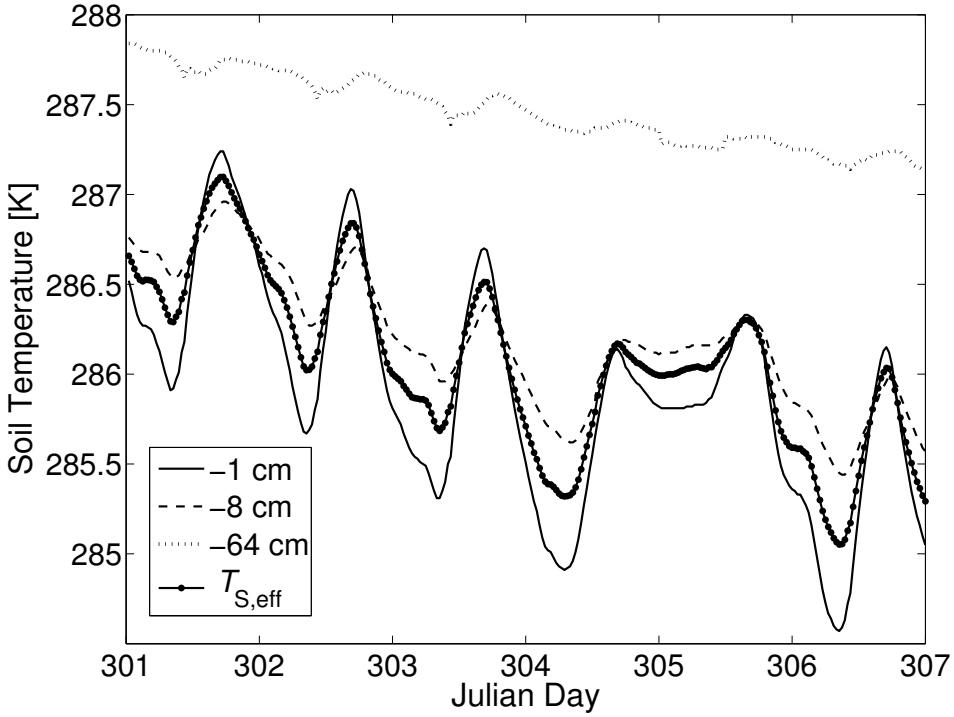

Figure 2-4: Measured soil temperatures at 1, 8 and 64 cm depth together with the effective soil temperature resulting from eq. 2-4 to 2-6, for Julian Day 302-307 (28 Oct. – 2 Nov.). All temperatures in [K].

Figure 2-5a shows a plot of volumetric soil moisture (SM) against gravimetric litter moisture (LM), for all measurements taken at the Bray site between July and December and therefore covering a wide range of moisture conditions. The linear patterns in the figure are caused by the drying up of the soil and litter layers in between rain events. This becomes more clear by looking at figure 2-5b, which shows a time series for SM and LM together with precipitation events. As an example, one of these drying patterns has been circled in both figures. It should be noted here that, due to a technical problem with the rain gauge at Bray, precipitation data between JD 252.8 (9th Sept.) and JD 347.2 (13th Dec.) were taken from a different gauge at approximately 3 km distance from the site.
Figure 2-5a shows that there is a strong relationship between soil and litter moisture, which will make it difficult to decouple the effects of the soil and litter layers in further analyses. Additional research on the dielectric behaviour of the litter layer is therefore necessary in order to better understand the radiometric signal above this type of forest system.

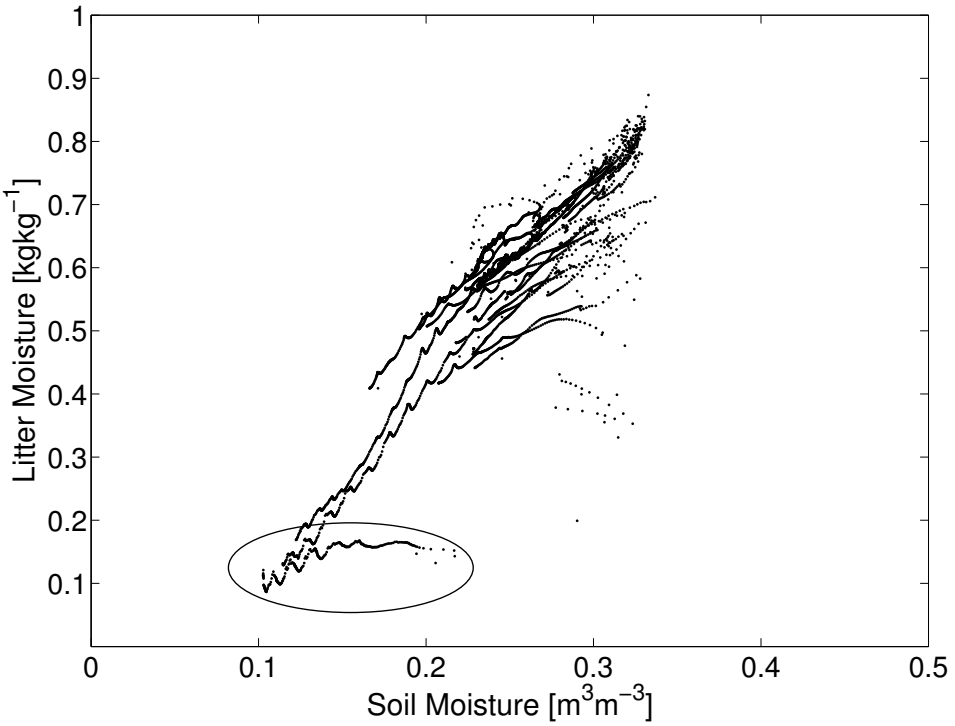

Figure 2-5a: Soil moisture content [m^3m^{-3}] *vs.* litter moisture content [$kgkg^{-1}$] measured at the Bray site between July and December 2004. R^2 = 0.84. The ellipse marks the same drying cycle as shown in figure 2-5b.

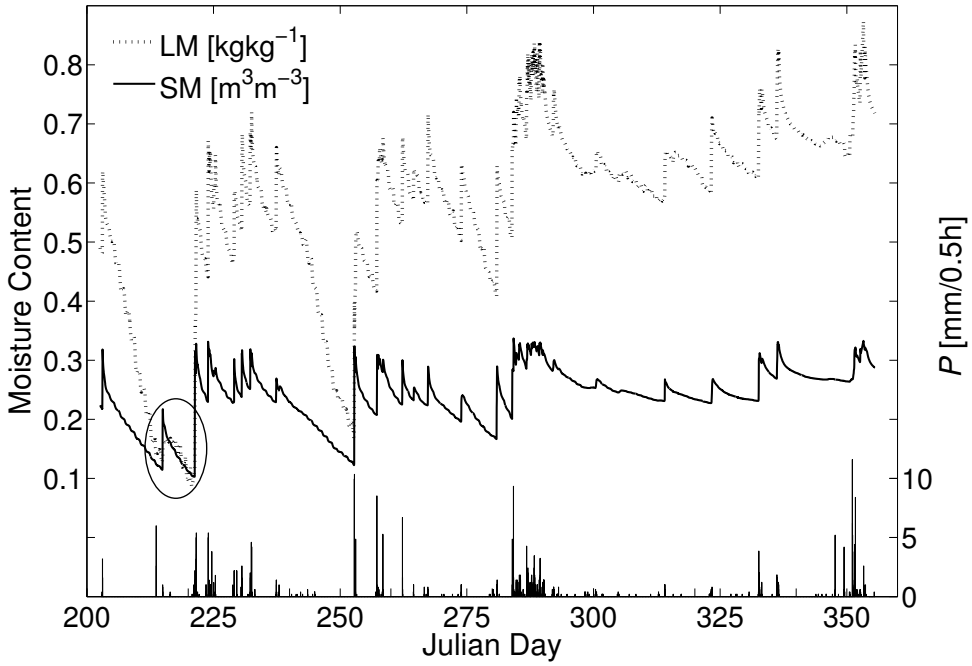

Figure 2-5b: Time series of soil and litter moisture content (in [m^3m^{-3}] and [$kgkg^{-1}$] repectively) and precipitation *P* [mm/half hour] measured at the Bray site between July and December 2004. Precipitation data between JD 252.8 (9th Sept.) and JD 347.2 (13th Dec.) were measured at 3 km distance of Bray. The ellipse marks the same drying cycle as shown in figure 2-5a.

2.4.3 Signal behaviour for different incidence angles

Brightness temperatures T_B were plotted against incidence angle for angles between 25º and 60º as shown in figure 2-6a. The figure shows measurements from the whole period split into 'wet' (when soil moisture SM > 0.25 m^3m^{-3}) and 'dry' (SM < 0.15 m^3m^{-3}) conditions. For both series of measurements, only observations with no precipitation during the preceding 12 hours were used.
The pattern of a decreasing emissivity with increasing viewing angle is a typical radiometric pattern for a soil layer at horizontal polarization and figure 2-6a (left) therefore shows that this medium dense forest does not completely block the soil signal. In a dense forest the canopy would block the soil emission and emissivity would be almost constant at all angles, giving the typical radiometric pattern for a vegetation layer. It follows from the Fresnel equations (eq. 2-3) that wet and dry bare soils show comparable angular patterns, with lower emissivity values for wet soils.

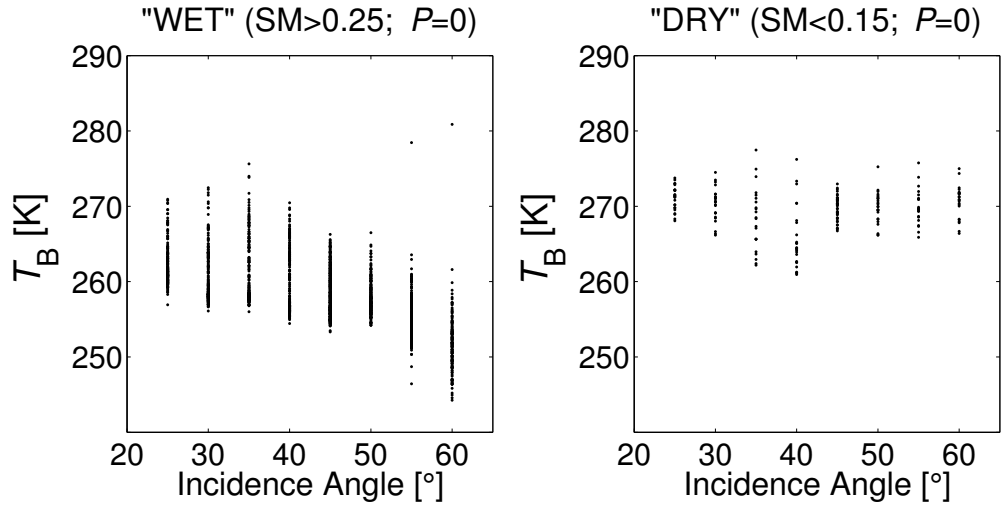

Figure 2-6a: All measured brightness temperatures (T_B) [K] for incidence angles 25°-60°, excluding those where precipitation had occurred in the past 12 hours. Left: 'wet' measurements at times when measured soil moisture SM > 0.25 m^3m^{-3}; Right: 'dry' measurements at times when measured soil moisture SM < 0.15 m^3m^{-3}.

However, in the case of fig. 2-6, the angular pattern for 'wet' and 'dry' conditions is quite different. Because precipitation events were excluded here, the condition of the vegetation canopy can be assumed similar in both cases, and can therefore not be the cause of this marked difference. A possible explanation for the difference between the 'wet' and 'dry' patterns in fig. 2-6 might lie in the behaviour of the thick litter layer, however more research is necessary in order to investigate this. Irregularities in the patterns in figure 2-6a (e.g. around θ = 35°-40°, especially for dry conditions) may be due to the effect of heterogeneity in the forest cover fraction.
The differences in the pattern of incidence angle *vs*. T_B for different soil moisture conditions can also be expressed by the angular index *AI* (eq. 2-10). Figure 2-6b shows the relationship between SM and *AI*, for which R^2 = 0.13. RMSE with the fitted line (*AI* = -0.0362 * SM + 0.0019) is 0.004. Because a dry soil gives higher emissivity values than a wet soil at all angles, the denominator in eq. 2-10 is higher under dry soil conditions and the *AI* approaches zero.

2.4.4 Signal behaviour with precipitation

Figure 2-7 shows (top-bottom) soil and litter moisture content, emissivity e_{gc} and precipitation plotted in time for Julian Day 257-263 (13-19 Sept.). In the figure, three events are marked by arrows, highlighting the varied response of the signal to changes in wetness conditions. Arrow 1 shows a drop in emissivity at a time with only very slight precipitation, though heavy rainfall has occurred previously as can be seen in the bottom graph. The increase in soil and litter moisture values is also very slight (approx. 0.02 m^3m^{-3} and 0.04 $kgkg^{-1}$ respectively), although they are still high following the earlier rainfall.

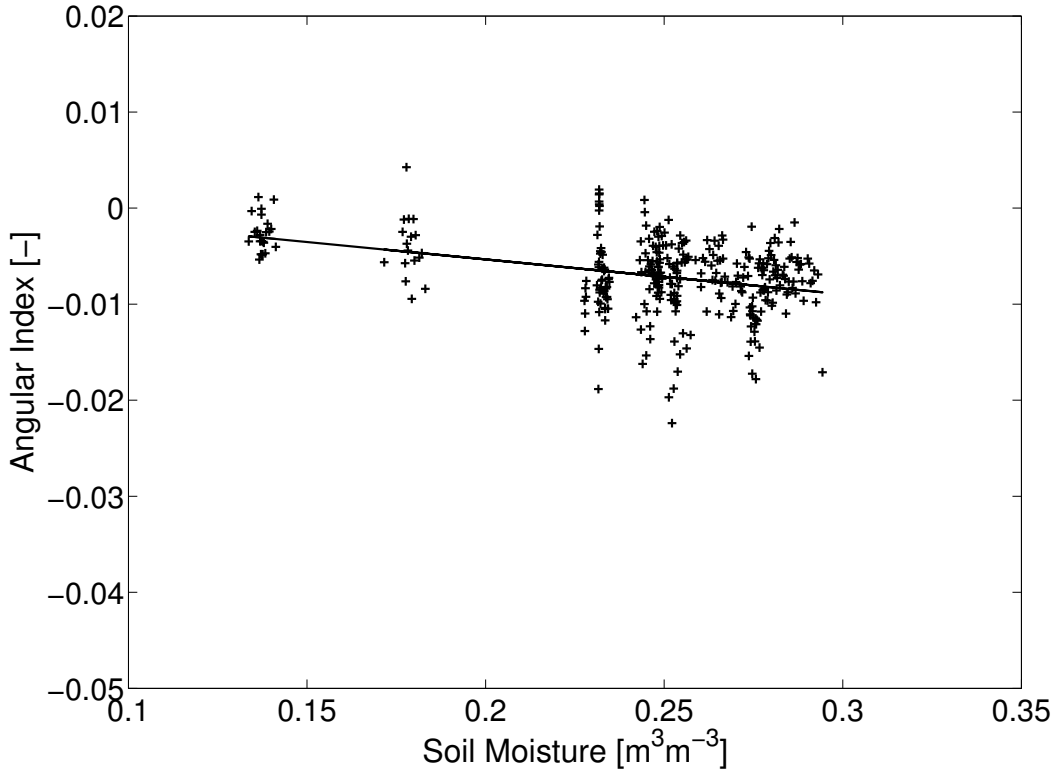

Figure 2-6b: Angular Index *AI* [-] resulting from eq. 2-10 with observations at 50º and 25º angles, *vs*. measured soil moisture (SM) content [m^3m^{-3}]. Fitted line: *AI* = -0.0362 * SM + 0.0019; R^2 = 0.13; RMSE = 0.004.

Arrow 2 points out a similar drop in emissivity for a situation where rainfall is higher (5.2 mm/half hour), although the increase in soil and litter moisture is still slight (again ~ 0.02 m^3m^{-3} and 0.04 $kgkg^{-1}$ respectively). Finally, arrow 3 shows the signal response for a situation with 'high' rainfall (6.7 mm/half hour) and a higher increase in soil and litter moisture (~ 0.07 m^3m^{-3} and 0.1 $kgkg^{-1}$ respectively). A quantitative relation between the amount of precipitation, the change in soil/litter moisture content and the change in emissivity can not be given here. However, the results do clearly show that emissivity decreases directly after rainfall, which would be in line with the hypothesis recently given by Hornbuckle *et al*. (2006).
Finally, a general increase in emissivity over time can be seen while soil and litter moisture content decrease (Julian Day ~ 258.5-262.3).

2.4.5 Sensitivity to surface moisture

In figure 2-8 the emissivity e_{gc} is plotted against soil moisture (left hand side) and litter moisture (right hand side) respectively. These figures comprise all radiometric measurements at 45° in the current dataset. Measurements for which no rainfall events occurred during the preceding 12 hours are marked by '+', otherwise the symbol '▪' is used. It should be noted that the same pattern was found when using only measurements for isothermal conditions (results not shown here), which again validates the calculation of T_{gc}.
In general, compared to the curve for a bare soil of the Bray type (fig. 2-2), the slope of the curve in fig. 2-8 is different and emissivity values found over the forest are much higher. This is not unexpected, as the canopy and possibly the litter layer also contribute to the overall emission. Emissivity values found here are of the same order of magnitude as values measured over Les Landes forest sites during the EuroSTARRS campaign (Saleh *et al*., 2004a).

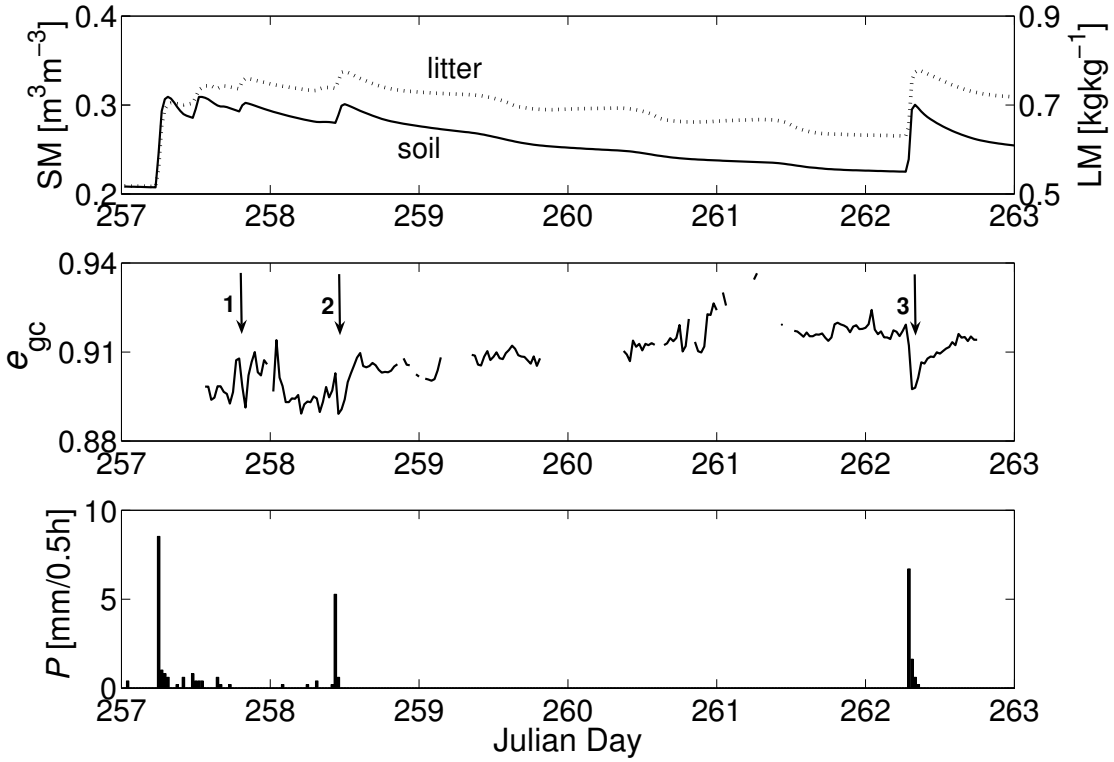

Figure 2-7: Emissivity response for varying wetness conditions, Julian Day 257-263 (13-19 Sept.). Top: litter [kgkg^{-1}] and soil [m^{3}m^{-3}] moisture content measured at the Bray site; middle: ground-canopy emissivity e_{gc} [-] from eq. 2-1 and 45° observations; bottom: precipitation P [mm/half hour] measured 3 km from the Bray site.

The small range in emissivity and the magnitude of around 0.91 emphasize the black-body character of this type of forest system. Linear correlation between *i)* e_{gc} and soil moisture, and *ii)* e_{gc} and litter moisture gives R^2-values of only 0.36 and 0.27 (statistically significant within a confidence interval of 95%). In addition to the low R^2 values, the sensitivity of the microwave signal to changes in soil or litter moisture is also very low: the dynamic range of emissivity e_{gc} is ~ 0.03 for a 0.2 m^{3}m^{-3} range in soil volumetric moisture and a 0.6 kgkg^{-1} range in litter gravimetric moisture. Therefore, the dynamic range in emissivity between wet and dry soil conditions is,

although detectable, probably too small for any meaningful soil moisture retrieval in this kind of environment.

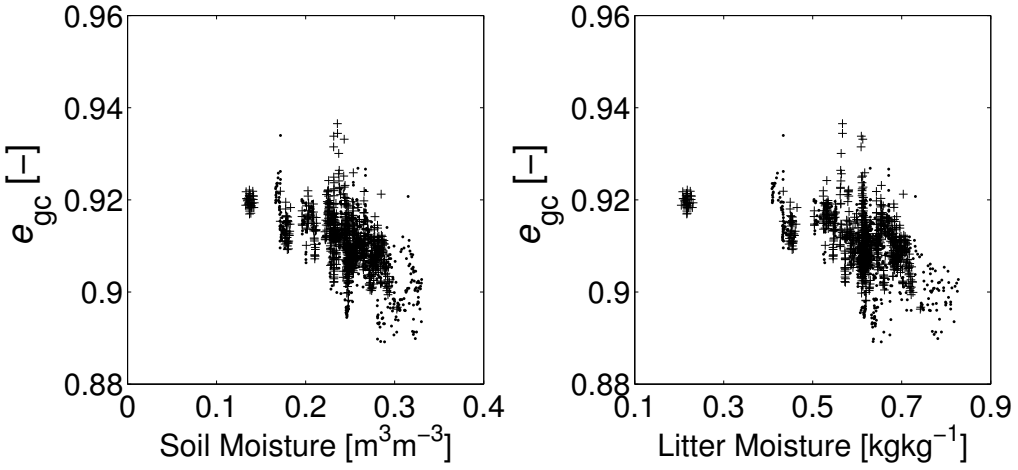

Figure 2-8: Measured soil (left) and litter (right) moisture content (in [m^3m^{-3}] and [$kgkg^{-1}$] repectively) at the Bray site *vs*. ground-canopy emissivity e_{gc} [-] from eq. 2-1 and 45° observations (symbol '+'). Radiometric measurements where precipitation occurred during the past 12 hours are marked by the symbol '▪'.

2.5 Summary and Conclusions

During the 'Bray 2004' experiment L-band microwave measurements were done at horizontal polarization over a temperate coniferous forest from July – December 2004. Ground measurements were taken of precipitation and soil and litter moisture content. This study describes the experiment and its objectives and gives some first results of multi-angular measurements of a pine forest under different wetness conditions. This work will contribute to future radiative transfer modelling of forested areas within the framework of the SMOS Level 2 algorithm.

Some interesting features of the behaviour and relative importance of the different forest layers at the 1.4 GHz frequency were shown in this study:

First, emissivity was calculated using the Rayleigh-Jeans approximation and a composite ground-canopy temperature T_{gc} as described by Kerr *et al*. (2006) and Wigneron *et al*. (2007), of which the site-specific parameters could be determined from *in situ* observations. Based on this analysis the average local optical depth ($\tau_0(\theta);\theta = 45^o$) of the Bray-forest was determined at 0.62 which corresponds to a vertical transmissivity of 54% ($\Gamma_0 = 0.54$). Second, emissivity values found over the forest are high (~ 0.91), as was also found during the EuroSTARRS experiment over other sites of Les Landes (Saleh *et al*., 2004a). Excluding periods of rainfall, the diurnal trend of T_B was dominated by the effect of surface temperature. Emissivity values were found to decrease following rainfall, however, a quantitative relation between the amount of precipitation, the change in soil/litter moisture content and the change in emissivity could not be given. The strong correlation found between the moisture content of litter and soil makes the decoupling of litter and soil effects difficult.

Finally, variations in soil moisture and/or litter moisture were also visible in both the angular index and the above canopy microwave emission e_{gc}. The dynamic range of

this last effect was assessed and amounted to $\delta e_{gc} \sim 0.03$ for a 0.2 m^3m^{-3} range in soil volumetric moisture. However, with an R^2 value of only 0.36, this range is probably too small to retrieve soil moisture with a meaningful precision in this kind of environment.

Earlier studies (Schmugge *et al*., 1988; Jackson and Schmugge, 1991; Saleh *et al*., 2006) suggest that the presence of a thick, highly absorbing root/litter layer can lead to high emissivity values for both dry and (especially) wet conditions. Together with the attenuating effect of the trees, this could contribute to the low sensitivity to surface moisture found in this study, as a substantial litter layer was also present at the Bray site. Also, it could be an explanation for the difference in angular signature found for wet and dry soil conditions. In general, separating the influence of each forest layer is a complex work and further research is currently in progress to gain a fuller understanding on this point.

Chapter 3

Calibration of the L-MEB Model over a Coniferous and a Deciduous Forest*

3.1 Introduction

The accuracy of radiometric (e.g. L-band or 1.4 GHz) soil moisture retrievals over vegetated land surfaces depends to a great amount on the properties of the vegetation layer. A vegetation layer covering the soil scatters and attenuates soil emission and will add its own emission to the total radiation measured above the canopy. This effect was modelled by Kirdyashev *et al*. (1979). The thicker or denser this layer, or the higher the frequency of measurement, the smaller the influence of the soil signal on the total above-canopy emission. Obviously, soil moisture retrievals will be less accurate over dense forests than over sparse vegetation. Previous microwave forest studies were therefore generally done at higher frequencies than L-band, focusing on the measurement of forest biometric properties rather than assessing surface properties underneath the canopy (for a summary see Pampaloni (2004)).
Besides the effect of vegetation, the effect of moisture conditions will also play a role in determining the sensitivity of the radiometric signal to soil moisture. Soil emission decreases with increased moisture content, but a vegetation layer such as a temperate deciduous or coniferous forest will show the opposite effect and have a higher emission with increased water content (Ulaby *et al*., 1986; Mätzler, 2006). These opposite effects are due to the different physical behaviour of each layer in terms of absorption and scattering, and they complicate our understanding of the L-band signal above vegetated surfaces.
From the few previous experimental forest studies at L-band (Macelloni *et al*., 2001; Lang *et al*., 2001; Grant *et al*., 2007; Guglielmetti *et al*., 2007) a high accuracy of soil moisture retrieval over forests is not to be expected. Not only may the vegetation layer of tree canopy and understory be relatively dense, in this type of environment a litter layer is often an additional cover of the mineral soil. Studies over grasslands (Schmugge *et al*., 1988; Jackson and Schmugge, 1991; Saleh *et al*., 2006) have hinted at the fact that this layer could highly attenuate soil emission, although radiative transfer properties of litter are still largely unknown.

The Soil Moisture and Ocean Salinity (SMOS) mission of the European Space Agency (ESA) will produce global measurements of soil moisture over land surfaces and salinity over the oceans on a temporal scale of 2-3 days (Kerr *et al*., 2001; Berger *et al*., 2003). Pixel dimensions will be on the order of 40 x 40 km^2. It is easy to see that at this scale many pixels will contain at least partial vegetation cover. In temperate, boreal and tropical zones, forests are a major occurring vegetation type and

---

will influence measurements in many pixels if not accounted for in the retrieval algorithms. However, *a priori* information on vegetation cover fraction will be available for SMOS, and if the emission behaviour of forests is also known beforehand, it could be possible to retrieve accurate soil moisture values for the non-forested parts of the mixed pixel in some cases (Van de Griend *et al*., 2004). For this reason, the understanding of forest radiative transfer properties is an important aspect within the context of SMOS.

The forward model used in the SMOS Level 2 soil moisture algorithm is 'L-band Microwave Emission of the Biosphere' or 'L-MEB' (Wigneron *et al*., 2007). This model is based on a zero-order radiative transfer approach, often called the tau-omega (τ-ω) approach in the literature after the two vegetation parameters τ and ω, linked to canopy transmissivity and scattering respectively. Although physically-based, it is a relatively simple approach which is easy to use and does not require detailed information on the vegetation/soil layers beforehand, making it well suited to operational use at a global scale.
Inversion of L-MEB for the SMOS Level 2 soil moisture algorithm requires calibration of the various soil and vegetation model parameters for different land cover types. Previous calibrations have included bare soils, grass and various types of crops (for a summary see Wigneron *et al*. (2007)). This study presents the first calibration of the forward model L-MEB over forests using experimental data. Previous forest studies in the context of SMOS were all based on modelling and/or very short-term experiments (e.g. Saleh *et al*., 2004a; Della Vecchia *et al*., 2006a).
Parts of the coniferous and deciduous data sets used in this study have previously been presented in Grant *et al*. (2007) and Guglielmetti *et al*. (2007) respectively. Main conclusions of those studies were (1) that branches are more important absorbers/emitters than leaves or trunks at L-band and (2) that at L-band variations in ground moisture over a medium dense forest (total aboveground biomass ~ 11 kg m^{-2}) with a distinctive litter layer are detectable, but have too small a dynamic range to result in soil moisture retrieval with a meaningful precision. Concerning litter, the current study does not focus specifically on that aspect, as the main purpose here was to calibrate the existing L-MEB algorithm over forests. Other studies are currently under progress to investigate the radiative transfer properties of such a layer.

This paper first gives an outline of the data sets and models used, including the description of a new experiment over conifers. Then, it presents the calibration of the relevant canopy and soil parameters in L-MEB, using experimental forest data. Results are given for two types of temperate forest (coniferous and deciduous), allowing for a general comparison. For the deciduous forest, a relationship between canopy optical depth and leaf area index (LAI) is also investigated. Finally, a sensitivity study is done for the focus parameters, temperature, soil moisture and precipitation.

3.2 Materials

In this study, three data sets were used. The first is the 'Bray' data set, consisting of measurements over a coniferous forest stand. The second is the 'FOSMEX' data set, consisting of measurements over a deciduous forest stand. The third data set consists of numerical simulations for three stands in Les Landes coniferous forest.

3.2.1 Bray site and data set

The Bray site lies within the forest of Les Landes, at approximately 20 km southwest of Bordeaux, France (latitude 44°42′ N, longitude 0°46′ W, altitude 61 m) and consists of Maritime Pines (*Pinus pinaster* Ait). Tree age was 34 years at the time of measurement, resulting in a stand height of approximately 22 m. Maximum values for canopy Leaf Area Index (LAI) are around 2.15 and the forest can thus be described as 'medium dense'. The understory consists mostly of grass (mainly *Molinia caerulea* L. Moench). Soils are sandy and hydromorphic podzols, with dark organic matter in the first 60 cm. On top of the soil lies a thick litter layer, the upper part of which consists mainly of dead grass and the lower part of grass roots, pine needles and other organic matter (humus).

Downward multi-angular microwave measurements at Bray were made using the L-band (1.41 GHz) EMIRAD radiometer of the Technical University of Denmark (Søbjærg, 2002). These measurements were made from a 40 m high tower at horizontal polarization and angles of 25º, 30º, 35º, 40º, 45º, 50º, 55º and 60º from nadir. Full (-3 dB) antenna beamwidth was 25º, resulting in a ~ 600 m^2 footprint at 45º. A thermal IR scanner (Heitronics KT 15.85D (9.6 – 11.5 μm)) was fixed next to the radiometer to obtain measurements of surface temperature over the same area. Vertically polarized microwave measurements were found to be influenced by some kind of disturbance and were therefore not used. Simultaneous ground measurements were made of soil and litter temperature, soil and litter moisture content, and precipitation. The experiment was performed between July and December 2004 and is described in detail in Grant *et al*. (2007).

Upward microwave measurements at Bray were made on 22nd of February 2006, again using the EMIRAD radiometer. The instrument was mounted on a structure (see Fig. 3-1 (top)), allowing it to take H and V polarized measurements of the forest at incidence angles between 90º and 0º relative to the upward vertical (zenith) as illustrated in Fig. 3-1 (middle). Three measurement series were taken at different azimuth angles, i.e. at 60º, 45º and 0º (parallel) relative to the row direction of the trees (see Fig. 3-1 (bottom)). Sky measurements were also taken for external calibration purposes, as explained in Grant *et a*l. (2007). Sky brightness temperature calculated from Pellarin *et al*. (2003a) was ~ 5 K.

3.2.2 Jülich site and FOSMEX data set

The FOSMEX experiment took place at the Jülich site, which lies within a mixed deciduous forest in West Germany (latitude 6° 21' 30'' E, longitude 50° 50' 30'' N, altitude 83 m). Within this site, the locations of the up- and downward radiometric measurements were in close proximity to each other. In the case of the upward measurements (Guglielmetti *et al*., 2007), the sole observed tree species was 70 years old Beech (*Fagus*) with an average crown height of approximately 20 m. At the location of the downward measurements (Guglielmetti *et al*., 2008) the forest comprised species of Oak (*Quercus*), Birch (*Betula*) and Beech (*Fagus*) in similar proportions. Tree age here was between 40 and 80 years old and the average crown height was approximately 24 m. In general, the forest can be described as 'rather dense'. The ground surface is covered by a 0-5 cm thick litter layer consisting of dead

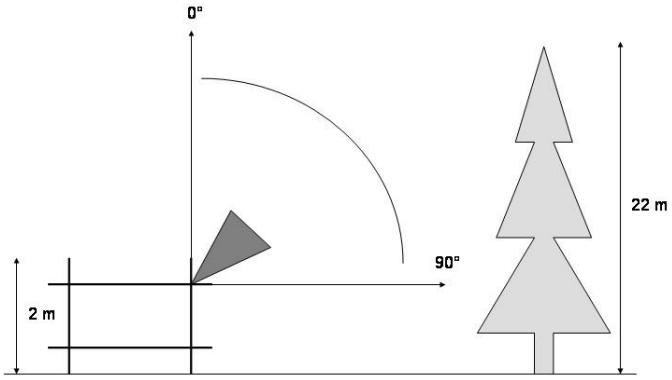

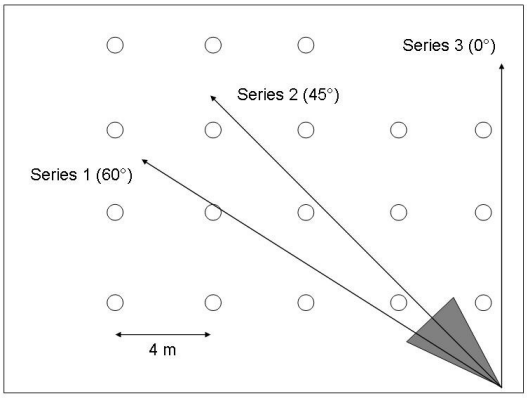

Figure 3-1: (top) Upward measurements of the canopy at the Bray site, using the EMIRAD L-band (1.4 GHz) radiometer mounted on a ~ 2 m high structure; (middle) Schematic drawing of the experimental set-up during the Bray upward measurements (side view). Measurements were made at incidence angles between 0° and 90°, with 0° being the upward vertical; (bottom) Schematic drawing of the Bray upward measurements, as seen from above. Trees are denoted by circles. Three series of measurements were made: at azimuth angles 60°, 45° and 0° relative to the row direction of the trees.

leaves, and the top 7 cm of the mineral soil also contains a large percentage of organic matter.

Downward radiometric measurements at Jülich were made during the whole of 2005, with two hiatuses between Julian Days 109-142 (19th April – 22nd May) and 227-280 (15th Aug. – 7th Oct.). The ETH Zürich radiometers ELBARA (1.4 GHz; dual polarization (Mätzler *et al*., 2003)) and MORA (11.4 GHz; vertical polarization (Institute for Applied Physics, 1991)) were installed on a 100 m high tower over the forest. Multiangular measurements were taken at angles of 46°, 50°, 54°, 58°, 62°, 66° and 70° from nadir, however only angles < 60° were included in the final data set. Full (-3 dB) antenna beamwidth was 12º, resulting in a footprint of ~ 1200 m^2 at 46°. Simultaneous ground measurements of soil temperature and soil moisture content were taken, together with precipitation and air temperature at 20 m. This experiment is described in detail in Guglielmetti *et al*. (2008).

Upward measurements at Jülich were made from September-November 2004 during the defoliation phase of the forest, again at multiple angles (40º and 60º) using the radiometers ELBARA and MORA. A detailed description of this experiment can be found in Guglielmetti *et al*. (2007). Soil surface temperatures were measured *in situ* with thermistors (Campbell S140 TL107) installed horizontally at 5 cm depth at 16 locations along two transects between the trees, in order to give representative temperatures of the forest ground.

3.2.3 Synthetic data set over Les Landes

Les Landes is a production forest in southwest France, consisting mainly of Maritime Pines (*Pinus pinaster* Ait). A synthetic brightness temperature data set was generated for purposes of initialization and comparison with the Bray brightness temperature measurements described in §3.2.1. The coniferous forest geometric database of Saleh *et al*. (2005) was used in combination with the 'Tor Vergata' model (§3.3.3) to produce simulated brightness temperatures, as also described in Saleh *et al*. (2004b). The synthetic data set includes brightness temperatures of three populations of trees (5, 26 and 32 years old) , at H and V polarization, incidence angles 10°, 20°, 30°, 40° and 50°, and soil moisture conditions from 0.05 to 0.4 m^3m^{-3} for a smooth soil of known temperature. The data set was compared with 'L-MEB' model (§3.3.1) simulations, and optimum values of the necessary L-MEB parameters were retrieved.

3.3 Models

3.3.1 L-MEB

The L-MEB model (Wigneron *et al*., 2007) is based on a simplified (zero-order) radiative transfer equation, often called the tau-omega or τ-ω model in the literature (Kirdyashev *et al*., 1979; Mo *et al*., 1982; Wigneron *et al*., 1995). In this model, multiple scattering is neglected, as is the reflection at the vegetation-atmosphere interface.

The main L-MEB equation is as follows:

$$T_B(\theta,P) = e_s T_s \gamma + (1-\omega)(1-\gamma)T_c(1+(1-e_s)\gamma) + T_{B,sky}(1-e_s)\gamma^2 \quad (3\text{-}1)$$

The total brightness temperature T_B (dependent on incidence angle θ and polarization P) results from addition of four terms: i) the soil emission attenuated by the canopy layer, ii) direct canopy emission, iii) canopy emission reflected by the soil back through the canopy and iv) sky emission reflected by the soil and twice attenuated by the canopy layer. In this model, the subscripts 's' and 'c' denote 'soil' and 'canopy' respectively. The sky brightness temperature $T_{B,sky}$ was calculated according to Pellarin *et al.* (2003a). The variable T is a thermodynamic temperature, e is the emissivity, and ω is the single scattering albedo of the canopy.
Finally, the variable γ describes the canopy transmissivity, which is related to the canopy optical depth τ according to:

$$\gamma(\theta,P) = \exp(-\tau_0(\theta,P)/\cos\theta) \quad (3\text{-}2)$$

where $\tau_0(\theta,P)$ denotes the nadir (0º) optical depth calculated from an observation at angle θ. Dividing by the cosine corrects for the difference in physical length through the canopy layer at different angles, but does not take into account the anisotropic effects of the canopy structure, which can change with incidence angle depending on the orientation of the canopy elements and the polarization of the measured signal. Therefore, the extra parameter $tt(P)$ has been introduced in the model to correct for canopy structure:

$$\tau_0(\theta,P) = \tau_{NAD}(\sin^2(\theta)\cdot tt(P) + \cos^2(\theta)) \quad (3\text{-}3)$$

where the subscript 'NAD' denotes theoretical nadir values.
The soil emissivity e_s in equation 3-1 is calculated by:

$$e_S(\theta,P) = 1 - R_S(\theta,P) \quad (3\text{-}4)$$

where R_s is the rough soil reflectivity. The Fresnel equations (Ulaby *et al.*, 1986; Mätzler, 2006) describe the reflectivity of a smooth soil (R_s*) with dielectric constant ε (calculated here using the method described in Dobson *et al.* (1985)), however in reality this rarely occurs. Therefore a roughness correction is applied in L-MEB using a version of the semi-empirical approach of Wang and Choudhury (1981):

$$R_s(\theta,P) = R_s^* \cdot \exp(-HR(\theta,P)\cdot\cos^{NR(P)}(\theta)) \quad (3\text{-}5)$$

HR and *NR* are parameters describing the soil effective (physical and dielectrical) roughness and the angular dependency of this roughness, respectively.

When using this model, infrared temperatures were used for T_c and soil temperatures for T_s (eq. 3-1). In the case of the Bray site, the latter consisted of effective soil temperatures calculated over a depth of several times the wavelength λ, as described by Grant *et al.* (2007). For the Jülich site, profiles were not available and measurements of soil temperature at 0-5 cm depth were used as input for T_s. As

effective soil temperatures were found to lie close to soil temperatures at 2-3 cm depth at the Bray site (Grant *et al*., 2007) this is considered a valid approximation.

3.3.2 Upward model

According to radiative transfer, when looking upward, measured brightness temperatures (T_B) for incidence angles < 90º are composed of a vegetation component and a sky component. As a first approximation, the soil emission reflected by the canopy is neglected. Equation 3-6 gives the model used for analysis of the upward measurements of brightness temperature:

$$T_B(\theta, P) = (1-\omega)\cdot(1-\gamma)\cdot T_c + T_{B,sky}\cdot\gamma \qquad (3\text{-}6)$$

3.3.3 Tor Vergata Model

The Tor Vergata model (Ferrazzoli and Guerriero, 1996; Ferrazzoli *et al*., 2002; Della Vecchia *et al*., 2006a) is based on radiative transfer theory and uses a discrete approach, representing vegetation elements (trunks, branches, leaves/needles) by geometrical shapes (cylinders) of suitable dimensions. The dielectric properties of each element are calculated using a semi-empirical approach requiring information on moisture status (Ulaby *et al*., 1986).
Scattering and extinction cross-sections of the crown and trunks are calculated according to the infinite length approximation. The understory layer is modelled as a simple absorbing layer, and the soil is represented by a uniform dielectric half-space with a rough interface. Soil permittivity is modelled using the semi-empirical model of Dobson *et al*. (1985). The soil bistatic scattering coefficient is obtained using the integral equation method (Fung, 1994).
By using the matrix doubling method (Ferrazzoli and Guerriero, 1996), first the scattering and extinction matrices of the whole crown are calculated, then the same algorithm is used to combine the crown with trunks, understory and soil. In this way the emissivity of the whole medium can be computed from the energy conservation law.

3.4 Methods

3.4.1 Minimization

Inversion of L-MEB is done by minimizing a cost function CF (Pardé *et al*., 2004):

$$CF = \frac{\sum_{1}^{N}\left(T_B^{\circ}(\theta,P) - T_B(\theta,P)\right)^2}{\sigma_{T_B}^{\ 2}} + \sum_{i=1}^{n}\frac{\sum_{1}^{N}\left(p_i - p_i^{\,ini}\right)^2}{\sigma_{p_i}^{\ 2}} \qquad (3\text{-}7)$$

In the first term, ° indicates the measured value of T_B. In the second term, p_i is the value of the retrieved parameter and p_i^{ini} the initial value of each parameter in the retrieval process corresponding to an *a priori* estimate of a parameter p_i. σ^2 in the first term is the variance of the simulated values of T_B, σ^2 in the second term is a fixed variance which can be used to constrain the model to a greater or lesser degree. The

possibility of constraining parameters is built into the model for future processing of SMOS observations, where a parameter can be constrained based on the previous day's value. However, in this study it was chosen to work without constraints (i.e. no *a priori* knowledge was assumed), in order to find the 'real' optimum for each parameter. Therefore the value $\sigma_p^2 = 1$ was used in all cases.
Parameter retrievals were assessed using the root mean square error (RMSE) between modelled and measured T_B. Several initializations for each parameter were tested in every case. For the Les Landes retrievals, no prior knowledge of possible initial values was available, therefore the retrievals were additionally assessed using the efficiency of the regression or skill score (SS). Best-fit canopy parameters were subsequently chosen by selecting initializations leading from min(RMSE) to 1.1*(min(RMSE)) and from 0.9*(max(SS)) to max(SS), then taking the average of the resulting values.

3.4.2 Analysis procedures

3.4.2.1 General

Before analysing the data, all measurements for which rainfall occurred during the past 24 hours were deleted from the data sets. Interception may lead to a significant increase in canopy opacity and a strong increase in the absorption and emission of the litter layer (Saleh *et al*., 2006). Under these types of conditions it will become difficult to accurately retrieve soil moisture. For this reason, an index flagging events during which interception effects are likely is built into L-MEB (Wigneron *et al*., 2007).
The six 'focus parameters' throughout this study were: ω, τ_{NAD}, tt(H), tt(V), HR and NR. In general, the approach taken was (1) to retrieve values of the canopy parameters ω, τ_{NAD}, tt(H) and tt(V) from the synthetic data set or the upward measurements, then (2) to run the forward model (L-MEB) using a) the values found in step (1), b) measured infrared and soil temperatures and soil moisture content, and c) the downward radiometric measurements, in order to calculate best-fit values of the soil parameters HR and NR.
In step (1), simultaneous 3- or 4-parameter retrievals were done for each time of measurement using the upward model (eq. 3-6) together with equations 3-2 and 3-3, and the minimization method given by equation 3-7. In step (2), the best-fit values of HR were assumed to lie between 0 and 2, and those of NR between -2 and 2, as this is the range in which these values have generally been found in other studies (Escorihuela *et al*., 2007). Criteria for the best-fit value here were i) lowest root mean square error (RMSE) and ii) lowest bias, in both cases resulting between observed and simulated values of T_B. The bias is a measure of the deviation of the observed-simulated values from the 1:1 line and was calculated as the average of $(T_{B,obs} - T_{B,sim})$ for all measurements.

3.4.2.2 Les Landes synthetic data (coniferous)

The canopy parameters ω, τ_{NAD}, tt(H) and tt(V) were simultaneously retrieved from the synthetic data set over Les Landes, using the L-MEB model and the minimization method as described in §3.4.1. In L-MEB, τ_{NAD} and ω are in fact effective and interdependent parameters, as the model is based on the assumption that scattering is predominantly in the forward direction (Mo *et al*., 1982). For this reason, direct measurement of these parameters is not possible and they can only be estimated from

inverse modelling. Simultaneous retrieval of two interdependent parameters such as τ_{NAD} and ω will only give reliable results when no constraints are used during retrieval and the data set is sufficiently large. For this last reason, a 4-parameter retrieval was done only in the case of the synthetic data set. The value of ω found here for the 32 year old population was then fixed during retrievals from the two experimental data sets (Bray and FOSMEX). The only known forest values for ω in the literature can be found in Della Vecchia *et al*. (2006b), however, this procedure was applied over average conditions at a large scale and it was therefore chosen to retrieve ω more specifically in the current study. Values found for the 32 year old population for the other three vegetation parameters were used as initial values in the retrievals from the experimental data sets.
In addition to the above parameters, it was also possible to calculate the canopy structure parameter b from the synthetic data set. This parameter relates τ_{NAD} to the vegetation water content VWC by $\tau_{NAD} = b * VWC$ (Jackson and Schmugge, 1991), and was found to be related to different vegetation types by Van de Griend and Wigneron (2004b). However, it does not take into account effects of canopy anisotropy. Measurements over corn (Hornbuckle *et al*., 2003) and grass covered soils (Schwank *et al*., 2005) have shown a rather pronounced dependence of transmissivity on polarization. To allow for such a possibility is the reason equation 3-3 has been incorporated in the L-MEB model.

3.4.2.3 Bray data (coniferous)

The upward measurements at Bray were used to simultaneously retrieve values of τ_{NAD}, tt(H) and tt(V), again using the upward model and the minimization method described in §3.4.1. As explained in the previous paragraph (§3.4.2.2), a fixed value of ω was taken from the Les Landes retrievals.
It should be noted that some caution should be exercised with these results as the upward measurements at Bray were made with the radiometer placed at the edge of the forest. This could result in side-lobe effects leading to an underestimation of brightness temperature (from a higher sky influence), especially at low angles (i.e. toward zenith). Also the side-lobes could result in a relatively high influence of the ground surface at high angles, although this would be expected to result in a polarized signal, which was not apparent here. As a precaution, the beamwidth of the main lobe (§3.2.1) plus first side-lobes (15° full beamwidth at half-power) was taken into consideration, and subsequently only measurements between 30° and 60° were used.

3.4.2.4 FOSMEX data (deciduous)

In the case of the FOSMEX data, the same procedure was used as described in the beginning of the previous paragraph (§3.4.2.3) for the Bray data. In the upward model, T_c was set equal to the T_{air} measured at 20 m height. As the upward measurements were made continuously throughout three months, they resulted in a time series of each canopy parameter, something not available for the Bray site. During the upward measurements, defoliation was calculated through sampling of fallen leaf biomass (LB) [gm^{-2}], as described by Guglielmetti *et al*. (2007), and it was therefore possible to relate τ_{NAD} to LAI. The average value of 0.0172 m^2g^{-1} for the specific leaf area (SLA) of Beech (*Fagus*) was taken from Bartelink (1997), as this was found to be irrespective of age and is an average value for sunlit and shady leaves (Masarovicova *et al*., 1996). Leaf water content measured at Jülich was around 50%.

Thus, LAI was calculated as follows:

$$LAI = 0.5 * LB * 0.0172 = 0.0086 * LB \quad (3\text{-}8)$$

3.5 Results and Discussion

3.5.1 Les Landes synthetic data (coniferous)

Results of parameter retrievals done over the synthetic data set of Les Landes are shown in table 3-1, together with the error associated with these retrievals (expressed by the RMSE in emissivity). The parameters for the 5 and 26 year old populations are not validated in this study, but are included here as useful initial parameter values in the case of younger trees, as no other information is currently available. They also allow for a comparison between the emission of different populations, with the 26 and 32 year old groups showing similar properties, and the 5 year old population dominated by higher transmissivity and scattering. Higher scattering could be due to a compensation effect of the model related to an underestimation of τ_{NAD}, as τ and ω are interrelated parameters (§3.4.2.2). However, it could also be caused by the smaller distances between the scatterers in the case of young vegetation, or by the different branch orientation in the 5 year old population (Saleh *et al*., 2005). Further validation with experimental data will be necessary to fully understand this effect.
The value of ω found here for the 32 year old population is similar to the values found by Della Vecchia *et al*. (2006b).

Table 3-1: Parameter values resulting from inversion of the L-MEB model using the synthetic data set of Les Landes. Calculations were done for coniferous forest stands of three different ages: 5, 26 and 32 years old. The first three rows give parameter values used in the data simulation, the following five rows give the retrieved L-MEB canopy parameter values together with the resulting RMSE in emissivity, and the final two rows show the b factor calculated from a combination of the above.

	'5 years'	***'26 years'***	***'32 years'***
Tree density [trees/ha]	1421	497	368
Branch water content (BWC) [kg m^{-2}]	0.2	1.5	1.3
Total water content (TWC)[kg m^{-2}]	1	10	8
τ_{NAD}	0.30	0.60	0.66
***tt*(H)**	0.41	0.59	0.62
***tt*(V)**	0.18	0.36	0.47
ω	0.12	0.07	0.07
RMSE (emissivity) of retrievals	0.010	0.005	0.0035
b_T tree structure parameter ($\tau_0=b_T$*TWC)	0.3	0.06	0.08
b_{Br} branch structure parameter ($\tau_0=b_{Br}$*BWC)	1.5	0.4	0.51

3.5.2 Bray data (coniferous)

Table 3-2a shows the retrieved canopy parameter values of τ_{NAD}, *tt*(H) and *tt*(V) for each of the three series of upward measurements at the Bray site. As can be seen, the results of measurement series 1 and 2 are more similar, whereas series 3 is slightly different, probably as a result of the different azimuth angle relative to the row direction in this case (see §3.2.1).

During the measurements made at the Bray site, the tree age was 34 years and the retrieved canopy parameters can therefore be compared to those in the last column of table 3-1. The values of τ_{NAD} are very similar in both cases, however the *tt*(P) parameters differ considerably. The upward measurements show a more isotropic canopy (i.e. *tt*(P) closer to 1) than expected from the simulations. However, in both cases *tt*(H) > *tt*(V), indicating that the effect of anisotropy on transmissivity is stronger at vertical polarization.
The average values of τ_{NAD}, *tt*(H) and *tt*(V) shown in table 3-2a were used as input in the L-MEB model (eq. 3-3) to obtain best-fit values of the soil parameters *HR* and *NR*(H) from the downward Bray data. Resulting values of RMSE and bias between measured and simulated values of T_B(H) using L-MEB are shown in table 3-2b. Figure 3-2 shows a comparison of all observed and simulated H polarized brightness temperatures.

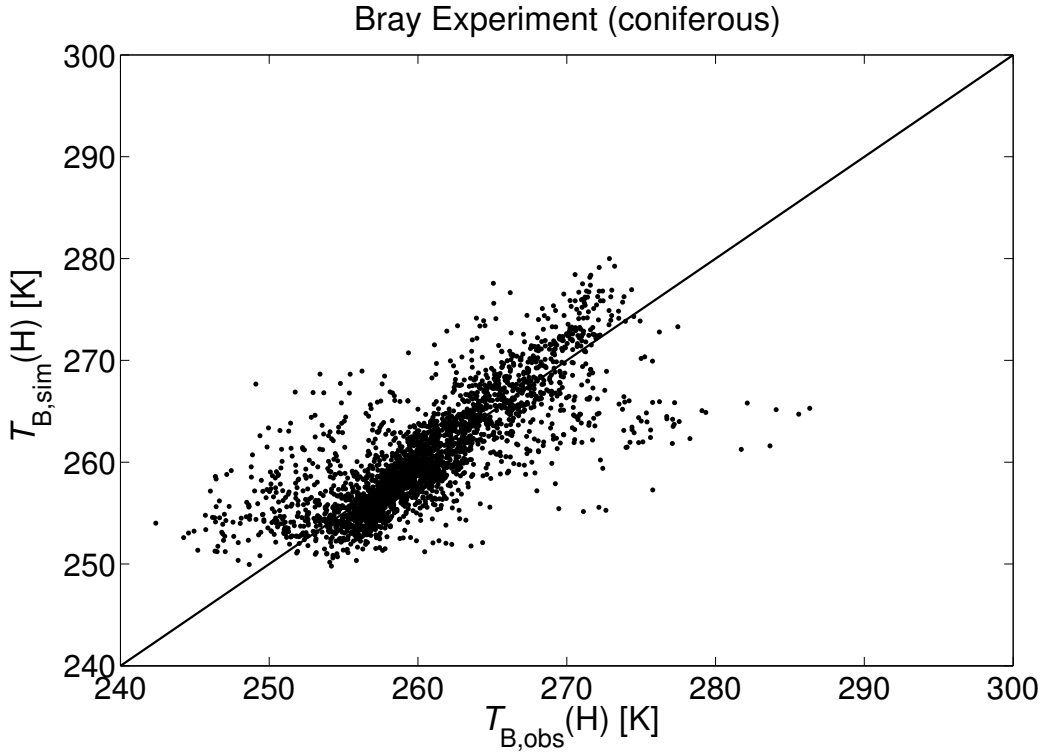

Figure 3-2: Comparison of observed ($T_{B,obs}$) and simulated ($T_{B,sim}$) H polarized brightness temperatures for the Bray experiment using the L-MEB forward model and downward measurements. Observations were excluded if rainfall had taken place during the past 24 hours. Model parameter values were used as given in table 3-2. RMSE = 3.75 K, bias = -0.01 K.

3.5.3 FOSMEX data (deciduous)

Table 3-3 shows the resulting parameter values found for the FOSMEX data following the analysis procedure as described in §3.4.2.4. Table 3-3a shows the average ± standard deviation over time of the retrieved values of τ_{NAD}, *tt*(H) and *tt*(V). The value for τ_{NAD} in table 3-3a is the average over all defoliation states. In the case of a deciduous forest, a more realistic approach might be to relate τ_{NAD} to the changing tree biomass throughout the year.

Table 3-2: L-MEB parameter values found for the (coniferous) Bray experiment; (**3-2a**) Retrieved values of canopy parameters τ_{NAD}, *tt*(H) and *tt*(V) for each of the three series of upward measurements at Bray, together with resulting values of RMSE. Average values ± standard deviations are shown for each parameter; (**3-2b**) Best-fit values of soil roughness parameters *HR* and *NR*(H) found for the Bray downward measurements, together with resulting values of RMSE and bias after forward modelling with L-MEB.

(3-2a)	τ_{NAD}	***tt(H)***	***tt(V)***	***RMSE [K]***
Series 1	0.66	0.83	0.81	1.5254
Series 2	0.64	1	0.92	1.9683
Series 3	0.71	0.83	0.67	2.3022
average ± stdev.	0.67 ± 0.04	0.89 ± 0.1	0.80 ± 0.13	

(3-2b)	***HR***	***NR(H)***	***RMSE [K]***	***Bias [K]***
H pol	1.2	1.8	3.7503	-0.0118

However, using the measurements made at Jülich, little to no correlation was found between τ_{NAD} and LAI, as illustrated in figure 3-3. Using this type of relationship for leaf biomass monitoring over forests is therefore not recommended. However, this comes as no surprise, as other studies have previously shown (Macelloni *et al*., 2001; Ferrazzoli *et al*., 2002; Guglielmetti *et al*., 2007) that at this frequency branches, not leaves (or trunks), are the main sources of emission.

The average parameter values given in table 3-3a were used as input in the L-MEB model, after which measured and simulated values of T_B were compared in order to find the best-fit values of *HR*, *NR*(H) and *NR*(V). These are shown together with the resulting values of RMSE and bias in table 3-3b. Figure 3-4 shows the result of forward modelling for all measurements at H and V polarization, respectively.

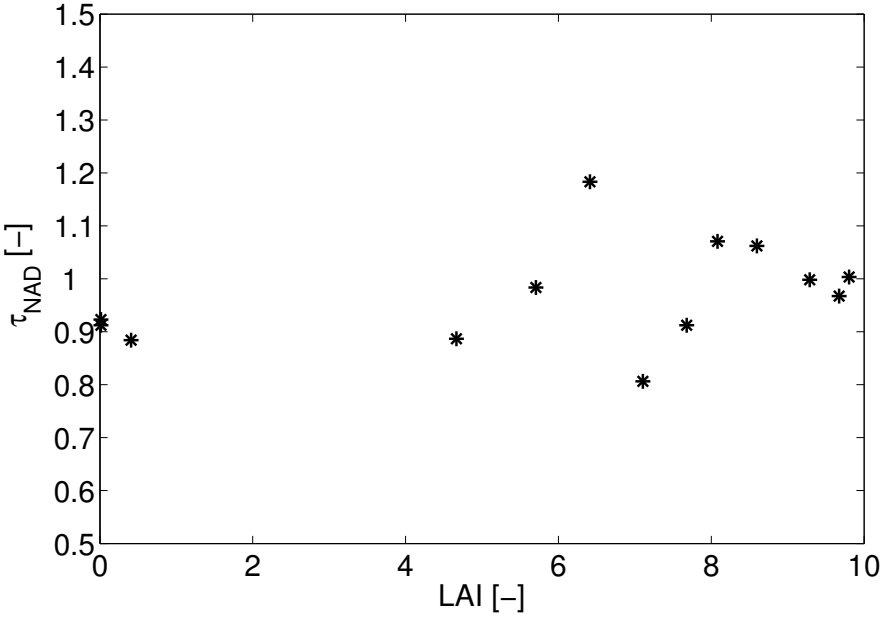

Figure 3-3: LAI (from eq. 3-8) plotted against retrieved values of τ_{NAD} during the defoliation period at the Jülich site (FOSMEX data set).

3.5.4 Comparison between experimental data sets

The results for both the Bray and FOSMEX data lead to errors in brightness temperature (expressed by the RMSE and bias) of a similar order of magnitude, although those for the Bray data set are slightly higher. However, some caution should be taken with a direct comparison of RMSE values, as the two experiments were not exactly identical in terms of set-up and measurements.
Comparisons per parameter lead to the following conclusions: First, the canopy optical depth at nadir τ_{NAD} is higher for the deciduous site, even when the LAI here is 0. Second, both sites show decreasing trends of $\tau_0(\theta,P)$ as a function of incidence angle, i.e. tt(H) and tt(V) are both < 1. In the case of an isotropic canopy, $tt(P) = 1$. The fact that the angular dependence is more pronounced over the deciduous site (i.e. lower values of $tt(P)$ are found; see tables 3-2 and 3-3) therefore indicates that this canopy is less isotropic than that at the coniferous site.

Table 3-3: L-MEB parameter values found for the (deciduous) FOSMEX experiment; (**3-3a**) UP = upward data set. Average values ± standard deviations over time of retrieved values of canopy parameters τ_{NAD}, tt(H) and tt(V), together with resulting values of RMSE; (**3-3b**) DOWN = downward data set. Best-fit values of soil roughness parameters *HR*, *NR*(H) and *NR*(V), together with resulting values of RMSE and bias for both polarizations after forward modelling with L-MEB.

(3-3a)	τ_{NAD}	*tt(H)*	*tt(V)*	*RMSE [K]*
UP	0.98 ± 0.08	0.54 ± 0.09	0.43 ± 0.06	1.7239 ± 0.7859

(3-3b)	*HR*	*NR(H)*	*NR(V)*	*H pol RMSE [K]*	*Bias [K]*	*V pol RMSE [K]*	*Bias [K]*
DOWN	1	1	2	2.791	-0.009	3.194	0.680

Third, the ratios between tt(V) and tt(H) (called *rtt* in L-MEB) are 0.90 and 0.80 for the Bray and FOSMEX data sets respectively, showing that at both sites the effect of anisotropy on canopy transmissivity and emissivity is greater at vertical polarization. From equations 3-2 and 3-3, it follows that when tt(V) is lower than tt(H), transmissivity will be higher at V polarization and canopy emissivity $(1-\omega)(1-\gamma)$ will therefore be lower. This confirms that at L-band the influence of vertically oriented canopy elements such as trunks is limited and horizontal elements such as branches play a greater role as a source of scattering and absorption, as noted in the previous paragraph (§3.5.3). Finally, concerning the soil roughness parameters *HR* and *NR*, it can be concluded that there is no significant difference in roughness between the two forests, both resulting in a best-fit when $HR \approx 1$, which corresponds to a rather high surface emission (eq. 3-5). The angular dependence of the roughness at horizontal polarization, as expressed by *NR*(H), is lower for the FOSMEX data than for the Bray data, possibly due to the difference in litter layer thickness between both sites. As expected, the understory/litter layer at Jülich is thinner than that at Bray, because although deciduous tree species generally produce more litter, decomposition is generally also faster than in the case of coniferous forests (Kavvadias *et al.*, 2001; Osono and Takeda, 2006). A thicker litter layer can be expected to attenuate more of the soil signal and consequently have a higher self-emission. However, the various aspects governing the behaviour of the *HR* and *NR* parameters are still relatively unknown and here they can mainly be seen as (effective) fitting parameters, although

in other studies the *HR* parameter was found to be a function of soil moisture in the cases of bare soil and grass covers (Escorihuela *et al.*, 2007 and Saleh *et al.*, 2007, respectively). Future research will have to show whether this is also the case under forests, however, in this study no such relationship was found.

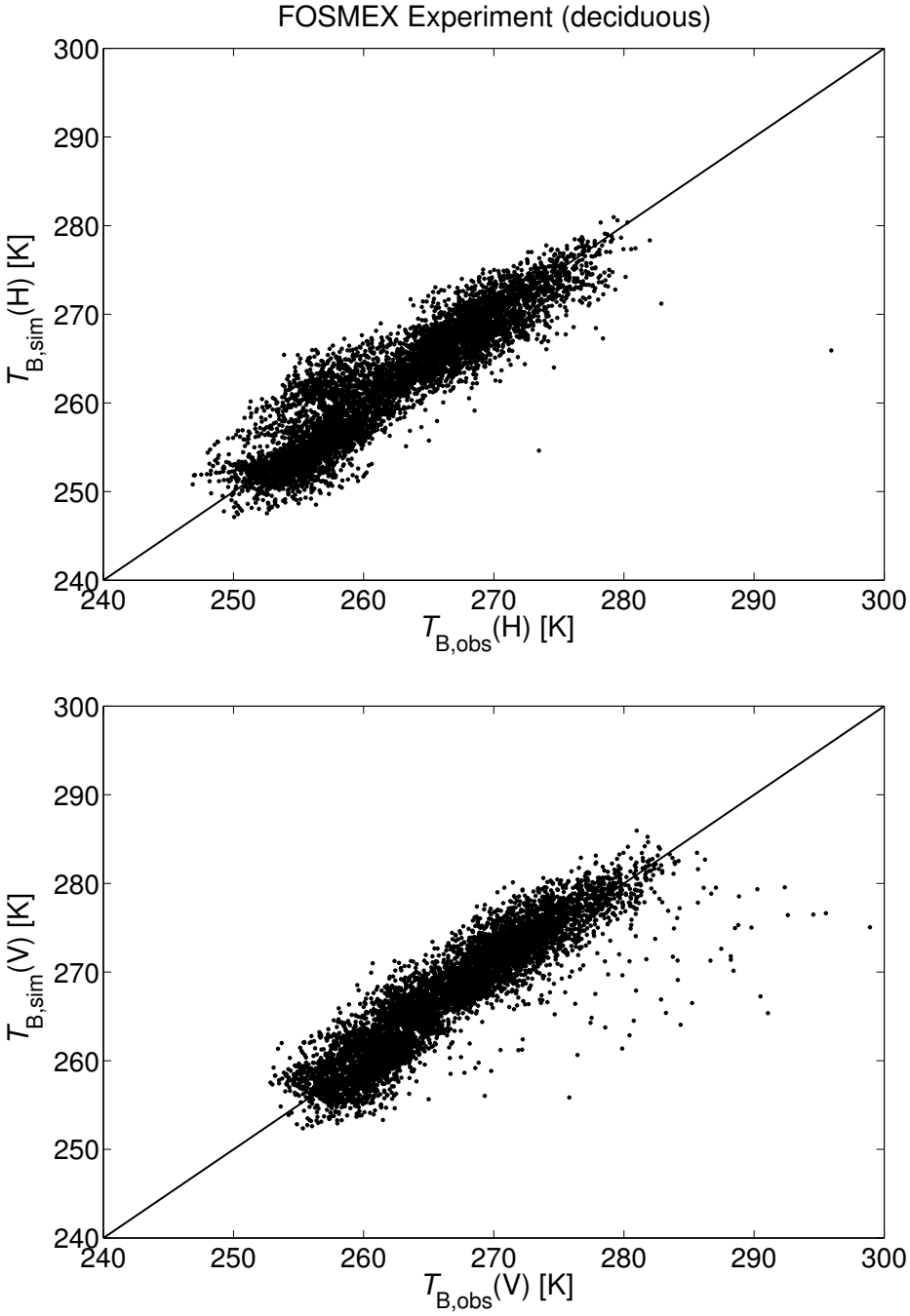

Figure 3-4: Comparison of observed ($T_{B,obs}$) and simulated ($T_{B,sim}$) H- (top) and V- (bottom) polarized brightness temperatures for the FOSMEX experiment using the L-MEB forward model and downward measurements. Observations were excluded if rainfall had taken place during the past 24 hours. Model parameter values used as given in table 3-3. H-pol: RMSE = 2.79 K, bias = -0.01 K; V-pol: RMSE = 3.19 K, bias = 0.68 K.

3.5.5 Sensitivity study

A sensitivity study was conducted by using the calibrated parameter values (from tables 3-2 and 3-3) in L-MEB as a reference situation, then introducing an error in one particular variable and running the forward model. The study consists of three parts: 1) errors introduced in the canopy and soil roughness parameters, 2) errors introduced in the physical temperatures and soil moisture values, and 3) including observations where precipitation had taken place during the previous 24 hours. Tables 3-4a to 3-4c show the respective results in terms of RMSE and bias in T_B.

Table 3-4: Values of RMSE and bias in T_B found after forward modelling with L-MEB when various types of errors are included in the data, respectively: (**3-4a**) errors in L-MEB canopy and soil roughness parameters, (**3-4b**) errors in temperature and soil moisture and (**3-4c**) including measurements where precipitation has taken place during the past 24 hours. Results in [K] shown for both Bray and FOSMEX (downward) data sets.

(3-4a)		***Bray (H)***	***FOSMEX (V)***	***FOSMEX (H)***
(0) reference	RMSE	3.7503	3.194	2.791
	Bias	-0.0118	0.680	-0.009
(1) *tt*(H) = *tt*(V) = 1	RMSE	3.9688	3.1730	4.1465
	Bias	0.7905	0.6039	2.7638
(2) ω = 0	RMSE	13.7688	14.4618	15.0988
	Bias	13.0381	14.0762	14.7977
(3) *HR* = 0	RMSE	14.6763	3.9350	8.0307
	Bias	-13.1282	-1.4293	-7.4224
(4) *NR* = +1 (H), -1 (V)	RMSE	4.0182	3.4248	2.7910
	Bias	0.5057	1.5698	-0.0093

(3-4b)		***Bray (H)***	***FOSMEX (V)***	***FOSMEX (H)***
(5) +2 K	RMSE	4.1747	4.0533	3.3491
	Bias	1.8351	2.5835	1.8511
(6) +0.04 m^3m^{-3}	RMSE	3.8262	3.1445	2.8554
	Bias	-0.6704	-0.0441	-0.5374

(3-4c)		***Bray (H)***	***FOSMEX (V)***	***FOSMEX (H)***
(7a) + rain, all data	RMSE	3.8317	3.2013	2.7398
	Bias	0.4067	0.2465	-0.6388
(7b) + rain, leaves	RMSE	-	3.3318	2.4265
	Bias	-	0.7832	-0.6650
(7c) + rain, no leaves	RMSE	-	3.0786	2.9967
	Bias	-	-0.2404	-0.6144

First shown in table 3-4a are the reference values as found in §3.5.2 and §3.5.3 (tables 3-2 and 3-3). When the assumption of an isotropic canopy is made in case (1), i.e. *tt*(H) and *tt*(V) are set to 1, the errors increase for H polarization, slightly with the Bray data but more so with the FOSMEX data set, resulting in model overestimations of ~ 1-3 K in T_B(H) respectively. At V polarization there is hardly any change in errors. As the main part of canopy emission is determined by horizontally oriented elements (e.g. branches), T_B at H polarization will be more affected by a possibly erroneous assumption of isotropy. Second, the assumption of no scattering, i.e. $\omega = 0$,

was tested in case (2). This led to very high errors in both RMSE and bias. The parameters ω and τ are interdependent, as mentioned previously (§3.4.2.2), and the values of τ_{NAD} in this study are based on the situation where $\omega = 0.07$. High errors are therefore not surprising; however, this does illustrate how sensitive L-MEB is to erroneous values of ω for a given value of τ_{NAD}.
In case (3), the assumption of a smooth soil was tested by setting *HR* to 0, which led to a high error with the Bray data. The errors with the FOSMEX data set were smaller, but it is interesting to see that at H polarization they are more than double those at V polarization. This is opposite to results predicted by the physically-based air-to-soil transition model in Mätzler (2006). However, the latter evaluation assumed isotropic soil permittivities and in doing so did not consider for any prevailing orientation of structures in the surface layer. The conflicting results found in the current study indicate that the assumption made on the isotropic soil permittivity might not be correct in the case of litter-covered soils or soils with a high percentage of organic matter.
In Escorihuela *et al*. (2007), it is found that for a bare loamy soil, best-fit values of *NR* were +1 at H polarization (which is close to the values found in the current study) and -1 at V polarization. Using these values in case (4) led to greater errors at H polarization with the Bray data and at V polarization with the FOSMEX data, as expected from the fact that the values found in these two cases for *NR*(*P*) (see tables 3-2 and 3-3) differed most from +/-1. However, these errors are much smaller than those found for erroneous values of *HR*, and we can conclude that *HR* has a much greater influence on modelling of the ground layer (soil and litter).

In table 3-4b, case (5) shows the results when a constant +2 K error is added to both soil and canopy temperatures and case (6) has a constant +0.04 m^3m^{-3} error added to the measured values of soil moisture. The value of 0.04 m^3m^{-3} was chosen bearing in mind that this is the SMOS anticipated accuracy for soil moisture retrievals. The 2 K error in temperature is often used in this type of modelling study.
Cases (5) and (6) show expected behaviour: case (5) shows that a 2 K increase in temperature leads to a ~2 K model overestimation (expected from the relationship $T_B \approx T * e$) and in case (6), an increase in soil moisture of course leads to a (small) model underestimation, as soil emissivity reduces with increasing moisture content. As expected, the resulting differences in RMSE compared to the reference situation are very small, in line with the knowledge that sensitivity to soil moisture is very low over forested areas.

Table 3-4c shows the effect of including rainfall data (observations where precipitation took place during the previous 24 hours) in the forward model. During the Bray experiment, precipitation occurred 8.2% of the time, versus 9.6% of the time during FOSMEX. Minimum, maximum and average precipitation values of all rainfall periods at Bray were 0.2, 17.8 and 1.2 mm/hour, respectively. At the Jülich site, the respective values were 0.1, 16.7 and 0.8 mm/hour. As mentioned previously (§3.4.2.1), canopy emission may increase significantly during rainfall. However, in the current study the inclusion of rainfall data only led to very small differences in errors in all cases; a slight overestimation with the Bray data and a slight underestimation with the FOSMEX data (case 7a). Because a large part of intercepted precipitation is caught by leaves (needles), the FOSMEX data were additionally split into a subset with leaves (17^{th} Apr. – 23^{rd} Nov.) and without (remaining days), to investigate whether this would lead to a significant difference in error. However, as

the results show (cases 7b and 7c, respectively), the differences in RMSE and bias found here are small in all cases, although the effects at H- and V-pol are reversed. At V polarization the error increases for the 'leaves' situation, whereas at H polarization this happens for the 'no leaves' situation.

3.6 Summary and Conclusion

Using up- and downward L-band measurements over both a coniferous and a deciduous forest together with a synthetic L-band data set over conifers, a calibration was made of the L-MEB model used in the SMOS Level 2 Soil Moisture algorithm. This has resulted in working values of the main canopy and soil roughness parameters τ_{NAD}, ω, tt(H), tt(V), HR and NR as shown in tables 3-1, 3-2 and 3-3. Using these values in the forward model resulted in an RMSE in brightness temperature of 2.8 to 3.8 K, depending on data set and polarization.

Previously, 'τ-ω' type modelling approaches at L-band often corrected for the dependence of canopy optical depth on incidence angle by dividing by the cosine of the angle. However, this corrects for the difference in path length only, and not for the difference in structure (i.e. polarization effects) encountered at different angles. Canopy optical depth was still found to decrease with increasing incidence angle for both forest types after a 'cosine' correction. At both sites this effect on optical depth was stronger for V polarization than for H polarization. This study therefore shows that an additional angular correction using the $tt(P)$ parameter in L-MEB is essential for non-isotropic canopies.

At L-band leaves are not the main sources of emission, and little to no correlation was found between canopy optical depth and LAI for the deciduous site. Using this type of relationship for leaf biomass monitoring over forests is therefore not recommended at this wavelength.

A sensitivity study was conducted by introducing various types of errors in L-MEB parameter values, then running the forward model and assessing the effect on $T_B(P)$ in terms of RMSE and bias. In most cases, the errors were small. Even when observations where precipitation had taken place during the previous 24 hours were included in the analysis, this resulted in only a very slight increase in RMSE. However, the model was found to be very sensitive to erroneous values of ω for a given value of τ_{NAD}, most likely because these two parameters are interdependent.

The results found in this study will be integrated in the operational SMOS Level 2 algorithm and used in future inversions of L-MEB for soil moisture retrievals over heterogeneous, partly forested areas.

Chapter 4

Observations and Modelling of a Pine Forest Floor at L-band *

4.1 Introduction

In view of ESA's upcoming Soil Moisture and Ocean Salinity (SMOS) satellite mission a better understanding of L-band forest emission is certainly needed, as many pixels over land will contain at least partial forest cover and thus complicate soil moisture retrievals. Over the past few years, several studies have focussed on passive L-band (1.4 GHz; $\lambda \approx 21$ cm) observations of forests (Lang *et al*., 2001; Macelloni *et al*., 2001; Grant *et al*., 2007; Guglielmetti *et al*., 2007; Guglielmetti *et al*., 2008). Results consistently revealed that it is crucial to know the L-band radiative properties of litter and understory in order to fully understand the microwave signatures. Until recently, the high L-band emissivity found over forests (Saleh *et al*., 2004a; Grant *et al*., 2007) was mainly attributed to the influence of the tree canopy. However, canopy transmissivity was subsequently shown to be higher than first assumed – typical average values for coniferous and deciduous forests being in the range of 0.4 to 0.5 (Guglielmetti *et al*., 2007; Grant *et al*., 2008). This implies that it might be possible to obtain information on forest floor emission transmitted through the canopy. Furthermore, the generally high emissivity values found over forests might not be predominantly due to a high opacity of the tree canopy, but could also be due to the litter and/or understory layers.

Ten years ago, a study over prairie grass (Schmugge *et al*., 1998) was the first to note that the thatched layer of dead vegetation in unburned grass areas has a considerable impact on L-band emission when wet. The issue was taken up again recently (Saleh *et al*., 2006) to confirm that, compared to a living grass layer, a mixed layer of dead grass and mulch shows an increased optical depth with higher moisture. Concerning forest litter, Guglielmetti *et al*. (2008) hypothesized that the below-canopy contribution to the L-band signal observed over forests might even be completely dominated by the litter layer, due to its high opacity and attenuation of soil emission. However, simulations at L-band (Della Vecchia *et al*., 2006a; Paloscia *et al*., 2008) found that above-canopy emission still showed a certain sensitivity to soil moisture, although the latter could be reduced by the presence of litter. Dielectric mixing models for litter have been developed by Della Vecchia *et al*. (2007) and Kleshchenko *et al*. (2002) for pine forest and needle litter, respectively, and lately by Schwank *et al*. (2008) for deciduous leaf litter. The latter study found that a deciduous litter layer is nearly transparent at L-band for dry conditions, but when wetted it acts as an important source of emission. Laboratory observations (Demontoux *et al*., 2008) have shown that the emission of a soil-litter system is quite complex, depending on litter layer thickness and the moisture contents of both the soil and litter layers. The three

studies (Guglielmetti *et al*., 2008; Schwank *et al*., 2008; Demontoux *et al*., 2008) consistently noted a transitional period just after wetting the litter, due to drainage and uptake/repartitioning of the water by the litter layer. However, none of the forest litter studies mentioned above were based on *in situ* field observations with the forest floor layers in their undisturbed state. The current study aims to fill this gap in the available information by performing forest floor observations in an experimental setting within the forest.
In a previous study calibrating the L-MEB model (Wigneron *et al*., 2007) over forests (Grant *et al*., 2008), the effect of the understory and litter was indirectly taken into account through the soil roughness parameter H_R. The current study takes a more physically-based approach by using the coherent Wilheit model (Wilheit, 1978) to simulate the emissivity of a soil-litter forest floor configuration. In general, the forest floor is modelled as a composition of soil, litter and grass layers. L-band observations were obtained of the tree canopy and of the forest floor in three different configurations (soil-litter-grass, soil-litter and bare soil). In order to investigate the behaviour of the various forest layers with varying ground moisture conditions, the emissivity of each configuration and the thermal sampling depth of the soil-litter configuration were related to varying soil moisture content. The main focus of this study is to obtain a better insight into the relative contribution of each forest layer to the overall L-band emission.

4.2 Materials

The current study uses data from two experiments both performed at the 'Bray' site, the most recent having taken place in 2007 and a previous one in 2004 (Grant *et al*., 2007). In 2007, L-band observations were performed below the canopy, whereas in 2004, this was done above the canopy. Throughout this text the two experiments will be named the 'below-canopy' and the 'above-canopy' experiments, respectively.

4.2.1 Site description

The 'Bray' site lies within the production forest of Les Landes, at approximately 20 km southwest of Bordeaux, France (latitude 44°42' N, longitude 0°46' W, altitude 61 m). Sole tree species at the experimental site is the Maritime Pine (*Pinus pinaster Ait*), with an age of 37 years in 2007 and an average height of 22 m during both experiments. The trees are planted in parallel rows along a northeast–southwest axis with an inter-row spacing of 4 m. The value of canopy Leaf (needle) Area Index (LAI) is around 2.15 m^2m^{-2} in summer and 1.95 m^2m^{-2} in winter. Corresponding total column biomasses (trunks, branches and needles) are approximately 11.28 kg m^{-2} and 10.58 kg m^{-2} which are typical values for a 'medium dense' forest and thus indicate the sheltered character of the forest floor. The understory includes a few scattered shrubs and young trees, but consists mostly of grass (mainly *Molinia caerulea* L. Moench). Green grass LAI is ≈ 1.55 m^2m^{-2} in summer and not applicable during winter. At the time of the below-canopy experiment, the grass was completely senescent, whereas the above-canopy experiment took place from July-December and therefore covered a range of grass phenological stages.
Soils at the Bray site are sandy and hydromorphic podzols, with dark organic matter in the first 60 cm. Percentages of sand and clay are around 80% and 3%, respectively. Average soil bulk density at the site is around 1.25 g cm^{-3}. The soil is covered by a

dense litter layer of spatially varying thickness (average 3 cm with thicknesses up to 10 cm; Demontoux *et al.*, 2008), consisting of decomposing grass and pine needles, cones and branches. The percentage of organic matter in this layer was determined to be around 85%.

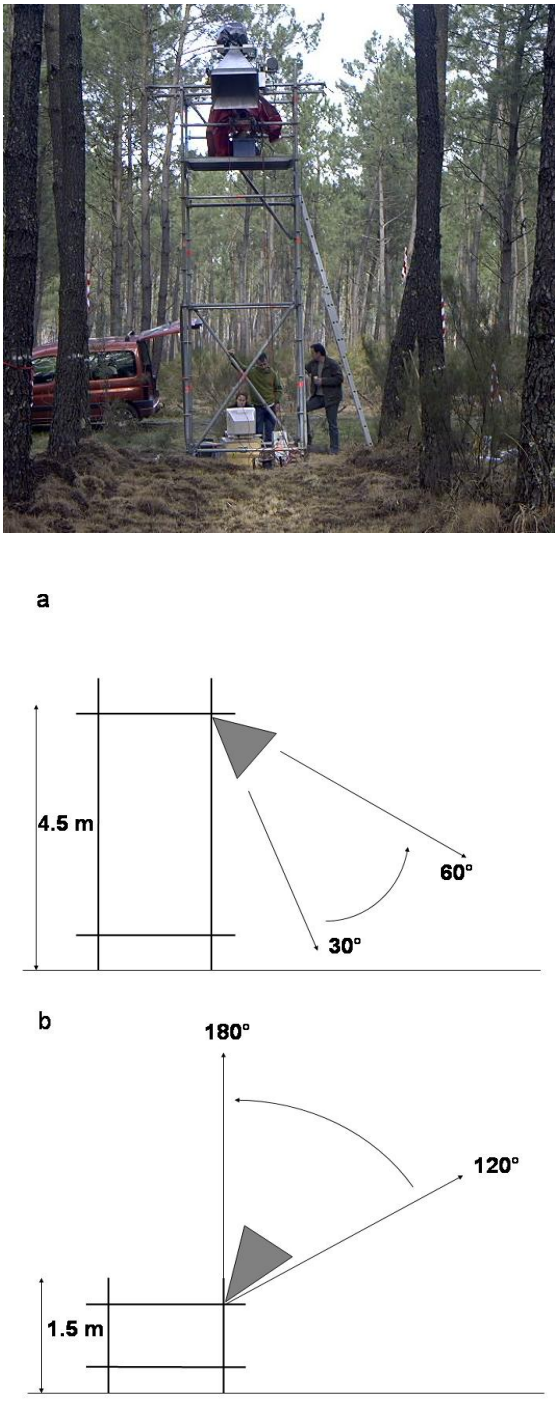

Figure 4-1: Experimental set-up of the radiometric observations during the below-canopy experiment using the EMIRAD L-band (1.4GHz) radiometer. Top: photograph; bottom left (a): sketch of downward observations of the forest floor; bottom right (b): sketch of upward observations of the tree canopy.

4.2.2 Data sets

Both experiments were conducted with the L-band polarimetric radiometer EMIRAD built at the Technical University of Denmark (Søbjærg, 2002). Table 4-1 summarizes the different data sets and observing configurations used in the current study, whereby the observed surface configurations can consist of various combinations of soil ('S'), litter ('L'), grass ('G'), tree canopy ('C') and sky ('Sky').

The above-canopy experiment was performed between July and December 2004 and is described in more detail in Grant *et al.* (2007). The radiometer was mounted on a 40 m tower over the forest and downward-looking observations were done at horizontal polarization (P = H) and angles $\theta = 25°$ to 60° relative to nadir. A thermal Infra Red (IR) radiometer (Heitronics KT 15.85D; 9.6–11.5 μm) was mounted next to the microwave radiometer to provide measurements of surface temperature T_{IR} over approximately the same footprint. At a fixed location, ground measurements of soil and litter moisture were taken every 10 s with ThetaProbes connected to a CS21X data logger, and averaged to half hourly values. Half-hourly precipitation totals were also recorded every 30 minutes. The L-band brightness temperatures $T_B^{H,45°}$ used from this experiment were those observed at $\theta = 45°$ (cf. table 4-1: configuration 'SLGC'). Moreover, only observations for which no rainfall had taken place in the past 24 hours were included in the analysis. As this concerned a long-term experiment, observations were done for a variation of temperatures and soil and litter moisture contents.

The below-canopy observations were made at the 'Bray' site from 15-19th February 2007 and consisted of two parts: i) downward observations of the forest floor from below the tree canopy, and ii) upward observations of the tree canopy in the direction of the sky. Figure 4-1 shows a photograph of the experimental set-up during the below-canopy downward observations and sketches of the set-ups for both the downward (fig. 4-1a) and the upward (fig. 4-1b) observations. An internal calibration of the radiometer was done automatically for each observation using internal hot- and cold loads with respective noise temperatures of 320 K and 120 K as described by Søbjærg (2002). An additional 'external calibration' was carried out in the same way as described for the above-canopy experiment in Grant *et al.* (2007), in order to correct for losses in the antenna and cables. For the latter calibration, sky brightness $T_{B,Sky}$ was measured at 30° from zenith before, during and after the experiment (cf. table 4-1: configuration 'Sky'). The measured values were then adjusted to the theoretical value $T_{B,Sky}$ = 4.6 K (Pellarin *et al.*, 2003a), and this correction was subsequently applied to all observations.

No precipitation occurred during any of the below-canopy observations; moreover, no precipitation occurred during the 24 hours before the upward observations of the canopy.

For the downward observations, the instrument was mounted on a 4.5 m high tower below the tree canopy. Full (-3 dB) antenna beamwidth was 25º, resulting in a footprint area ≈ 10 m^2 at $\theta = 40º$. Three forest floor configurations were observed: i) soil-litter-grass (SLG), ii) soil-litter (SL) and iii) bare soil (S) (cf. table 4-1). Layers were manually removed between each of the three series and observations were done at horizontal (P = H) and vertical (P = V) polarization and angles $\theta = 30º$ to 60º with 5º increments. The experiment was intended to study how the emission properties of the different ground configurations change with the removal of each layer, not to obtain temporal information on layer properties. Therefore, each configuration (i.e. each angular series) was only observed for a short period of time (15 minutes, cf. table 4-1).

It should be noted that in all cases some tree trunks partly covered the edges of the footprints, especially at higher observation angles. Furthermore, some grass tufts (cut off at the surface) and roots remained in the footprints of the 'S' and 'SL' configurations, as it was impossible to remove these without severely influencing surface roughness. However, as tree trunks and grass tufts/roots were present in all configurations, the relative differences in emissivity between the different configurations can be assumed to be correct. Finally, the 'S' configuration probably still contained some organic material in the topsoil as the depth of the litter layer was highly variable.
Directly before and after the radiometric observations, in situ measurements of temperature and moisture were performed. Soil temperatures were measured with a standard lab-calibrated digital thermometer, yielding the average temperature of the top 7 cm of the forest floor. Soil moisture was obtained with a Time Domain Reflectometer (TDR) probe (TRIME FM2 (IMKO), type P2) and by gravimetric sampling. Furthermore, grass and litter samples were taken for determining the moisture of the litter and grass layers. Finally, air temperature within the canopy at 20 m height was obtained from ongoing meteorological measurements at the Bray site. As vertical temperature gradients in such a forest system are expected to be relatively small (e.g. Grant *et al*., 2007) the air temperature was used in the model as an approximation for grass and tree canopy temperatures.

Table 4-1: Summary of data sets and observing configurations used in the current study. Observed surface: S = soil, L = litter, G = grass, C = tree canopy, Sky = sky. Variables: *T* = temperature, *SM* = soil moisture, *LM* = litter moisture.

configuration	***year***	***direction***	***θ [°]***	***φ [°]***	***P***	***duration***	***varying parameters***
S	2007	down	30-60, per 5	180	H,V	15 mins.	-
SL	2007	down	30-60, per 5	180	H,V	15 mins.	-
SLG	2007	down	30-60, per 5	180	H,V	15 mins.	-
SLGC	2004	down	45	65	H	3-6 months	*T*, *SM*, *LM*
Sky	2007	up	150	0	H,V	5 mins.	-
CSky	2007	up	120-180, per 5-10	75, 53 and 0	H,V	50, 45 and 30 mins.	-

The upward radiometric observations through the canopy were done at a slightly different location forest-inwards, in order to avoid an overly high contribution of sky emission at the forest edge. However, canopy conditions at the locations of the downward and upward observations were very similar. For the upward observations, the radiometer was mounted on a 1.5 m structure and directed upwards in order to obtain canopy observations analogous to those described in Grant *et al*. (2008). Three series of observations were done at angles between 120º and 180º relative to the downward vertical direction (nadir) (see figure 4-1b). Each series was taken at a

different azimuth angle φ, i.e. at 75º, 53º and 0º (parallel) relative to the row direction of the trees (cf. table 4-1: configuration 'CSky').

4.3 Methods

4.3.1 L-MEB model (SLGC configuration)

In the current study, the L-MEB model (Wigneron *et al*., 2007) was used to model the emission of the whole forest system (i.e. a soil-litter-grass-canopy or SLGC configuration) from above-canopy observations. The model is based on the zero-order radiative transfer approach shown in equation 4-1, which considers the upwelling radiation emitted by the forest floor (first term), and the combination of up- and downwelling canopy radiation (second term). The downwelling canopy radiation is reflected at the forest floor and subsequently transmitted back upwards through the canopy. The third term of the equation considers the sky radiation reflected by the canopy, the sky radiation reflected by the forest floor and an additional sky term which represents an approximation of multiple scattering between the forest floor and the canopy in order to satisfy Kirchhoff's Law (Mätzler, 2006). In L-MEB, the latter contribution is neglected, as both scattering within the canopy and sky radiation are low. Although in consequence L-MEB does not fulfil Kirchhoff's Law, the error is insignificant and the numerical results are very similar to those of a physically correct expression (see also Appendix A).

$$\begin{aligned} T_{\mathrm{B}}^{P,\theta} &= T_{\mathrm{F}} \cdot \left(1 - R_{\mathrm{F}}^{P,\theta}\right) \cdot \gamma_{\mathrm{C}}^{P,\theta} + \left(1 - \omega_{\mathrm{C}}^{P}\right) \cdot \left(1 - \gamma_{\mathrm{C}}^{P,\theta}\right) \cdot T_{\mathrm{C}} \cdot \left(1 + R_{\mathrm{F}}^{P,\theta} \cdot \gamma_{\mathrm{C}}^{P,\theta}\right) \\ &+ \left[\omega_{\mathrm{C}}^{P} \cdot \left(1 - \gamma_{\mathrm{C}}^{P,\theta}\right) \cdot \left(1 + \left(R_{\mathrm{F}}^{P,\theta} \cdot \gamma_{\mathrm{C}}^{P,\theta}\right)^2\right) + R_{\mathrm{F}}^{P,\theta} \cdot \left(\gamma_{\mathrm{C}}^{P,\theta}\right)^2\right] \cdot T_{\mathrm{B,Sky}} \end{aligned} \qquad (4\text{-}1)$$

In equation 4-1, the subscript 'F' denotes the forest floor, while the variables T_{F} and T_{C} indicate the thermodynamic temperatures of the forest floor and the tree canopy, respectively. The forest floor reflectivity $R_{\mathrm{F}}^{P,\theta}$ is related to forest floor emissivity $e_{\mathrm{F}}^{P,\theta}$ through $R_{\mathrm{F}}^{P,\theta} = 1 - e_{\mathrm{F}}^{P,\theta}$. Depending on the observed configuration (§4.2.2), $e_{\mathrm{F}}^{P,\theta}$ can be either the bare soil emissivity $e_{\mathrm{F}}^{P,\theta} = e_{\mathrm{S}}^{P,\theta}$, the emissivity of the soil-litter configuration $e_{\mathrm{F}}^{P,\theta} = e_{\mathrm{SL}}^{P,\theta}$, or the emissivity of the soil-litter-grass configuration $e_{\mathrm{F}}^{P,\theta} = e_{\mathrm{SLG}}^{P,\theta}$. The sky brightness temperature $T_{\mathrm{B,Sky}}$ was calculated according to the method outlined in Pellarin *et al*. (2003a).
The variable ω_{C}^{P} is the effective single scattering albedo of the tree canopy and the variable $\gamma_{\mathrm{C}}^{P,\theta}$ describes canopy transmissivity, which is related to the canopy optical depth $\tau_{\mathrm{C}}^{P,\theta}$:

$$\gamma_{\mathrm{C}}^{P,\theta} = \exp\left(-\tau_{\mathrm{C}}^{P,\theta} / \cos\theta\right) \qquad (4\text{-}2)$$

The optical depth $\tau_{\mathrm{C}}^{P,\theta}$ is derived from brightness temperatures measured at angles θ in upward direction. Dividing by the cosine corrects for the difference in physical path length through the canopy layer at different angles, but does not take into account the effects of uniaxial canopy anisotropy with a vertical axis of symmetry. Such effects are taken into account by the parameter tt_{C}^{P} used in the L-MEB model (Wigneron *et al*., 2007). This results in $\tau_{\mathrm{C,NAD}}$, with the subscript 'NAD' denoting theoretical nadir values:

$$\tau_{\mathrm{C}}^{P,\theta} = \tau_{\mathrm{C,NAD}}\left(\sin^2(\theta)\cdot tt_{\mathrm{C}}^{P} + \cos^2(\theta)\right) \tag{4-3}$$

In the current study, all L-MEB-related retrievals were done using the cost function *CF* (Pardé *et al*., 2004) as a minimization criterion for model inversion:

$$CF = \frac{\sum_{1}^{N}\left(T_{\mathrm{B}}^{\circ} - T_{\mathrm{B}}\right)^2}{\sigma_{T_{\mathrm{B}}}^{\ 2}} + \sum_{i=1}^{n}\frac{\sum_{1}^{N}\left(p_i - p_i^{\mathrm{ini}}\right)^2}{\sigma_{p_i}^{\ 2}} \tag{4-4}$$

The error computed by this cost function represents the sum of the squared differences T_{B}° - T_{B} in observed and simulated brightness temperatures plus the squared differences p_i - p_i^{ini} in retrieved and initial parameter values. The parameters $\sigma_{T_{\mathrm{B}}}^{\ 2}$ and $\sigma_{p_i}^{\ 2}$ are the corresponding variances. In the current study all retrievals were done without constraints. Also, several initial values were always tested.

4.3.2 Canopy and forest floor emissivities

The procedure used to obtain the forest floor emissivities was the following: First, the upward canopy observations were analysed to obtain values of the canopy parameters $\tau_{\mathrm{C,NAD}}$ and tt_{C}^{P}. Subsequently, these were used to account for canopy emission reflected by the forest floor in the downward observations.

4.3.2.1 Canopy emission (CSky configuration)

The upward-observed (i.e. downwelling) brightness temperatures $T_{\mathrm{B}}^{P,\theta}$ comprise the contributions of i) upwelling forest floor radiation reflected by the tree canopy, ii) downwelling radiation from the tree canopy and iii) downwelling sky radiation. The zero-order radiative transfer model used for the analysis of the upward canopy observations (Mätzler, 1994a; Guglielmetti *et al*., 2007; Grant *et al*., 2008) is shown in equation 4-5:

$$T_{\mathrm{B}}^{P,\theta} = T_{\mathrm{F}}\cdot\left(1-R_{\mathrm{F}}^{P,\theta}\right)\cdot\omega_{\mathrm{C}}^{P}\cdot\left(1-\gamma_{\mathrm{C}}^{P,\theta}\right) + \left(1-\omega_{\mathrm{C}}^{P}\right)\cdot\left(1-\gamma_{\mathrm{C}}^{P,\theta}\right)\cdot T_{\mathrm{C}} + T_{\mathrm{B,Sky}}\cdot\gamma_{\mathrm{C}}^{P,\theta} \tag{4-5}$$

In this equation, multiple interactions between the forest floor and the canopy have been neglected, as the product of the canopy and forest floor (SLG configuration) reflectivities is << 1. The equation fulfils Kirchhoff's Law (see Appendix A).
Following a previous study over the same forest (Grant *et al*., 2008), the single scattering albedo was set to $\omega_{\mathrm{C}} = 0.07$. Canopy temperature T_{C} was taken from the air temperature at 20 m, as explained in §4.2.2, and T_{F} was taken from an infrared temperature measurement of the forest floor during the upward observations. $R_{\mathrm{F}}^{P,\theta}$ was set to 0.05 in accordance with an estimation of $e_{\mathrm{F}}^{P,\theta}$ = 0.95 in Mätzler (1994a), which was based on experimental data covering a range of moisture conditions and frequencies (Mätzler, 1994b). The precision of this parameter is not very critical at this point because of its small impact on $T_{\mathrm{B}}^{P,\theta}$.

By combining equation 4-5 with equations 4-2 and 4-3, it was then possible to simultaneously retrieve the parameters $\tau_{C,NAD}$ and tt_C^P, using the cost function *CF* defined in equation 4-4 as a minimization criterion.

4.3.2.2 Forest floor emission (S, SL and SLG configurations)

Because the downward observations were performed below the tree canopy, the forest floor emissivities ($e_S^{P,\theta}$, $e_{SL}^{P,\theta}$ or $e_{SLG}^{P,\theta}$) were obtained from the measured brightness temperatures $T_B^{P,\theta}$ using an adapted zero-order radiative transfer approach:

$$T_B^{P,\theta} = T_F \cdot \left(1 - R_F^{P,\theta}\right) + \left(1 - \omega_C^P\right) \cdot \left(1 - \gamma_C^{P,\theta}\right) \cdot T_C \cdot R_F^{P,\theta} + R_F^{P,\theta} \cdot T_{B,Sky} \cdot \gamma_C^{P,\theta} \qquad (4\text{-}6)$$

As with the previous equation (eq. 4-5), equation 4-6 fulfils Kirchhoff's Law and neglects multiple interactions (see Appendix A). With T_C, ω_C^P and $\gamma_C^{P,\theta}$ obtained from the upward canopy observations (§4.3.2.1), and T_F from ground measurements ($T_F = T_{soil}$ in the case of a soil or litter layer, $T_F = T_{air}$ in the case of a grass layer), it was then possible to calculate the forest floor emissivity $e_F^{P,\theta} = 1 - R_F^{P,\theta}$.

4.3.3 Modelling of soil-litter (SL) emissivity

4.3.3.1 Footprint emissivity

Previously the L-MEB model has been used to model a litter layer using the τ-ω approach (Saleh *et al.*, 2006). However, the τ and ω parameters in L-MEB, representing volume effects such as extinction and scattering, are relevant for a vegetation layer but potentially less so for litter due to its higher volume density. Therefore, the current study uses a more physically based approach.
The emissivity $e_F^{P,\theta} = e_{SL}^{P,\theta}$ of the soil-litter forest floor configuration was simulated following the method proposed by Schwank *et al*. (2008). The basic ideas behind this approach are: i) the dielectric depth profile $\varepsilon(z)$ of a specific ground configuration is represented by an empirical approach which describes gradual transitions between the dielectric regimes; ii) coherent reflectivities $R_{coh}^{P,\theta}$ associated with $\varepsilon(z)$ are computed with a coherent radiative transfer model. $R_{coh}^{P,\theta}$ accounts for roughness with lateral dimensions below the resolution limit (Bragg limit) and iii) $R_{coh}^{P,\theta}$ is averaged over the thickness range of the considered dielectric layers (e.g. litter) in order to model the partial cancellation of coherence due to variations at lateral scales above the resolution limit. The resulting reflectivity $R_F^{P,\theta}$ is then used to model the measured $T_B^{P,\theta}$.
In the current study two modifications were applied to the approach used by Schwank *et al.* (2008): i) instead of a matrix formulation of Maxwell's boundary conditions at dielectric discontinuities the Wilheit model (Wilheit, 1978) was used to compute $R_{coh}^{P,\theta}$ and ii) a more realistic averaging approach was used to derive $R_F^{P,\theta}$ from $R_{coh}^{P,\theta}$.
As in Schwank *et al*. (2008), Fermi functions were used to represent the dielectric profile $\varepsilon_{ALS}(z)$ of the litter-soil configuration:

$$\varepsilon_{\mathrm{ALS}}(z) = \varepsilon_{\mathrm{A}} + \frac{\varepsilon_{\mathrm{L}} - \varepsilon_{\mathrm{A}}}{1 + \exp\left(-2.197 \cdot \frac{z - z_{\mathrm{AL}}}{\Delta_{\mathrm{AL}}}\right)} + \frac{\varepsilon_{\mathrm{S}} - \varepsilon_{\mathrm{L}}}{1 + \exp\left(-2.197 \cdot \frac{z - z_{\mathrm{LS}}}{\Delta_{\mathrm{LS}}}\right)} \qquad (4\text{-}7)$$

The parameters ε_{L} and ε_{S} are the effective litter and soil permittivities and z is the downward vertical direction. The mean depths of the dielectric transitions between air and litter (AL), and litter and soil (LS) are z_{AL}, and z_{LS}, respectively. Consequently, the litter layer thickness is $D_{\mathrm{L}} = z_{\mathrm{LS}} - z_{\mathrm{AL}}$. The sharpness of the dielectric transitions are parameterized by $2{\cdot}\Delta_{\mathrm{AL}}$, and $2{\cdot}\Delta_{\mathrm{LS}}$, defined as the differences in z from 10% to 90% of the corresponding permittivity differences.

An example of a permittivity profile $\varepsilon_{\mathrm{ALS}}(z)$ of the litter-soil configuration is plotted in figure 4-2, using parameter values typical for the Bray forest floor. Given $\varepsilon_{\mathrm{ALS}}(z)$, the Wilheit modelling procedure was performed for a total depth of 30 cm with the thickness of each of the $N = 300$ homogeneous layers set to 0.1 cm, which is less than one-tenth of the wavelength in the medium. No temperature gradients were considered over the total depth. This procedure resulted in the coherent reflectivities $R_{\mathrm{coh}}{}^{P,\theta}$.

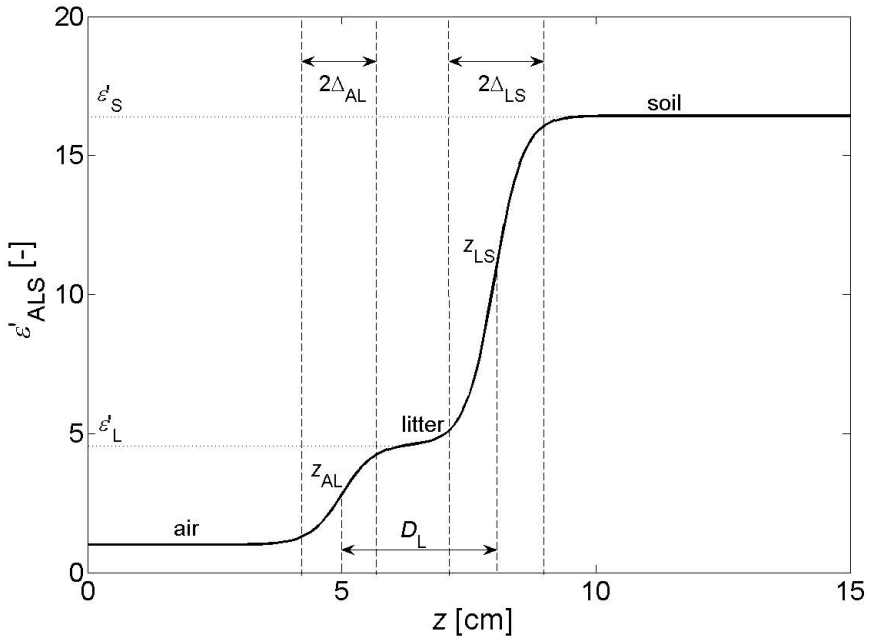

Figure 4-2: Example of a dielectric profile $\varepsilon'_{\mathrm{ALS}}(z)$ according to equation 4-7 representative for the soil-litter configuration. $\theta = 45°$, $D_{\mathrm{L}} = 3$ cm, $2{\cdot}\Delta_{\mathrm{AL}} = 1.39$ cm, $2{\cdot}\Delta_{\mathrm{LS}} = 1.25$ cm, $\varepsilon_{\mathrm{A}} = 1$ and $\varepsilon_{\mathrm{S}} = 16.428 + 2.977\mathrm{i}$ and $\varepsilon_{\mathrm{L}} = 4.613 + 0.104\mathrm{i}$, corresponding to soil and litter moistures of 0.205 $m^3\ m^{-3}$ and 0.453 $kg\ kg^{-1}$. These values are typical for the Bray forest floor.

As mentioned above, compared with Schwank *et al.* (2008) an improved averaging approach was used in the current study to compute the experimentally relevant footprint reflectivities $R_{\mathrm{F}}{}^{P,\theta}$ from the coherent reflectivities $R_{\mathrm{coh}}{}^{P,\theta}$. Instead of linearly averaging $R_{\mathrm{coh}}{}^{P,\theta}$ over the range of the litter layer thickness D_{L} within the footprint, a normalized gamma probability distribution $P(D_{\mathrm{L}})$ was used, as shown in equation 4-8 (with Γ = Gamma function). This is a more realistic approach as the spatial variability of D_{L} is accounted for and weighed.

$$R_{\mathrm{F}}^{P,\theta} = \int_0^{\infty} P(D_{\mathrm{L}}) \cdot R_{\mathrm{coh}}^{P,\theta}(D_{\mathrm{L}})\, dD_{\mathrm{L}} \quad \text{with} \tag{4-8}$$

$$P(D_{\mathrm{L}}) = \frac{1}{b^a \Gamma(a)} \cdot {D_{\mathrm{L}}}^{a-1} \cdot \exp\left(\frac{-D_{\mathrm{L}}}{b}\right)$$

The distribution $P(D_{\mathrm{L}})$ with a = 3.85 and b = 1.05 cm shown in figure 4-3 was based on the distribution of D_{L} observed in the field (Demontoux *et al.*, 2008). Combining the coherent reflectivities ${R_{\mathrm{coh}}}^{P,\theta}$ with $P(D_{\mathrm{L}})$ yielded the footprint reflectivities ${R_{\mathrm{F}}}^{P,\theta}$. The general procedure for model calibration of the below-canopy observations of the soil-litter configuration was to simultaneously retrieve the parameters Δ_{AL} and Δ_{LS} (eq. 4-7) using an unconstrained nonlinear optimisation procedure, in which several initial values were tested.

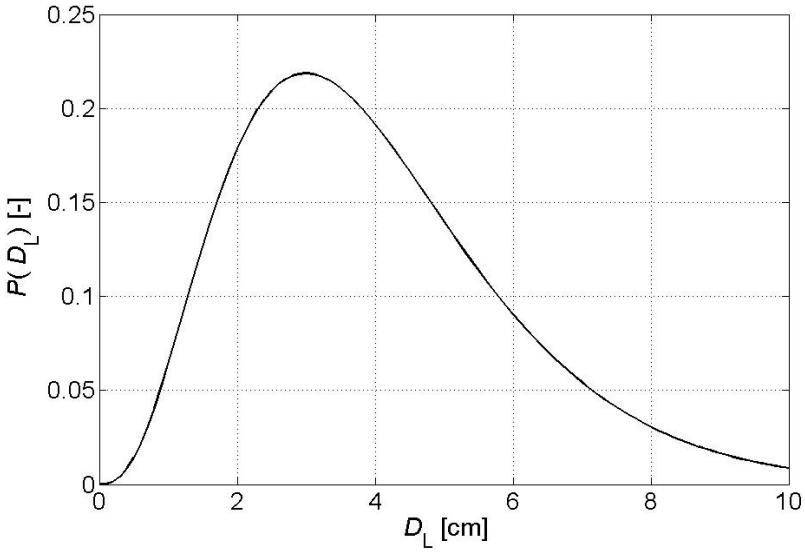

Figure 4-3: Normalized gamma probability distribution $P(D_{\mathrm{L}})$ (eq. 4-8) with a = 3.85 and b = 1.05 cm used for modelling the distribution of litter layer thickness D_{L}.

4.3.3.2 Soil and litter permittivity

For the calibration of the Wilheit model with the below-canopy observations of ${e_{\mathrm{SL}}}^{P,\theta}$, gravimetric litter moisture *LM* [kgkg^{-1}] was estimated from volumetric soil moisture *SM* [m^{3}m^{-3}] using the site-specific empirical relation observed during a period of 6 months in 2004 (Grant *et al.*, 2007):

$$LM = 3.0971 \cdot SM - 0.1816 \quad (R^2 = 0.84) \tag{4-9}$$

Effective soil and litter permittivities ε_{S} and ε_{L} are represented in the empirical dielectric profile $\varepsilon_{\mathrm{ALS}}(z)$ (eq. 4-7). The Dobson dielectric mixing model (Dobson *et al.*, 1985) was used to compute ε_{S} as a function of the volumetric soil moisture *SM* [m^3 m^{-3}] with soil parameters as given in §4.2.1 and table 4-2 (§4.4.1). Estimates of $\varepsilon_{\mathrm{L}} = \varepsilon_{\mathrm{L}}' + \mathrm{i}\ \varepsilon_{\mathrm{L}}''$ were taken from laboratory measurements relating *LM* to litter permittivity, for litter samples with bulk density 0.1 g cm^{-3} taken from the Bray site (Demontoux *et al.*, 2008):

$$\varepsilon'_{\mathrm{L}} = 2.3 \cdot \tanh\left(8 \cdot \left(LM - 0.65\right)\right) + 5.8 \cdot LM + 4.1 \quad \text{(4-10a)}$$

$$\varepsilon''_{\mathrm{L}} = 1.25 \cdot \tanh\left(18 \cdot \left(LM - 0.63\right)\right) + 1.35 \quad \text{(4-10b)}$$

4.4 Results and Discussion

4.4.1 Ground measurements during the below-canopy experiment

Results of the ground measurements during the below-canopy experiment are shown in table 4-2. Temperatures and soil moisture values in this table are averages of measurements done before and after each series of radiometric observations of a given configuration (S, SL or SLG, see §4.2.2). Gravimetric litter moisture is obtained from soil moisture according to the empirical relation given by equation 4-9.

Table 4-2: Temperature and moisture values obtained from ground measurements done before and after each radiometric observation series of the three different configurations S, SL and SLG.

	Soil-litter-grass	***Soil-litter***	***Bare soil***
Date	15/02/07	15/02/07	16/02/07
T_{soil} 0-7 cm [K]	281.55	282.75	283.53
T_{air} at 20 m [K]	284.05	287.6	288.41
Soil moisture 0-5 cm [m^3 m^{-3}]	0.194	0.205	0.220
Litter moisture [kg kg^{-1}] (from eq. 4-9)	0.450	0.481	-
Litter fresh biomass [kg m^{-2}]	-	6.74	-
Grass moisture [kg kg^{-1}]	0.67	-	-
Grass fresh biomass [kg m^{-2}]	2.58	-	-

4.4.2 Canopy observations

Figure 4-4 shows values of the forest canopy transmissivity $\gamma_{\mathrm{C}}^{P,\theta}$ derived from the three different azimuthal observation series, plotted against observation angle θ. The lines in the figure trace the polarization-averaged values of $\gamma_{\mathrm{C}}^{P,\theta}$ for each of the three azimuthal series. The figure shows a general increase in $\gamma_{\mathrm{C}}^{P,\theta}$ for θ = 120º-180º, which illustrates the effect of difference in path length through the canopy at different angles (cf. the 1/cos θ term in eq. 4-2). Depending on θ the observed dispersion between azimuth series can amount up to 0.10. This is due to the fact that, especially at shallower incidence angles, each azimuthal measurement series observed a different part of the canopy and the dispersion in $\gamma_{\mathrm{C}}^{P,\theta}$ thus reflects the canopy heterogeneity. Furthermore, the figure shows that the differences in $\gamma_{\mathrm{C}}^{P,\theta}$ for each pair of H- and V polarizations are very small at the lower angles but increase at observation angles ≥ 150º. This might be due to the tree structure, which shows a more horizontal orientation of the branches close to the trunk but a more vertical one towards the outer ends, as reported by Saleh *et al*. (2005). At the lower observation angles the footprint will predominantly contain the more central parts of the trees, which consist of both horizontal and vertical elements, whereas at the higher observation angles it mainly covers the more vertical branch ends. This may explain the fact that the vertically polarized transmissivity $\gamma_{\mathrm{C}}^{\mathrm{V},\theta}$ is lower at the higher observation angles. At θ = 180º, the antenna plane of incidence is horizontal and perpendicular to the ground.

Differences in $\gamma_C^{P,\theta}$ for each pair of H- and V signals must therefore be interpreted as azimuthal differences rather than actual horizontal and vertical differences. As figure 4-4 shows, none of the three observation series shows a difference between the paired H- and V values at $\theta \approx 180º$. Also, values of $\gamma_C^{P,\theta}$ for each of the three azimuth observation series are very similar at this observation angle. This indicates that at $\theta \approx 180º$, as can be expected from the tree structure described above, the influence of row structure disappears and the tree canopy is isotropic.

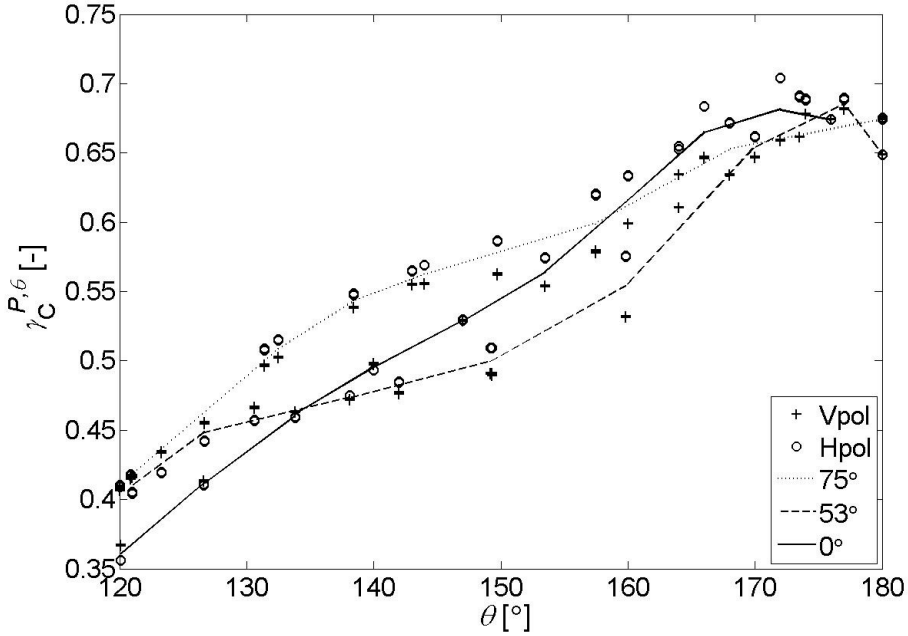

Figure 4-4: Forest canopy transmissivity $\gamma_C^{P,\theta}$ (eq. 4-5) plotted against observation angle θ for three different azimuth angles (75°, 53° and 0°) relative to the row direction of the trees. Dotted, dashed and solid lines trace the polarization-averaged values of $\gamma_C^{P,\theta}$ for the 75°, 53° and 0° azimuth angles, respectively.

Following the procedure explained in §4.3.1 and §4.3.2.1, values of the canopy parameters $\tau_{C,NAD}$ and tt_C^P were retrieved from observations at angles θ = 120º-180º. The results are shown in table 4-3 for each of the three azimuth observation series, together with the resulting root mean square (RMS) error in $T_B^{P,\theta}$. Average values were used as model inputs in all further parts of this study.

The differences in $\tau_{C,NAD}$ for each azimuthal series show the spatial variability of the canopy optical depth. This will of course have some impact on the derivation of ground emissivities and thus on the modelling results.

It should be noted that the values given in table 4-3 differ slightly from those found in a previous study concerning an experiment made in 2006 (Grant *et al.*, 2008). The reason for this lies in the fact that the 2006 observations were done at the edge of the forest, and consequently only observations at angles between 120°-150° were used in the analysis in order to minimize sky influence. Furthermore, the model used previously by Grant *et al.* (2008) neglected the ground radiation reflected by the canopy. The current study has extended on the previous results by using a more complete model (eq. 4-5) together with observations done within the forest, and a greater range of angles (120°-180°), to obtain more realistic values of $\tau_{C,NAD}$ and tt_C^P.

Table 4-3: Values of tree canopy parameters $\tau_{C,NAD}$ and tt_C^P retrieved from observations at angles 120º-180º for each of the three azimuth observation series, together with the resulting RMS error in $T_B^{P,\theta}$.

	$\tau_{C,NAD}$	tt_C^H	tt_C^V	***RMS error [K]***
75º azimuth	0.43	1.08	1.14	5.450
53º azimuth	0.46	1.18	1.16	13.035
0º azimuth (// rows)	0.41	1.44	1.44	7.878
average ± stdev.	0.43 ± 0.03	1.23 ± 0.19	1.25 ± 0.17	

4.4.3 Forest floor emissivities

The forest floor emissivities $e_F^{P,\theta}$ for H- and V-polarizations derived using equation 4-6 are shown in figure 4-5 for each of the three observed forest floor configurations (bare soil (S), soil-litter (SL) and soil-litter-grass (SLG)).

Two aspects of this figure are noticeable. Firstly, emissivities are high, especially those of the soil-litter-grass system, which are slightly over 1 for V polarisation. The latter result is non-physical. Although forest floor emission is expected to be high, especially when litter and grass layers are involved, in this case the experimental set-up probably has an additional effect. Because these observations were done below the canopy and inside the forest, the situation is in fact quite similar to being inside a black box. As the forest floor emission is already high, it is easy to overestimate $e_{SLG}^{P,\theta}$ unless all other contributions to the observed $T_B^{P,\theta}$ are exactly known. However, the set-up was specifically chosen in order to obtain *in situ* measurements with the forest floor layers in their undisturbed state and, as said previously (§4.2.2), to better understand the relative layer contributions to emissivity.

A second noticeable aspect of figure 4-5 is that it clearly shows that the contributions of both the litter and the grass layers to overall radiance are important. In a previous study (Schmugge *et al*., 1998), the thatch structure of an unburned grass cover was found to result in very high emissivities and low sensitivity to moisture status of the underlying soil. A later study over grass (Saleh *et al*., 2006) found a similar effect for a 'mixed layer' consisting of mulch, plant debris and a tight layer of grass roots and stems, especially when wet, however the respective contributions of these components could not be separated. Finally, Schwank *et al*. (2008) found that a layer of dead leaves on the ground of deciduous forests is almost transparent at L-band if dry, but an important radiation source when wet. Figure 4-5 indicates that although the effect of the litter layer on overall radiance is certainly not negligible, a layer of moist senescent grass can have an additional important effect. This could contribute to the low sensitivity to soil moisture found for above-canopy radiometric observations at the Bray site (Grant *et al*., 2007), an effect which until now was attributed mainly to the litter layer.

4.4.4 Model calibration

Model calibration for the soil-litter configuration was done as described in §4.3.3 by retrieving parameter values Δ_{AL} and Δ_{LS}, which describe the vertical extents of the air-litter and litter-soil transitions. Because equations 4-9, 4-10a and 4-10b were all based on experimental data obtained from the Bray site, it should be kept in mind that in this procedure, ε_S and ε_L were not independent.

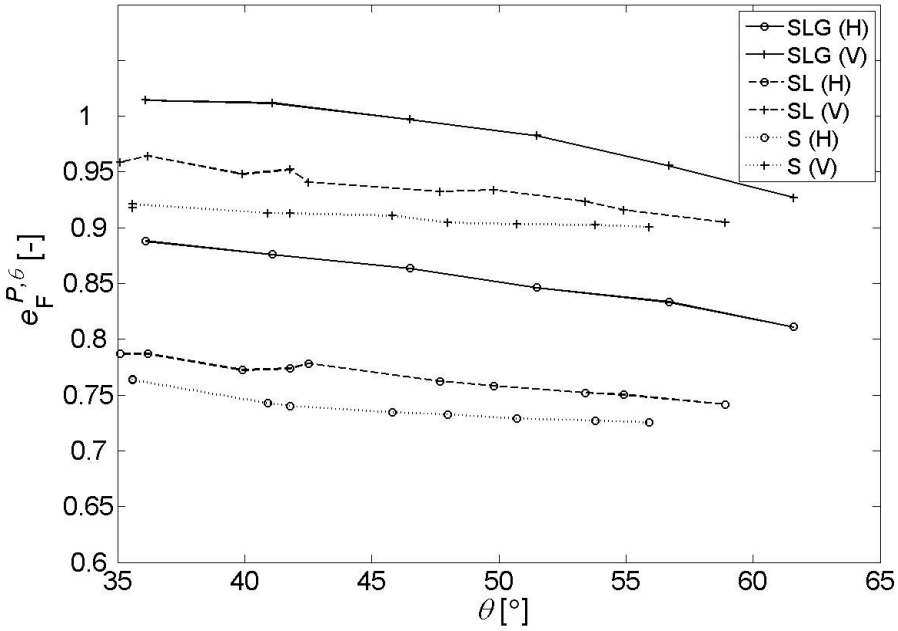

Figure 4-5: Forest floor emissivities $e_F^{P,\theta}$ corrected for the contributions of the reflected downwelling canopy and sky radiation (eq. 4-6) plotted against observation angle θ for each of the three observed forest floor configurations (bare soil (S), soil-litter (SL) and soil-litter-grass (SLG)).

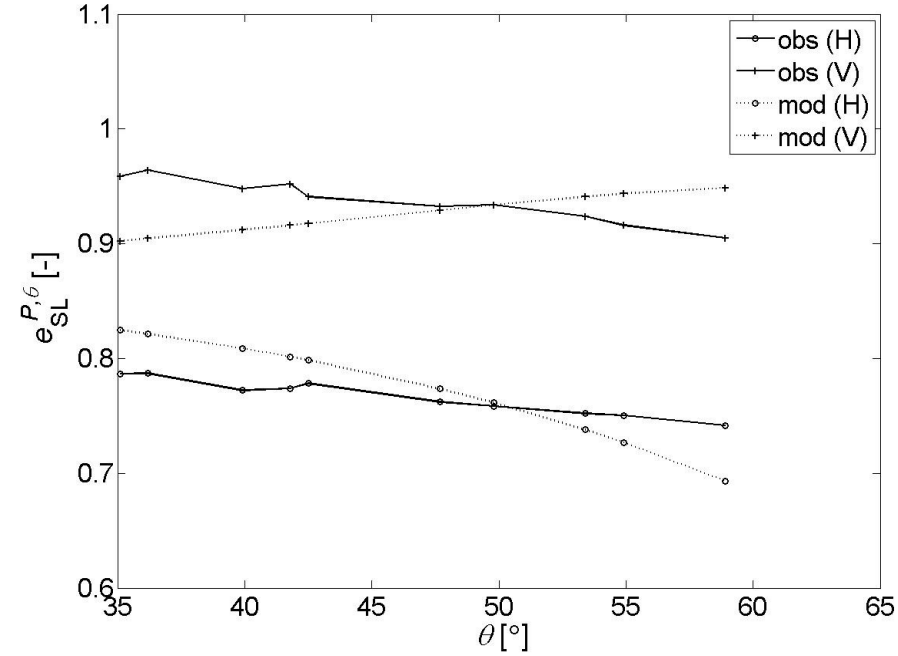

Figure 4-6: Comparison between values of forest floor emissivity for a soil-litter configuration $e_{SL}^{P,\theta}$ derived from below-canopy observations and simulations. The latter were done using the Wilheit model with air-litter and litter-soil dielectric transitions.

The values resulting from the retrievals were Δ_{AL} = 0.695 cm and Δ_{LS} = 0.624 cm, associated with RMS errors in emissivity $e_{SL}^{P,\theta}$ of 0.036 (V) and 0.029 (H), respectively. These values of Δ_{AL} and Δ_{LS} resulted in the dielectric profile $\varepsilon'_{ALS}(z)$ shown previously in figure 4-2, for $\theta = 45°$, D_L = 3 cm, SM = 0.205 m^3m^{-3} (cf. table 4-2) and LM = 0.453 $kgkg^{-1}$ (eq. 4-9). Corresponding soil and litter permittivities are $\varepsilon_S = 16.428 + 2.977i$ and $\varepsilon_L = 4.613 + 0.104i$. The coherent reflectivities resulting from this profile are $R_{coh}^{H,45°} = 0.083$ and $R_{coh}^{V,45°} = 0.06$. Subsequently accounting for the distribution $P(D_L)$ yields the values $R_F^{H,45°} = 0.213$ and $R_F^{V,45°} = 0.077$ for the footprint reflectivities.

Figure 4-6 shows simulated footprint emissivities (dotted lines) compared with the soil-litter emissivities derived from the below-canopy observations (solid lines) for observation angles 35°-60°.
The fact that the emissivities derived from observations show different angular dependences to the simulated values could be due to various causes: First, an imperfect calculation of forest canopy radiance, in which the spatial variability of $\tau_{C,NAD}$ (§4.4.2), i.e. the effect of canopy heterogeneity, is not completely accounted for. Second, the neglected effect of grass tufts and trunks in the footprint. Third, the large beamwidth of the antenna. Finally, an incorrect probability distribution and/or an (as yet unknown) angular dependency of litter emissivity could be important. The errors are larger at vertical polarisation, where the slope orientation of the observations is opposite to that of the simulations. In a study concerning deciduous leaf litter (Schwank *et al*., 2008), larger modelling errors at vertical polarisation were attributed to possible anisotropic properties of the observed litter type. The results found in the current study suggest that anisotropy might also occur in the case of coniferous litter.

4.4.5 Emissivity and soil moisture

A compilation was made of the results of both the above- and below-canopy experiments in order to present a comprehensive image of the emission of each layer of the forest system as a function of *SM* conditions. This was done for the H polarization only, as only this polarization was available during the above-canopy experiment (§4.2.2).
Figure 4-7 shows four different emissivities plotted against soil moisture content: i) above-canopy observed emissivity $e_{SLGC,obs}^{H,45°}$ (published previously by Grant *et al*. (2007)), ii) below-canopy emissivity of the soil-litter-grass system $e_{SLG,'obs'}^{H,45°}$, derived from the above-canopy observations, iii) simulated values of soil-litter emissivity $e_{SL,sim}^{H,45°}$ and iv) simulated values of smooth bare soil emissivity $e_{S,sim}^{H,45°}$.
It should be noted that in all observed and simulated results presented in figure 4-7, values of *SM* and *LM* were taken from the ground measurements made during the above-canopy experiment (§4.2.2), and not from equation 4-9, which was used for model calibration only (§4.3.3.2 and §4.4.4).
The observed emissivities of the soil-litter-grass-canopy ($e_{SLGC,obs}^{H,45°}$) were obtained from the above-canopy data set by calculating $T_B^{H,45°}/T_{gc}$ with T_{gc} being the effective ground-canopy temperature (Grant *et al*., 2007). Then, soil-litter-grass emissivity $e_{SLG,'obs'}^{H,45°}$ was calculated from these measurements by removing the contribution of the tree layer from the above-canopy observations (eq. 4-1), using the canopy parameters obtained from the below-canopy upward observations (eq. 4-5). It was assumed that significant changes in the tree canopy would not have taken place in the

period between the two experiments. The suffix 'obs' in the subscript indicates that values of $e_{SLG,'obs'}^{H,45°}$ are not the actual observations themselves, but have been derived from observations. T_{gc} was used for both the tree canopy temperature and for the temperature of the soil-litter-grass system.
The soil-litter emissivities ($e_{SL,sim}^{H,45°}$) were simulated with the Wilheit model (§4.3.3.1), using the calibrated values of Δ_{AL} and Δ_{LS} and the probability distribution shown in figure 4-3. Soil-litter temperatures T_{SL} were approximated by the effective soil temperatures $T_{S,eff}$ (Grant *et al.*, 2007) obtained during the above-canopy experiment. In the simulations, it was assumed that the parameters Δ_{AL} and Δ_{LS} do not depend on moisture conditions.
Finally, a time series of smooth bare soil emissivity ($e_{S,sim}^{H,45°}$) was obtained with the Fresnel equations, the Dobson dielectric mixing model (Dobson *et al.*, 1985), $T_{S,eff}$ (Grant *et al.*, 2007) and soil parameter values as given in §4.2.1.

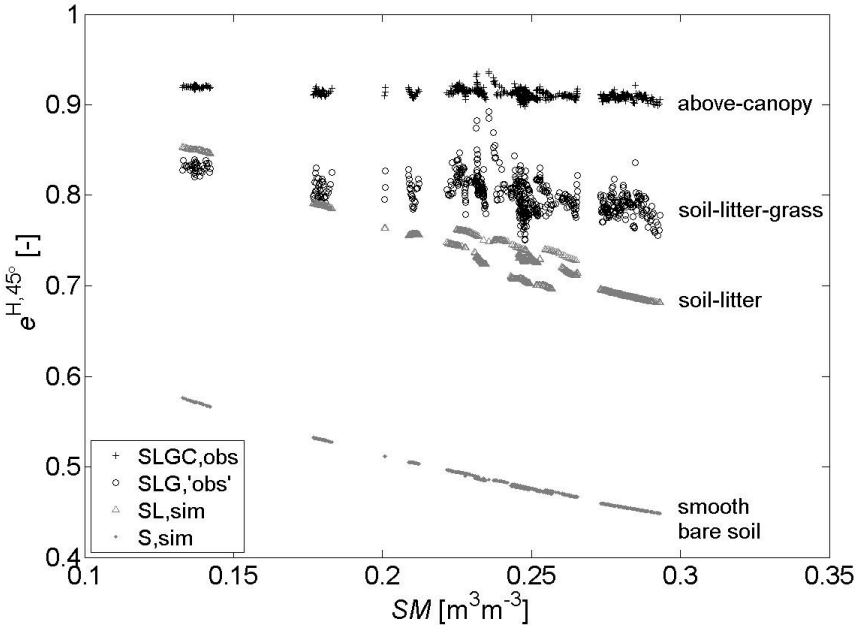

Figure 4-7: Horizontally polarized surface emissivities derived from above-canopy observations ($e_{SLGC,obs}^{H,45°}$ and $e_{SLG,'obs'}^{H,45°}$; black) and simulations ($e_{SL,sim}^{H,45°}$ and $e_{S,sim}^{H,45°}$; grey), plotted against volumetric soil moisture content.

The respective decreases in gradient de_F/dSM from $e_{SL,sim}^{H,45°}$ through $e_{SLG,'obs'}^{H,45°}$ to $e_{SLGC,obs}^{H,45°}$ show that the sensitivity to soil moisture is already substantially suppressed by the presence of a grass layer. This corroborates the low above-canopy sensitivity of emissivity with respect to ground moisture conditions found by Grant *et al.* (2007), even though the average transmissivity of the tree canopy lies around 0.55 (cf. fig. 4-4). This sensitivity loss is clearly due to the effect of the grass understory as well as that of the tree canopy.
The scatter in $e_{SLG,'obs'}^{H,45°}$ values can be explained by temperature variations between subsequent observations. When deriving these below-canopy emissivities, the effective temperature T_{gc} was used for both the tree canopy and the soil-litter-grass system. However, it is very well possible that the latter case especially is a rather coarse approximation. The variation inherent in the above-canopy data set is for a great deal due to the changing phenological conditions of the grass understory from

summer to winter. Furthermore, some variation, especially such as seen around $SM \approx$ 0.21-0.26 m^3m^{-3}, could also be the result of different *LM* conditions for a given *SM*.
Under dry conditions, the grass layer is almost transparent and emission originates mainly from the soil-litter system ($e_{SLG,'obs'}^{H,45°} \approx e_{SL,sim}^{H,45°}$ for $SM \leq 0.16$ m^3m^{-3}). This transparency of dry grass is similar to the behaviour of a dry litter layer found by Schwank *et al*. (2008), therefore under dry conditions the overall forest floor emission will in fact mainly originate in the soil layer.
For $SM \approx$ 0.21-0.26 m^3m^{-3} multiple emissivity values $e_{SL,sim}^{H,45°}$ can sometimes be seen, which result from periods with differing litter moisture *LM* at the same *SM*. For a given value of *SM*, emissivity becomes lower for increasing *LM*.
Finally, figure 4-7 includes the simulated $e_{S,sim}^{H,45°}$ for a smooth bare soil of the Bray type in order to provide a reference against which to view the other three emissivities. It can be seen when comparing the gradients of $e_{S,sim}^{H,45°}$ and $e_{SL,sim}^{H,45°}$ that the addition of a litter layer does not change the sensitivity to soil moisture, but merely increases emissivity values. This suggests that the effective roughness H_R (Wang and Choudhury, 1981) of the soil-litter configuration does not change with changing soil moisture. A previous study (Saleh *et al*., 2007) over grass covers found that the relationship $H_R(SM)$ became less pronounced with increased litter cover, and was non-existent in the case of a sandy soil, both of which conditions apply to the Bray site. However, the physical behaviour of the 'effective' soil roughness parameter is not yet understood well enough to conclude whether this is a general or a site-specific result.

4.4.6 Thermal sampling depth

The thermal sampling depth of a medium is defined as the depth δ_T above which ~ 63% ($1\text{-}e^{-1}$) of the upwelling thermal radiation originates (Wilheit, 1978). Consequently, δ_T is determined by both the real and imaginary parts of the dielectric constant (Ulaby *et al*., 1986). In the current study, δ_T (measured from the top of the litter layer) was obtained from simulations performed for the soil-litter configuration using the Wilheit model (§4.4.5). These simulations were run for the soil and litter moisture contents measured during the above-canopy experiment, and for three different litter layer thicknesses D_L, in order to give an insight into the relative contribution of each layer to the total emission in the case of a soil-litter system.
In the results, the litter layer thickness D_L was subtracted from the thermal sampling depth (δ_T-D_L), i.e. the thermal sampling depth was defined relative to the litter-soil interface. The advantage of this approach is the fact that it gives the depth *within the soil layer* at which 63% of the total upwelling emission originates, as a function of D_L.
Values of δ_T-D_L are plotted against *SM* in figure 4-8a for $\theta = 45°$ and three different values D_L = 1, 3, 10 cm. Values of δ_T were almost identical for H and V polarizations, therefore polarization averaged values are shown. It should be repeated here that temperature gradients within the soil-litter system were ignored (§4.3.3.1).
Figure 4-8b shows the corresponding $e_{SL,sim}^{H,45°}$ plotted against *SM* for each value of D_L.
In figure 4-8a it can be seen that for a given *SM* and D_L, various values of δ_T- D_L are visible between $SM \approx$ 0.21-0.26 m^3m^{-3}, which reflect different conditions of *LM* as indicated by the arrows in the figure (values of *LM* given for SM = 0.25 m^3m^{-3}). This effect of *LM* of course increases with increasing thickness D_L. It can be seen that the thermal sampling depth increases with decreasing *LM* for a given value of *SM*.

The depth δ_T-D_L below the soil-litter interface will of course increase with decreasing litter cover, however, the magnitude of this increase depends on the moisture conditions present. In general, low *SM* conditions were associated with low *LM* conditions. The fact that the differences between δ_T-D_L for D_L = 1 cm and D_L = 10 cm are very small for low *SM* confirms that the litter layer is rather transparent in dry *LM* conditions (cf. figure 4-7).
For higher moisture (i.e. *SM* and *LM*) conditions, litter layer emission becomes more important, resulting in a changeover in δ_T (observed here at $SM \approx 0.2$ m^3m^{-3}) and subsequent decreasing δ_T-D_L with increasing moisture content for D_L = 3 cm and D_L = 10 cm. The positive gradients in δ_T-D_L with increasing *SM* in certain cases, such as for D_L = 1 cm and for D_L = 3 cm and D_L = 10 cm at $SM < 0.2$ m^3m^{-3}, are in accordance with the results of a recent modelling study (Schwank *et al.*, 2008), which predicted that both negative and positive gradients of reflectivity can occur with changing soil moisture. This behaviour was explained by coherent effects becoming relevant for particular combinations of litter- and soil permittivities ε_L and ε_S present in the ground system. Due to such coherent effects even a litter layer much thinner than the wavelength λ (e.g. D_L = 1 cm) can affect the ground emission significantly.
This figure (fig. 4-8a) shows that only when the litter layer is very thick and very wet does the emission originate predominantly in the litter layer, resulting in negative values of δ_T-D_L. In all other cases, the radiometric signal still contains a certain contribution of soil emission.

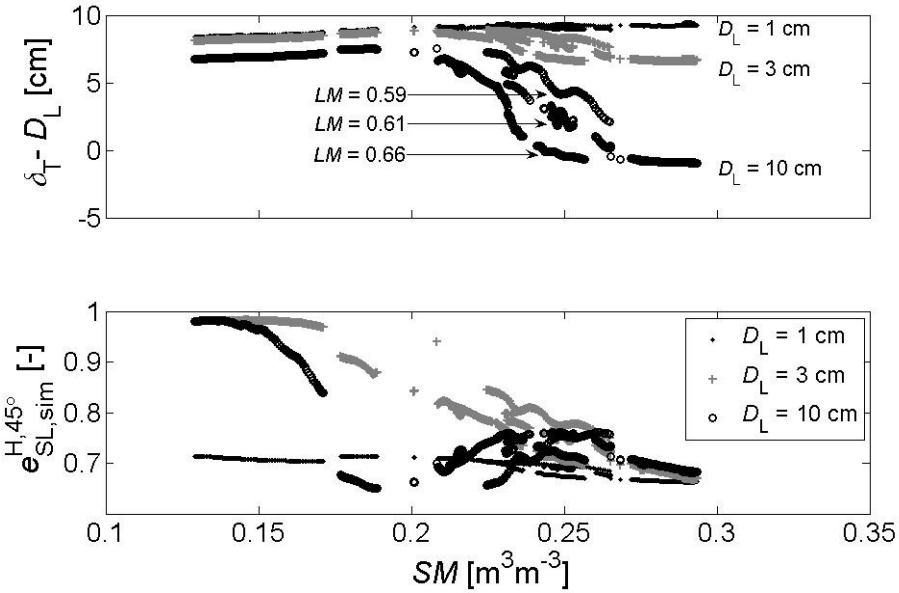

Figure 4-8a (top) and 4-8b (bottom): Values of δ_T-D_L (average of H and V polarizations) of $e_{SL,sim}^{P,45°}$ emissivities plotted against volumetric soil moisture content *SM* for three different values of D_L. Arrows indicate values of *LM* for $SM = 0.25$ m^3m^{-3} (**a**). Corresponding $e_{SL,sim}^{H,45°}$ plotted against *SM* for three different litter layer thicknesses D_L (**b**).

The patterns in emissivity shown in figure 4-8b are similar to those found previously from simulations by Della Vecchia *et al.* (2007) and Demontoux *et al.* (2008), and show the effect of coherence occurring in the presence of a litter layer, as a function of D_L. The unexpected patterns in the case of D_L = 1 cm, such as the positive gradient $d(\delta_T\text{-}D_L)/dSM$ in figure 4-8a and the shallow slope in corresponding $e_{SL,sim}^{H,45°}$ in figure 4-8b, can be explained by the fact that coherent effects can occur even for layer

thicknesses much smaller than the observation wavelength (e.g. Schmugge and Jackson (1998)). In field observations, these effects will cancel each other out to a certain degree because of the spatial variation in D_L within a footprint, and will therefore not necessarily be visible.

4.5 Summary and Conclusions

The main objective of this study was to better understand the L-band emission properties of the different layers of a forest system as a function of varying ground moisture conditions. The study involved the combined use of two unique data sets and two well-established models (L-MEB and Wilheit).

L-band radiometric observations were made *in situ* below the canopy over three different configurations of a forest floor: i) a soil-litter-grass (SLG) configuration, ii) a soil-litter (SL) configuration and iii) bare soil (S). Layers were manually removed between each of the three series of observations. Upward-looking observations were made of the tree canopy in order to derive the radiative transfer properties of the crown vegetation. Above-canopy observations of soil-litter-grass-canopy (SLGC) emission were available from a long-term data set previously obtained at the same site. The emissivities of S, SL, SLG and SLGC configurations were related to varying soil moisture contents.

The emissivities of the smooth bare soil and the soil-litter configuration showed a similar sensitivity to variations in soil moisture content. As expected, this sensitivity then decreased with each additional vegetation layer.

Under dry conditions, the grass layer was almost transparent, as is also the case for a dry litter layer. Therefore, in such conditions the below-canopy emission originates almost entirely in the soil layer. However, under wetter conditions, the L-band sensitivity to soil moisture is substantially suppressed by the presence of a wet grass understory, whether living or senescent. This explains why such low above-canopy sensitivity to ground moisture conditions was found previously over forests, even though the tree canopy was rather transparent.

The thermal sampling depth of the soil-litter forest floor configuration was investigated for a range of soil moisture values. It was found that the thermal sampling depth generally exceeded the thickness of the litter layer, indicating that the radiometric signal still contained a certain contribution of soil emissivity. Only in the case of a rather thick and wet litter layer was the soil emission almost completely obscured.

Altogether, this study gives a comprehensive image of the L-band emission of the various forest layers (soil, litter, grass and tree canopy) with varying ground moisture conditions. The study is the first on this subject to use undisturbed, *in situ* experimental data and it confirms several results of recent modelling and/or laboratory-based studies. This knowledge can help to improve the analysis of above-canopy forest observations at L-band, an important issue in the context of space borne sensors such as SMOS.

Chapter 5

On the Influence of Forest Cover Fraction on L-band Soil Moisture Retrievals from Heterogeneous Pixels using Multi-Angular Observations*

5.1 Introduction

ESA's Soil Moisture and Ocean Salinity (SMOS) mission, planned for launch in 2009, will carry a multi-angle interferometric L-band (1.4 GHz) radiometer for monitoring soil moisture and ocean salinity at global scale (Kerr *et al.*, 2001). Spatial resolution of the instrument is around 40 km at nadir view, which means that most pixels of the earth's surface will be heterogeneous, consisting of a mixture of forest, crops, grass and bare soil. The target error for SMOS is below 0.04 m^3m^{-3} volumetric soil moisture. Studies involving soil moisture retrievals over crops and grassland have indicated that this target error can be achieved (e.g. Pardé *et al.*, 2004; Wigneron *et al.*, 2007; Saleh *et al.*, 2007). However, soil moisture retrievals over forested areas are expected to give poorer results, due to the higher attenuating effect of the denser vegetation cover. Previously, soil moisture retrievals over homogeneous forested areas using experimental observations at L-band have been attempted in several small-scale studies (e.g. Chauhan *et al.*, 1999; Lang *et al.*, 2001; Lang *et al.*, 2006). The results of these studies showed some sensitivity to soil moisture, depending on forest biomass and ground conditions. However, Lang *et al.* (2001) indicated the need for accurate measurement of ground temperature in order to achieve these results. A modelling study by Della Vecchia *et al.* (2006a) also found an appreciable sensitivity to soil moisture over forests. Although temperate deciduous and coniferous forests have been found to have a reasonably high transmissivity, ranging from 0.4-0.6 (Grant *et al.*, 2008; Guglielmetti *et al.*, 2008; Guglielmetti *et al.*, 2007; Della Vecchia *et al.*, 2006b; Hallikainen *et al.*, 2000), above-canopy L-band observations can show only a small sensitivity to changes in soil moisture content due to the obscuring effect of the litter and understory layers, if these are present (e.g. Grant *et al.*, 2009). This relatively invariable forest emission can actually be an asset in soil moisture retrievals over heterogeneous pixels containing forest, as the soil moisture of the non-forested part of the pixel might still be retrieved with the required accuracy if the emission of the forested part of the pixel is modelled correctly enough. The current study will investigate the latter hypothesis.

To date, all known existing studies concerning soil moisture retrievals from heterogeneous forest pixels have been based on model simulations (Van de Griend *et al.*, 2003; Van de Griend *et al.*, 2004; Loew, 2008), rather than experimental data. The first two of these studies concluded that ignoring the *a priori* knowledge of the forest cover fraction α gives large errors in soil moisture retrieval if $\alpha \geq 10\%$, but if α is

* This chapter has been submitted for publication as: Grant, J.P., Van de Griend, A.A., Wigneron, J.-P., Saleh, K., Panciera, R. and Walker, J.P. (2009). On the Influence of Forest Cover Fraction on L-band Soil Moisture Retrievals from Heterogeneous Pixels using Multi-Angular Observations. *Remote Sensing of Environment*.

known and ≤ 50%, soil moisture in the non-forested area can be determined with a precision better than the 0.04 m^3m^{-3} target error for SMOS. The third study found a similar result, but again stressed the importance of knowing the surface temperature to within 4 K. That study also indicated that soil moisture retrievals over mixed forest pixels can show a good temporal evolution of soil moisture although the retrieval results themselves are biased. Retrieval accuracy was also found to depend on scale, increasing with decreasing spatial resolution until levelling out above a 10 km resolution.
While the above modelling studies present rather optimistic results, the studies are restricted to a limited range of moisture and land cover conditions, and, importantly, the results have not been verified with experimental data. Moreover, significant assumptions are made concerning parameter values. Especially, forest optical depth was assumed to be much higher than values found from recent field experiments (1-1.5 compared to 0.4-0.6).
In view of the impending launch of SMOS, the current study seeks to validate the results of previous modelling studies using large-scale experimental data which include both homogeneous and heterogeneous pixels, different land cover fractions, and different soil moisture conditions. The National Airborne Field Experiment 2005 (NAFE '05) field campaign (Panciera *et al.*, 2008) is well suited to this task. The main objective of the current study is thus to better understand and quantify the influence of forested areas on the soil moisture retrieval from heterogeneous pixels, in view of the upcoming SMOS mission.

5.2 Materials

5.2.1 Site description

The area of study (lat/lon (32º 8' 42" S, 150º 6' 43.1994" E) to (32º 11' 6" S, 150º 9' 7.1994" E)) covered part of the 'Roscommon' farm. This area was part of the larger 'Krui' study area covering the Krui River subcatchment, which lies within the Goulburn River catchment in southeast Australia. The location of Roscommon within the catchment is outlined in (Panciera *et al.*, 2008), while figure 5-1 shows the farm boundaries, forest areas and flight lines in more detail.
The study area has an average elevation of 300 m above sea level and is characterised by native grassland and relatively open Eucalypt forest areas. The forested surfaces were generally found on the more steep and rocky parts of the landscape (gently rolling with elevation differences up to ~15 m), whereas the flatter parts had been cleared for grazing.
The grassland areas consisted of native grass spp., with an average vegetation height estimated to be ~ 30 cm. Average grass Normalized Difference Vegetation Index (NDVI) during the experiment was 0.60. Estimates of leaf area index (LAI) derived from MODIS data at 250 m resolution were around 1.8 m^2m^{-2} for the entire campaign. Vegetation water content was estimated to be around 0.5 ± 0.2kg based on measurements of the weight difference between wet and dry biomass.
The forest areas consisted mainly of Box (*Eucalyptus spp.*), Ironbark (*Eucalyptus spp.*) and some Black Cypress-pine (*Callitris endlicheri*). Fish-eye photographs were taken of the Eucalypt vegetation, from which the fraction cover was determined to be ~39% and the LAI was estimated at 2.5. MODIS images showed that forest LAI did not noticeably change during the experiment. The understory was an open-heath

formation consisting mainly of Sifton bush (*Cassinia quinquefaria*). Some litter was present on the ground and formed a generally very thin (~ 0.5 cm) layer. Litter dry bulk density was 0.15 ± 0.05 gcm^{-3}. It is estimated that around 10-15% of the forest floor consisted of bed rock, with the remainder covered by sandy soil (67% sand, 15% clay) with a bulk density of 1.22 $kg.m^{-3}$ and a porosity of 0.437. Field observations found the thickness of the soil layer to be highly variable, however, more detailed information on this parameter is unavailable.

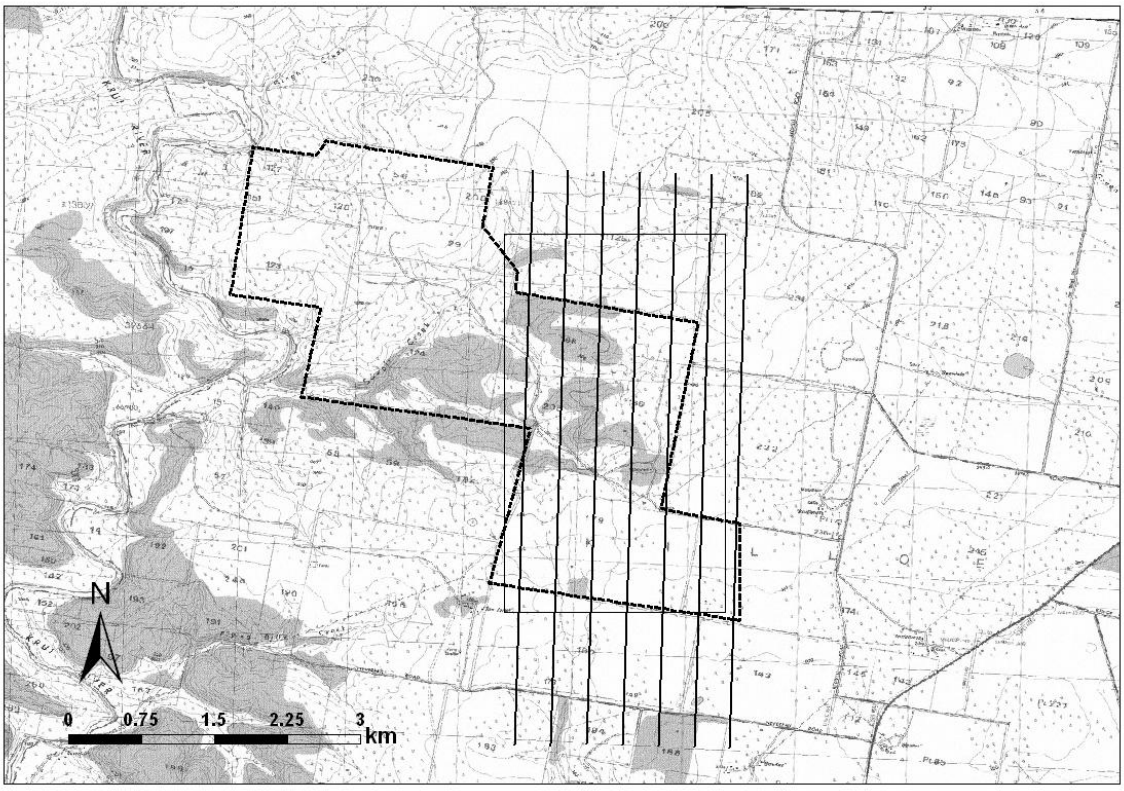

Figure 5-1: Topographic map of the area around Roscommon farm. The farm boundary is given by the dotted line, the thick solid lines show the seven PLMR flight lines at approximately 150 m altitude above ground level and the thin-lined rectangle indicates the approximate study area. The forest areas are coloured in grey.

5.2.2 Data

The airborne L-band measurements used in the current study were made using the dual-polarised Polarimetric L-band Multibeam Radiometer (PLMR) on 1st, 8th, 10th, 15th, and 22nd November 2005. Rather heavy precipitation occurred at the very beginning of the experiment, followed by a long drying-up period and finally some scattered rainfall at the end of the experiment. Precipitation data recorded at the Stanley station (approx. 8 km northwest of Roscommon) were available from the Goulburn River experimental data set (Rudiger *et al.*, 2007). Table 5-1 shows an overview of climatic conditions over the study area on the relevant flight days and times.

Table 5-1: Overview of climatic conditions for the Roscommon farm study area on the relevant flight days and times. $\overline{SM}$ = area-averaged soil moisture ± standard deviation, $T_{IR,av}$ = area-averaged swath-average infrared temperature ± standard deviation, Subscripts 'G' and 'F' denote grass and forest, respectively.

Day	*Local time [h]*	$\overline{SM_G}$ $[m^3m^{-3}]$	$\overline{SM_F}$ $[m^3m^{-3}]$	$T_{IR,av,G}$ [K]	$T_{IR,av,F}$ [K]	*Precipitation*
1/11	14.35-14.45	0.283 ± 0.028	0.184 ± 0.019	301.88 ± 1.03	302.06 ± 1.20	± 16.5 mm on previous two days; 0.4 mm on this day
8/11	10.30-10.40	0.217 ± 0.011	0.127 ± 0.059	300.24 ± 1.56	300.72 ± 1.90	rain just before flights; previous 2 days dry
10/11	10.10-10.20	0.097 ± 0.002	0.055 ± 0.030	304.73 ± 1.65	305.37 ± 2.08	0.2 mm previous day; 8.8 mm two days ago
15/11	10.05-10.15	0.068 ± 0.011	0.035 ± 0.019	312.04 ± 1.59	312.91 ± 1.84	dry
22/11	10.00-10.10	0.031 ± 0.008	0.014 ± 0.003	313.57 ± 3.11	317.66 ± 2.51	dry

PLMR observations were made in a pushbroom configuration at four different altitudes; however, the current study used only the lowest (approximately 190 m above ground level) altitude data in order to obtain a sufficient number of swaths. At this altitude the nominal ground resolution (-3 dB footprint) was 62.5 m at nadir. Observations were made every second at incidence angles of +/-7º, +/-21.5º and +/-38.5º, with the six footprints covering a total swath of approximately 375 m. Observations where the aircraft pitch/roll angle was > 5° were filtered out. More detailed information on PLMR and the flight characteristics can be found in (Panciera *et al.*, 2008).

Thermal infrared temperatures T_{IR} were obtained with a FLIR ThermaCam S60 thermal imager (spectral range 7.5-13 μm), which was also on board the aircraft carrying PLMR. The FLIR had a ~1 m resolution at the lowest altitude flight and obtained T_{IR} using an overall scene emissivity of 0.98, which is a value often used for vegetation in the thermal infrared range. One FLIR image covered approximately the same area as the PLMR swath. For each PLMR swath, only minimum, maximum and average T_{IR} values for the whole swath were used.

A Landsat 5 TM image from October 2005 (spatial resolution 25 m) was used to define seven land cover types (dense forest, open woodland, native grass, bare soil/low LAI, crops, cloud and cloud shadow), based on a combination of supervised and unsupervised classification methods. In the current study, the 'dense forest' and 'open woodland' classes were joined together to define forest areas, while the 'native grass' class was used to define the grassland areas (cf. figure 5-1).

Ground measurements of the top 5 cm soil moisture content were taken using a portable Stevens Water Hydraprobe® sensor. A site-specific calibration of this sensor against gravimetric samples in the field and laboratory has indicated that the data are accurate to within ± 0.033 m^3m^{-3} (Merlin *et al.*, 2007). Approximately 10-15 measurements were taken at random throughout the forest area per day and approximately 60-100 throughout the grassland areas, although these were

concentrated in the south-west part of the farm. These measurements were part of the 'farm-scale' sampling (cf. Panciera *et al.*, 2008) done at Roscommon. All available data points within the current study area (§5.2.1) were taken into account, irrespective of the resolution grid they belonged to.
Finally, field measurements of temperature were done at two fixed locations on Roscommon farm: one in a grassland area and one in the forest. Soil temperatures at the grassland location were obtained at 1 cm depth with Unidata 6507A/10 sensor, and (for 22nd Nov. only) at 2.5 cm depth with a T107 sensor, every 20 minutes. At the fixed forest location, temperatures were obtained every 10 minutes from thermocouples installed at 2 cm depth in the soil, on the soil surface, 2 cm within the tree trunk at breast height, and at 5m and 7.5 m in the canopy.

5.3 Methods

5.3.1 L-MEB

The radiative transfer model used was the L-band Microwave Emission of the Biosphere (L-MEB) model (Wigneron *et al.*, 2007), which forms the base of the SMOS Level 2 Soil Moisture Algorithm. The main L-MEB equation for a vegetation-covered soil is based on a simplified zero-order radiative transfer approach of the 'τ-ω' type (Kirdiashev *et al.*, 1979; Mo *et al.*, 1982), as shown in equation 5-1:

$$T_B^{P,\theta} = T_S \cdot \left(1 - R_S^{P,\theta}\right) \cdot \gamma^{P,\theta} + \left(1 - \omega^P\right) \cdot \left(1 - \gamma^{P,\theta}\right) \cdot T_C \cdot \left(1 + R_S^{P,\theta} \cdot \gamma^{P,\theta}\right) + R_S^{P,\theta} \cdot T_{B,sky} \cdot \left(\gamma^{P,\theta}\right)^2 \quad (5\text{-}1)$$

The respective terms describe the upwelling ground radiation, the combination of up- and downwelling canopy radiation, and the sky radiation reflected by the ground surface. The sky radiation reflected by the canopy is neglected, as is multiple scattering between the ground and the canopy. The parameters T_S and T_C are the physical temperatures of the soil and vegetation canopy, respectively. The vegetation canopy can consist of either grass or forest, indicated by the respective subscripts 'G' and 'F' from here onwards. The sky brightness temperature $T_{B,sky}$ is calculated according to the method outlined in (Pellarin *et al.*, 2003a). The variable ω^P (P = H or V polarization) is the single scattering albedo of the vegetation layer and the variable $\gamma^{P,\theta}$ (θ = observation angle) describes the transmissivity of the vegetation layer, which is related to vegetation optical depth $\tau^{P,\theta}$ according to:

$$\gamma^{P,\theta} = \exp\left(-\tau^{P,\theta} / \cos\theta\right) \quad (5\text{-}2)$$

Dividing the optical depth by the cosine corrects for the difference in physical pathway length through the canopy layer at different angles, but does not take into account the effects of canopy anisotropy. In the L-MEB model, an extra parameter (tt^P) has been introduced to account for such remaining angular effects. The relation between canopy anisotropy (i.e. structure) effects at V and H polarization is expressed by rtt = tt^V / tt^H. The correction using tt^P results in τ_{NAD}, with the subscript 'NAD' denoting theoretical nadir values:

$$\tau^{P,\theta} = \tau_{NAD}\left(\sin^2(\theta) \cdot tt^P + \cos^2(\theta)\right) \quad (5\text{-}3)$$

The reflectivity $R_S^{P,\theta}$ of a rough soil is obtained with a semi-empirical approach combining the Fresnel equations with a roughness correction based on the approach in (Wang and Choudhury, 1981):

$$R_S^{P,\theta} = \left[(1-Q_R)\cdot R^{*H,\theta}_S + Q_R \cdot R^{*V,\theta}_S\right]\cdot \exp\left(-H_R \cdot \cos^{N_R^P}(\theta)\right) \quad (5\text{-}4)$$

In this equation, $R^{*P,\theta}_S$ is the smooth soil reflectivity calculated from the Dobson dielectric mixing model (Dobson *et al.*, 1985) and the Fresnel equations. H_R and N_R^P are parameters describing the soil effective (topographic and dielectric) roughness and the angular dependency of this roughness, respectively. The parameter Q_R describes polarization mixing and is set to 0 in L-MEB.
An overview of default parameter values for L-MEB is given in table 5-2a, together with the relevant references.

Table 5-2a: Default values used as input in L-MEB for non-retrieved (i.e. 'fixed') parameters.

Parameter	***Default value***	***Reference***
tt_F^P	1	Kerr *et al.*, 2007
tt_G^P	1	"
$H_{R,F}$	0.5	"
$H_{R,G}$	0.4	Saleh *et al.*, 2009
N_R^P	1	Wigneron *et al.*, 2007
Q_R	0	"

Table 5-2b: Initial values used in L-MEB for retrieved parameters.

Parameter	***Initial value***	***Reference***
$\tau_{NAD,F}$	0.45	Grant *et al.*, 2009
$\tau_{NAD,G}$	0.14	Saleh *et al.*, 2007
ω_F^P	0.087	Della Vecchia *et al.*, 2006b
ω_G^P	0.05	Saleh *et al.*, 2007
SM	0.15	-

In this study, an extra (polarization-independent) parameter, denoted β, was introduced in the model to correct for uncertainties resulting from the lack of detailed information on soil emission properties (e.g. field measurements of *SM*, percentages sand and clay, and roughness) and the possibly imperfect choice of dielectric mixing model. To this end, the value of rough soil reflectivity calculated in L-MEB was multiplied by β:

$$R^{P,\theta}_{S,corr} = R^{P,\theta}_S \cdot \beta \quad (5\text{-}5)$$

The introduction of this 'correction parameter' β allows the assumption of a correct roughness value in the *SM* retrievals, as will be discussed in more detail in the following paragraph (§5.3.2).

5.3.2 Retrievals

As stated in §5.2.2, dual-polarized PLMR observations were made at incidence angles of +/-7º, +/-21.5º and +/-38.5º, the six angular footprints together forming one swath.

The assumption was made that, within one swath, all forest-covered parts were homogeneous (i.e. they had the same physical properties), and the same for the grass-covered parts. In some cases angular footprints were missing, therefore only swaths containing more than 2 angular footprints were selected for the retrievals, giving a minimum of 4 and a maximum of 12 observations per swath (i.e. 2 polarizations and 2-6 angles).
The retrieval procedure for L-MEB is based on the minimization of the cost function *CF* shown in equation 5-6:

$$CF = \frac{\sum_{1}^{N}\left(T_{\mathrm{B}}^{\circ} - T_{\mathrm{B}}\right)^2}{\sigma_{T_{\mathrm{B}}}^{\ 2}} + \sum_{i=1}^{n}\frac{\sum_{1}^{N}\left(p_i - p_i^{\mathrm{ini}}\right)^2}{\sigma_{p_i}^{\ 2}} \qquad (5\text{-}6)$$

The error computed by this cost function represents the sum of the squared differences in observed and simulated brightness temperatures $(T_{\mathrm{B}}^{\circ} - T_{\mathrm{B}})^2$ plus the squared differences in retrieved and initial parameter values $(p_i - p_i^{\mathrm{ini}})^2$ for N observations and n parameters. The parameters $\sigma_{T_{\mathrm{B}}}^{\ 2}$ and $\sigma_{p_i}^{\ 2}$ are the corresponding variances, and allow for the possibility of constraining parameters. However, no constraints were used in the current study (i.e. large values of $\sigma_{p_i}^{\ 2}$ were used) and all retrievals were tested for model convergence. Initial values for retrieved parameters are given together with the relevant references in table 5-2b.

5.3.2.1 Methodology

First, retrievals over homogeneous swaths were done with field measurements of soil moisture as input, in order to obtain site-specific values of the main L-MEB parameters. Then, retrievals of soil moisture and optical depth were performed over heterogeneous swaths. In both cases it was assumed that physical footprint temperatures T_{S} and T_{C} were known, which is also the assumption of the SMOS processor. Non-retrieved parameters were fixed to the default values given in table 5-2.

5.3.2.2 Homogeneous swaths

The retrievals over homogeneous swaths were done per observation day, per flight line. Homogeneous forest and grass swaths within a given flight line were selected and the assumption was made that all areas of a particular vegetation type (grass or forest) within a given flight line were identical. Then, one single retrieval was performed using all the homogeneous forest swaths of a given flight line, and one using all the homogeneous grass swaths. Note that only four of the six flight lines covered forest areas (cf. fig.5-1). The choice to do the retrievals per flight line rather than for the whole area at once was made in order to obtain a better insight into the spatial variability of the parameters and the errors in their retrieval.
Input values of *SM* were taken from the available field measurements. Swath *SM* was calculated as follows: if a PLMR swath contained Hydraprobe point measurements, the *SM* value for that swath was calculated by taking the average of the ground measurements. However, a majority of the swaths, especially in the forest areas, did not contain any Hydraprobe measurements. In these cases, an ‘observed’ soil moisture

for the swath was calculated as $SM_{swath} = \alpha \cdot \overline{SM_F} + (1-\alpha) \cdot \overline{SM_G}$, with $\overline{SM_F}$ and $\overline{SM_G}$ indicating average forest and grassland soil moisture, respectively. These averages (cf. table 5-1) were calculated from all Hydraprobe *SM* measurements in the relevant homogeneous swaths (forest or grassland). An estimate of the errors involved in using the area-averages rather than having exact swath values of *SM* is given by the standard deviations of $\overline{SM_F}$ and $\overline{SM_G}$ in table 5-1, which are rather low.

Each of the parameters H_R, N_R^P and tt^P was fixed rather than included in the retrievals because the latter option systematically resulted in model instability, i.e. bad convergence, when tested for each parameter separately. Therefore, the actually retrieved parameters over homogeneous swaths were τ_{NAD}, ω^H, ω^V and β.

By introducing the parameter β in the model (§5.3.1), all errors related to soil emission which can influence retrieval results will be taken into account by β rather than by H_R, which would be the case if the retrievals were performed without β and including H_R. The advantage of this approach becomes apparent in the next step when *SM* is retrieved. Although a date-specific relationship remains between *SM* and β, the retrieved values of *SM* are at least not directly influenced by erroneous values of H_R. The errors in the retrieved values of *SM* will therefore give a better idea of the actual retrieval errors involved, rather than merely being a reflection of errors in the previously retrieved H_R. In other words, the inclusion of the correction parameter β allows the assumption of a correct roughness value in the *SM* retrievals. Indirectly, the parameter β might also partly correct for errors in soil temperature.

5.3.2.3 Heterogeneous swaths

Retrievals over heterogeneous swaths were performed using the *a priori* information on land cover fractions obtained from the land use map (§5.2.2). In the case of heterogeneous swaths, two modelling approaches were tested: 1) simultaneous retrieval of swath-effective values of soil moisture and optical depth (SM_{swath} and $\tau_{NAD,swath}$), and 2) simultaneous retrieval of grassland soil moisture and optical depth values (SM_G and $\tau_{NAD,G}$). These two methods were chosen in order to show two extremes in the range of possible retrieval configurations consisting of combinations of *SM* and τ_{NAD}.

In the first modelling approach, it was assumed that the soil moisture content under grassland and forest areas was equal, i.e. $SM_{swath} = SM_G = SM_F$. While this assumption is incorrect in reality, it should be kept in mind that the soil emission from forested surfaces is assumed to make only a minor contribution to the observed brightness temperature, with the majority of the forest signal coming from the vegetation itself. The errors involved in this approach are therefore less extreme than might be thought.

In this approach, footprint temperature $T_{footprint}$ was approximated by $T_{footprint} = \alpha \cdot T_F + (1 - \alpha) \cdot T_G$. Further model inputs were the default parameters given in table 5-2 and the daily area-averages of ω^H, ω^V and β taken from the retrievals over homogeneous swaths (previous section).

Model inputs for the second approach differed from those for the first approach in the following ways: SM_F was fixed to the area average value, $\tau_{NAD,F}$ was fixed to the average daily value resulting from the retrievals over homogeneous swaths (previous section), and T_F and T_G were separate input values. Although this approach is not likely to be implemented operationally due to the unavailability of initial information on the above parameters, the results are included in this study as a theoretical exploration of the hypothesis that 'the soil moisture of the non-forested part of the

pixel might still be retrieved with the required accuracy if the emission of the forested part of the pixel is modelled correctly enough'. In theory, the first (swath-effective *SM* retrievals) and second (grassland *SM* retrievals) approaches respectively represent worst- and best-case scenario's in terms of the amount of initial available model input. It should be specifically noted that model convergence for this second approach was only achieved if a given swath contained at least two angular footprints containing 100% grass cover. The reason for this is, of course, the fact that in order to retrieve two (here: grassland) parameters, at least two independent (grassland) observations are needed. This fact should be kept in mind for any future studies dealing with within-pixel retrievals. As a result of this restriction, there were less heterogeneous swaths available for analysis in the second approach than in the first.
It should be noted that the antenna pattern was not taken into account during the retrievals over heterogeneous swaths, i.e. simulated T_B values were not weighted by the distribution of intensity within the PLMR footprint. However, the resulting errors are negligible; as an indication, a comparison of weighted and non-weighted values of α on 1st Nov. (N = 1552) resulted in a correlation coefficient of 0.999 and a root mean square error (RMSE) in α of 0.0268. In other words, at most 2.7% of the swath emission was incorrectly calculated by not taking the antenna pattern into account, while a considerable reduction in computing time was won.

5.4 Results and Discussion

5.4.1 Footprint temperature and emissivity

5.4.1.1 Thermodynamic temperatures

Field measurements of temperature were done at one fixed location in the forest and one fixed location in the grassland area (§5.2.2). The field measurements, together with the average T_{IR} value for the corresponding swath, are shown in table 5-3. T_F was approximated by taking the average of soil (2 cm depth), bole and canopy temperatures at the forest location, whereas T_G was approximated by soil temperature at 1 cm depth at the grass location. These approximations were justified by the fact that the field measurements of soil and canopy temperatures were very similar (differences in the order of 1.5 - 3 K). In theory, soil temperatures at depth could also be important in the case of a dry, sandy soil. However, in the NAFE '05 data set the temperature and moisture data necessary for a correct calculation of effective soil temperature were lacking. Given the high spatial variability in temperature, besides the presence of a vegetation cover, neglecting the soil temperature at depth in the overall temperature calculations is not expected to introduce large errors in the resulting patterns of soil moisture retrieval found in this study.

Table 5-3: Thermal infrared (T_{IR}) and field (T) measurements of temperature in a forest (F) and a grassland (G) footprint.

Date	$\mathbf{T_{IR,F}}$ ***[K]***	$\mathbf{T_F}$ ***[K]***	***bias(F)***	$\mathbf{T_{IR,G}}$ ***[K]***	$\mathbf{T_G}$ ***[K]***	***bias(G)***
1st Nov.	302.11	300.85	1.26	302.93	301.05	1.88
8th Nov.	299.57	292.83	6.74	299.28	296.14	3.14
10th Nov.	306.91	296.44	10.47	305.76	299.05	6.71
15th Nov.	309.62	294.25	15.37	313.02	299.05	13.97
22nd Nov.	315.17	294.40	20.77	320.28	301.93	18.35

The bias for forest and grassland in table 5-3 gives the difference between the thermodynamic temperatures derived from thermal infrared observations ($T_{IR,F}$ and $T_{IR,G}$) and those derived from field measurements (T_F and T_G). It can be seen that in the wettest conditions (1st Nov.), T_F and T_G were very similar at the time of flight. In drier conditions, T_G was generally higher than T_F. Furthermore, in drier conditions the T_{IR}-derived values clearly start to overestimate those derived from field measurements quite substantially, mainly due to the difference in sampling depth between the two methods. Table 5-3 shows that, for both vegetation types, this overestimation (i.e. the bias) increases almost linearly with time. Besides resulting from the difference in sampling depth, the discrepancies are also partly instrumental in origin. In order to correct for both effects, the thermodynamic temperature ($T_{footprint}$) of a footprint with a given forest fraction α was calculated as in equation 5-7, using the bias(F) and bias(G) of the observation day in question.

$$T_{footprint} = \alpha \cdot \left(T_{IR,F} - bias(F)\right) + \left(1-\alpha\right) \cdot \left(T_{IR,G} - bias(G)\right) \qquad (5\text{-}7)$$

5.4.1.2 Emissivity

Figure 5-2 gives examples of the angular emissivities of homogeneous grassland and forest footprints, respectively, using observations made on 1st and 22nd November, under 'wet' and 'dry' conditions respectively.
Grass and forest emissivities e_G and e_F were calculated according to the Rayleigh-Jeans approximation (T_B - $T_{B,sky}$) / ($T_{footprint}$ - $T_{B,sky}$) (Ulaby *et al.*, 1986) and plotted against incidence angle θ. The figures show that, as expected, e_G is slightly lower than e_F , and e_G shows greater angular variation than e_F. The figures are in agreement with theory, showing increasing and decreasing emissivities with θ for V and H polarization, respectively. This implies that the (polarised) soil emission is only partly attenuated by the vegetation. The difference in emissivity between wet and dry conditions shows that there is a certain sensitivity of above-canopy brightness temperature to changing moisture conditions for open Eucalypt forests. The fact that there is less scatter present in the 'dry' data is most probably due to the inherently high emission from a dry soil, in which case the relative influence of vegetation and surface roughness on the signal becomes smaller, as suggested earlier by (Crosson *et al.*, 2005). Also, soil moisture usually becomes more homogeneous in dry conditions. The few outliers in the data are assumed to be the result of wrongly classified landuse for those footprints.
It was found that in wet conditions the range in brightness temperature was much larger than the range in thermodynamic temperature, indicating a large spatial variation and large effect of non-temperature variables such as canopy parameters, soil moisture and/or effective surface roughness. For dry conditions, the variation in these surface characteristics is clearly smaller and thermodynamic temperature may play a more important role. These conclusions were found to be valid for any given α, i.e. for both homogeneous and heterogeneous footprints.

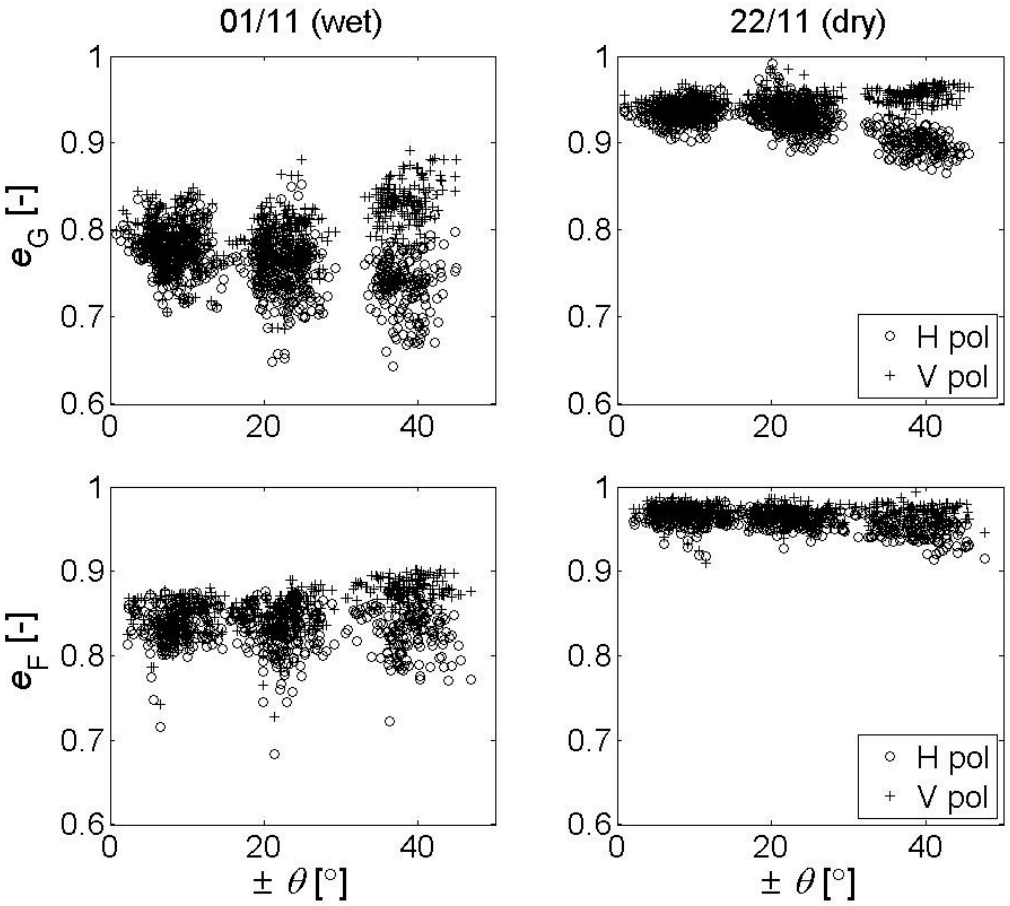

Figure 5-2: Example of angular emissivities of (top) 100% grassland footprints (e_G) and (bottom) 100% forest footprints (e_F) under 'wet' (left) and 'dry' (right) conditions on 1st and 22nd Nov. respectively. Corresponding area-average soil moisture values are $SM_G \approx 0.28$ m^3m^{-3} and $SM_F \approx 0.18$ m^3m^{-3} (wet) and $SM_G \approx 0.03$ m^3m^{-3} and $SM_F \approx 0.01$ m^3m^{-3} (dry).

5.4.2 Retrievals

5.4.2.1 Retrievals from homogeneous swaths

The parameter values retrieved from homogeneous swaths are shown in tables 5-4a (forest) and 4b (grass). There are differences in parameter values between flight lines, owing to the fact that in reality the vegetation cover is of course not homogeneous, however, although the large spatial variability is visible, the general orders of magnitude remain fairly consistent. The single scattering albedo for H-pol is systematically somewhat higher than for V-pol, while β varies somewhat between flight days, as expected. Still, temporal interpretation of the parameter values, i.e. between flight days, might not give a realistic impression because of the daily corrections of temperature (§5.4.1) and β (§5.3.2), which have been performed separately for each flight day as explained earlier. Therefore the main focus of this study is on spatial variation.

Table 5-4a: Retrieved parameter values for homogeneous forest swaths (N = number of swaths)

Date	**flightline**	N	τ_{NAD}	ω^{H}	ω^{V}	β	**RMSE(T_B) [K]**
1/11	1	103	0.47	0.02	0.02	2.66	7.688
	2	161	0.35	0.06	0.05	1.83	6.321
	3	153	0.36	0.04	0.03	1.93	6.911
	4	130	0.45	0.04	0.03	2.31	5.894
8/11	1	107	0.36	0.00	-0.01	1.89	6.550
	2	185	0.38	-0.01	-0.03	1.93	6.795
	3	171	0.46	0.01	-0.00	2.27	6.720
	4	120	0.47	-0.01	-0.02	2.33	5.328
10/11	1	125	0.63	0.04	0.04	3.76	6.127
	2	119	0.48	0.04	0.04	2.58	6.704
	3	155	0.54	0.06	0.05	2.86	5.592
	4	97	0.52	0.03	0.04	2.90	4.911
15/11	1	93	0.50	0.05	0.04	1.83	3.289
	2	103	0.46	0.05	0.04	1.67	4.760
	3	169	0.43	0.05	0.04	1.54	4.668
	4	95	0.52	0.05	0.04	1.79	3.245
22/11	1	88	0.66	0.04	0.03	2.46	3.977
	2	164	0.35	0.08	0.06	1.06	4.502
	3	144	0.78	0.03	0.02	3.34	3.986
	4	128	0.76	0.03	0.03	3.19	4.204

The negative values of forest single scattering albedo on 8th November could be due to the fact that rainfall occurred just before the flights. This effect is, however, not seen in the grass swaths, where the shorter vegetation might have resulted in the precipitation already having dried up. In further analyses, daily averages of ω^{H}_{F} and ω^{V}_{F} for 8th November were therefore estimated by taking the averages of the 1st and 10th November, i.e. the observation days before and after Nov. 8th. Both forests and grass show high retrieved values of either τ_{NAD} (especially) or ω^{P} on 22nd of November, the reason for which is not well understood. The values of beta are reasonable given the low reflectivity of a sandy soil and the physical condition $0 < R_{S,corr}{}^{P,\theta} \cdot \beta < 1$ was valid in all cases.

Table 5-4b: Retrieved parameter values for homogeneous grass swaths (*N* = number of swaths)

Date	**flightline**	***N***	τ_{NAD}	ω^{H}	ω^{V}	β	**RMSE(T_B) [K]**
1/11	1	198	0.39	0.02	0.02	1.88	6.368
	2	184	0.36	0.05	0.04	1.67	6.442
	3	106	0.34	0.05	0.04	1.54	7.687
	4	95	0.23	0.05	0.03	1.26	7.320
	5	100	0.23	0.14	0.11	1.20	9.681
	6	68	0.28	0.09	0.07	1.32	9.361
8/11	1	215	0.39	0.04	0.03	1.58	5.242
	2	165	0.34	0.05	0.03	1.41	6.090
	3	134	0.23	0.05	0.03	1.16	7.206
	4	122	0.28	0.02	0.01	1.42	9.061
	5	110	0.26	0.06	0.04	1.24	8.166
	6	96	0.23	0.05	0.04	1.13	7.588
10/11	1	205	0.58	0.06	0.06	2.76	4.310
	2	165	0.52	0.06	0.06	2.36	5.371
	3	140	0.42	0.09	0.09	1.93	6.649
	4	101	0.41	0.11	0.10	1.93	7.645
	5	64	0.21	0.16	0.15	1.26	6.703
	6	48	0.30	0.10	0.10	1.50	7.509
15/11	1	247	0.41	0.06	0.05	1.21	4.179
	2	159	0.37	0.09	0.08	0.96	4.136
	3	120	0.59	0.06	0.05	1.59	4.540
	4	113	0.38	0.08	0.07	1.13	5.758
	5	127	0.31	0.08	0.07	0.93	4.585
	6	45	0.48	0.09	0.07	1.02	4.285
22/11	1	215	0.26	0.08	0.08	0.97	4.382
	2	162	0.65	0.05	0.04	2.12	4.402
	3	113	0.77	0.05	0.04	2.51	3.992
	4	108	0.62	0.06	0.05	1.53	4.255
	5	110	0.72	0.05	0.04	2.29	4.184
	6	51	0.22	0.09	0.08	0.88	4.259

5.4.2.2 Retrievals from heterogeneous swaths

In order to give an idea of the distribution of forest fraction α per swath, the histogram in figure 5-3 shows an example for the 1st November. Note that only heterogeneous swaths ($0.01 < \alpha < 0.99$) have been included in the figure. The distribution varies slightly per observation day, but the overall pattern is very similar in all cases. The total number of 87 heterogeneous swaths was relatively small, as the forested parts of Roscommon were not very extensive. In comparison, there were 185 homogeneous grass swaths ($\alpha < 0.01$) and 98 homogeneous forest swaths for this day.

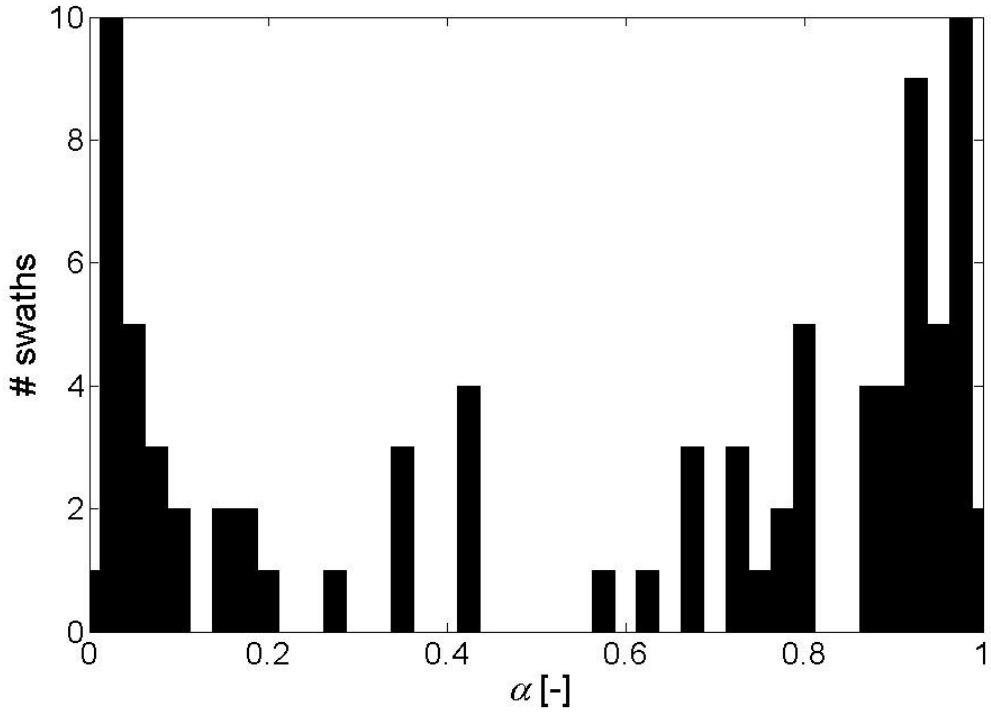

Figure 5-3: Example of the distribution of forest fraction α for 375 m by 62.5 m heterogeneous swaths ($0.01 < \alpha < 0.99$) in the Roscommon farm area on 1st November.

The results of the retrievals from heterogeneous swaths ($0.01 \leq \alpha \leq 0.99$) are shown in tables 5-5a and 5-5b, and figure 5-4.

Table 5-5a shows the results for the first retrieval approach, i.e. simultaneous retrieval of SM_{swath} and $\tau_{NAD,swath}$. It can be seen that, except on the driest day, the average retrieved SM_{swath} slightly overestimates the average observed value, which was also found for pixels in (Loew, 2008). On the other hand, the high standard deviation of the retrievals seems to reflect the actual spatial variability, which is much higher than that of the observations. The field observed standard deviation, however, is based on only a few measurements, insufficient to characterize the actual spatial variability. It should also be realized that, in this case, the retrieved values refer to 'swath-effective' values of which the exact physical meaning is difficult to identify because of non-linear mixing effects, and because the soil properties between the forest and the grass soils are different.

As indicated in the study by Loew (2008), it is important to observe the bias in *SM* together with the RMSE, as a low RMSE can still be coupled to a high bias. In the current study it should be kept in mind that, due to the limited number of field observations, many of the observed values of SM_{swath} are based on α-weighted area-averages and great caution should thus be taken with the interpretation of RMSE(SM_{swath}) and bias(SM_{swath}).

The retrieved values of $\tau_{NAD,swath}$ are slightly higher than expectations based on tables 5-4a and 5-4b, an effect which will be discussed later in more detail in the context of figure 5-4. Finally, the values of RMSE(T_B) indicate that, overall, the model is able to match T_B simulations to observations reasonably well, although this of course becomes more difficult with increasing wetness, when soil and vegetation emission become increasingly opposed.

Table 5-5a: Results of SM_{swath} and $\tau_{NAD,swath}$ (method 1) retrievals from heterogeneous swaths ($0.01 \leq \alpha \leq 0.99$). N = number of swaths, with number of removed outliers in parentheses. Retrieved and observed values indicated by 'ret' and 'obs', respectively. Values shown are average +/- standard deviation swath soil moisture (SM_{swath} [m^3m^{-3}]), root mean square error (RMSE) and bias between retrieved and observed SM_{swath}, average +/- standard deviation swath optical depth ($\tau_{NAD,swath}$ [-]), and the RMSE in brightness temperature (T_B [K]).

Date	**N**	**SM_{swath} *(ret)***	**SM_{swath} *(obs)***	***RMSE* (SM_{swath})**	***bias* (SM_{swath})**	**$\tau_{NAD,swath}$ *(ret)***	***RMSE*(T_B)**
1/11	81 (6)	0.27 ± 0.12	0.23 ± 0.05	0.13	0.04	0.47 ± 0.20	3.798
8/11	97 (12)	0.17 ± 0.12	0.17 ± 0.03	0.10	0.01	0.50 ± 0.21	4.623
10/11	82 (3)	0.09 ± 0.09	0.07 ± 0.02	0.09	0.02	0.68 ± 0.28	3.007
15/11	69 (7)	0.07 ± 0.06	0.05 ± 0.01	0.07	0.02	0.68 ± 0.37	2.013
22/11	80 (3)	0.01 ± 0.03	0.02 ± 0.01	0.03	-0.01	0.73 ± 0.29	1.611

The results for 1st November (wet) and 22nd November (dry) are shown in more detail in figure 5-4 (note that y-axis scales differ) using the first retrieval approach, i.e. simultaneous retrieval of SM_{swath} and $\tau_{NAD,swath}$. Results are presented as averages ± 75th percentile for 0.2 increments in α. The choice to use percentiles instead of standard deviation was based on the obviously skewed distribution of the results. If no error bars are present in the figure, the number of swaths in that class was too small to allow it. Although figure 5-4 does also reflect the large amount of spatial variability in the data, due to the variability in field conditions and the many uncertainties involved in the analysis, the general patterns are clear. The retrieved values of $\tau_{NAD,swath}$ show, as expected, a generally increasing pattern with increasing forest fraction α. Excepting the outlier on 22nd Nov., the values of $\tau_{NAD,swath}$ for low α are of the same order of magnitude as those found for grassland areas in table 5-4b. However, the values of $\tau_{NAD,swath}$ for higher α are higher than would be expected according to table 5-4a and it thus appears that increased forest fraction does influence retrievals of optical depth by resulting in an increased overestimation.

The retrieved values of SM_{swath} in the right-hand images show maximum values of retrieved SM_{swath} at intermediate α. Even though these plots do not show the actual errors in retrieved *SM* (because, as said previously, values of RMSE(SM_{swath}) are not completely reliable), an idea of the errors involved can be derived from subtracting the area-average observed *SM* (the middle of the two solid lines) from the retrieved values. In this case, an approximately convex curve remains. Such a shape was also found in a modelling study by Van de Griend *et al.* (2003) for retrievals over pixels containing a mix of bare soil ($\tau = 0$) and vegetation with $\tau = 0.4$. That study also found a flatter curve in drier conditions, as seen here in figure 5-4. However, contrary to the current study, the modelling study assumed that no *a priori* knowledge of α was available. Another modelling study by Loew (2008) which did assume *a priori* knowledge of α to be available, shows a result for mixed forest/grassland pixels which could be interpreted as a similar curved shape, although it is not conclusive as forest fractions above 65% are sparse. However, that study assumed higher values of forest optical depth (τ = 0.8-1) than the current study does. It seems that the mix of optical depth values, i.e. the contrast present between forested and non-forested areas,

determines the shape of the curve, whereas the un-/availability of *a priori* knowledge of α mainly influences the absolute error values. Modelling studies by Van de Griend *et al*. (2003 and 2004) both with and without *a priori* knowledge of α, show that when higher values of τ are introduced in the mixed pixel, the maximum of the error curve shifts towards higher values of α. It is therefore too general a statement to simply say that if α is known *a priori*, all pixels containing more than 50% forest fraction will give errors in retrieved *SM* greater than 0.04 m^3m^{-3}. The value of α at which this 0.04 m^3m^{-3} boundary will be crossed (if it is crossed) will differ according to the different land use optical depths within the pixel and their values relative to each other. This makes sense, as optical depth and soil moisture are indirectly linked in the tau-omega model. Unfortunately, the consequence for SMOS is that it will be extremely difficult to find reliable flags for the maximum allowed forest fraction in mixed pixels.

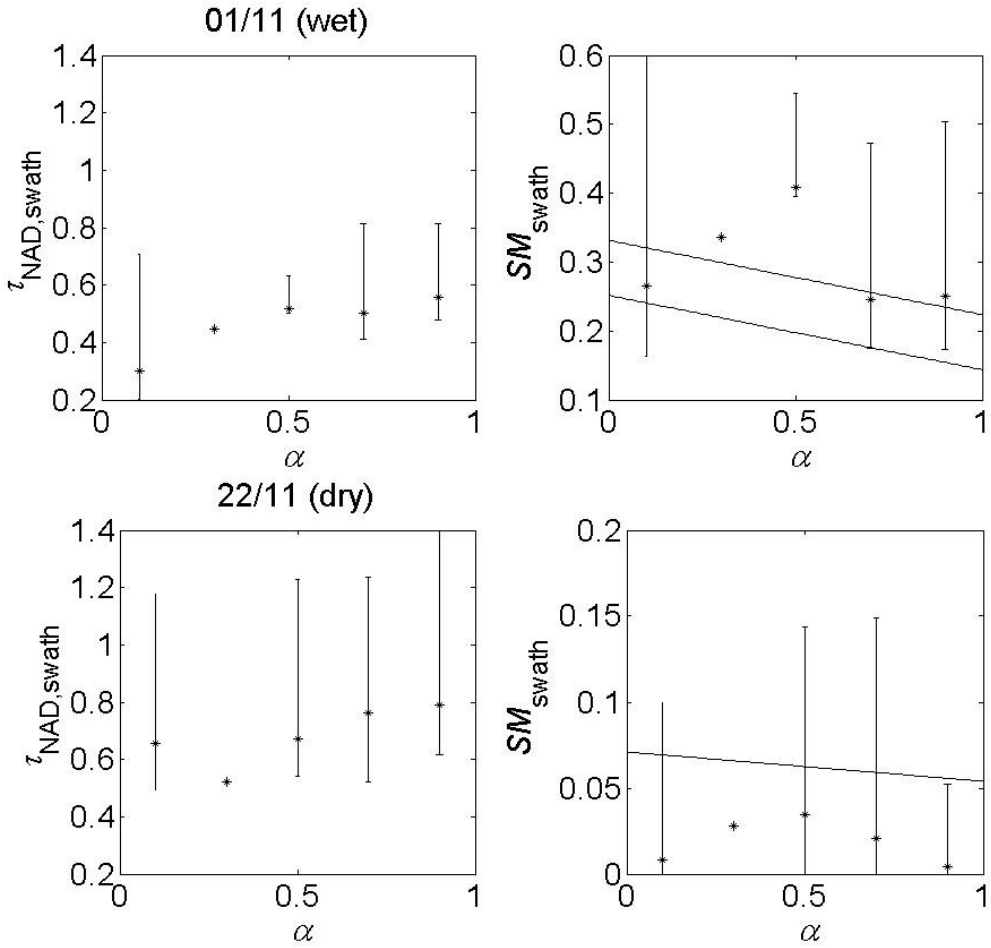

Figure 5-4: Retrieved 'swath-effective' values of soil moisture (SM_{swath} [m^3m^{-3}]) and optical depth ($\tau_{NAD,swath}$ [-]) plotted against forest fraction α for heterogeneous swaths ($0.01 \leq \alpha \leq 0.99$) on (top) 1st November (wet) and (bottom) 22nd November (dry). Left: average and 75th percentile of retrieved $\tau_{NAD,swath}$. Right: average and 75th percentile of retrieved SM_{swath}. Solid lines indicate area-average $SM\left(=\alpha\cdot\overline{SM_F}+(1-\alpha)\cdot\overline{SM_G}\right)$ ± 0.04 m^3m^{-3} (with $\overline{SM_F}$ and $\overline{SM_G}$ from table 5-1). NB. Note different ranges of y-axes in right-hand plots.

Table 5-5b shows the results for the second retrieval approach, i.e. simultaneous retrieval of SM_G and $\tau_{NAD,G}$ while the emission of the forested part of the swath is modelled with parameter values as retrieved from the homogenous forest parts. The table shows that in dry conditions the results are generally very reasonable. The results will, at least partly, reflect a compensation for the forward modelled emission of the forested part of the swath. Retrieved values of $\tau_{NAD,G}$ are generally close to observed values (taken from table 5-4b), except for 22nd Nov. which had very high values of 'observed' $\tau_{NAD,G}$ (table 5-4b). No relationship can be seen between moisture conditions and the degree of over- or underestimation in $\tau_{NAD,G}$. As also said for table 5-5a, the values of RMSE(SM_G) and bias(SM_G) should be taken with extreme caution. The study by Loew (2008) found that the bias(*SM*) increases with increasing dryness, therefore the low error values for dry conditions found in the current study should not lead straight to the conclusion that *SM* retrievals over forested areas are reliable enough as long as the moisture content is low. This issue is important for SMOS and deserves further attention in future.

Table 5-5b: Results of SM_G and $\tau_{NAD,G}$ (method 2) retrievals from heterogeneous swaths ($0.01 \leq \alpha \leq 0.66$). *N* = number of swaths, with number of removed outliers in parentheses. Retrieved and observed values indicated by 'ret' and 'obs', respectively. Values shown are average +/- standard deviation grassland soil moisture (SM_G [m^3m^{-3}]), root mean square error (RMSE) and bias between retrieved and observed SM_G, average +/- standard deviation grassland optical depth ($\tau_{NAD,G}$ [-]; observed values from table 5-4b), and the RMSE in brightness temperature (T_B [K]).

Date	**N**	**SM_G *(ret)***	**SM_G *(obs)***	***RMSE* (SM)**	***bias* (SM)**	**$\tau_{NAD,G}$ *(ret)***	**$\tau_{NAD,G}$ *(obs)***	***RMSE* (T_B)**
1/11	22 (8)	0.24 ± 0.13	0.29 ± 0.01	0.13	-0.05	0.26 ± 0.15	0.30 ± 0.07	3.776
8/11	35 (5)	0.24 ± 0.15	0.21 ± 0.01	0.15	0.03	0.33 ± 0.19	0.29 ± 0.07	3.582
10/11	26 (5)	0.09 ± 0.06	0.09 ± 0.01	0.06	-0.00	0.44 ± 0.20	0.41 ± 0.14	3.383
15/11	18 (8)	0.05 ± 0.03	0.07 ± 0.01	0.03	-0.02	0.39 ± 0.28	0.42 ± 0.10	1.999
22/11	17 (10)	0.02 ± 0.02	0.03 ± 0.01	0.02	-0.01	0.35 ± 0.32	0.54 ± 0.24	1.272

Values and patterns of RMSE(T_B) are very similar to those in table 5-5a, therefore it can be concluded that the model does not have more difficulty in fitting simulations to observations when the forest part of the swath emission is known from forward modelling.

It should be noted here that, as explained in §5.3.2, this second approach only works for swaths with more than 2 angular footprints containing 100% grass. As in this study a maximum of 6 angles was observed for each swath, the consequence of this requirement is that at least 33% of the swath will cover grassland. Therefore, this analysis only includes swaths with $\alpha < 0.66$ and a possible heightened influence of high forest fraction is thus not taken into account.

Due to this limited range of α and, as a result, the low number of suitable swaths, a figure similar to figure 5-4 was not drawn up for this retrieval approach (retrieval of SM_G and $\tau_{NAD,G}$).

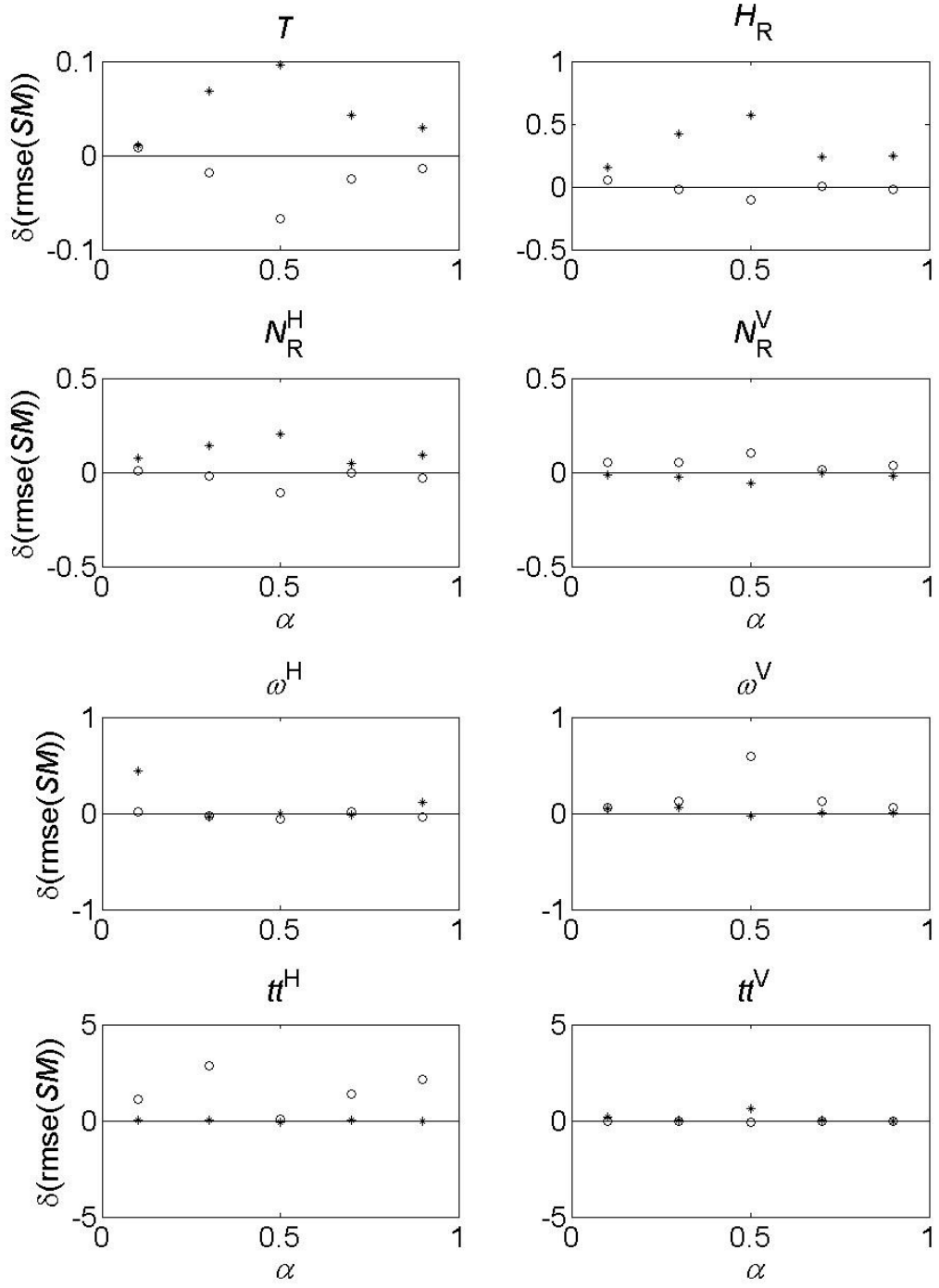

Figure 5-5: Results of superimposing errors on each of the fixed L-MEB parameters for 1/11 (wet conditions), then simultaneously retrieving SM_{swath} and $\tau_{NAD,swath}$ for heterogeneous swaths ($0.01 \leq \alpha \leq 0.99$) only. The vertical axis shows the difference (δ [m^3m^{-3}]) between the mean RMSE(SM_{swath}) found with and without (cf. table 5-5a) superimposed errors. Legend per focus parameter: T: 'o' = default -5 K, '*' = default + 5 K; H_R: 'o' = H_R= 0, '*' = default + 0.5; N_R^P: 'o' = default -1, '*' = default + 1; ω^P: 'o' = ω^P = 0, '*' = default + 0.1; tt^P: 'o' = default -0.5, 'Δ' = default + 0.5. All non-focus parameters were fixed to default values during the retrievals. NB. Y-axes differ in range.

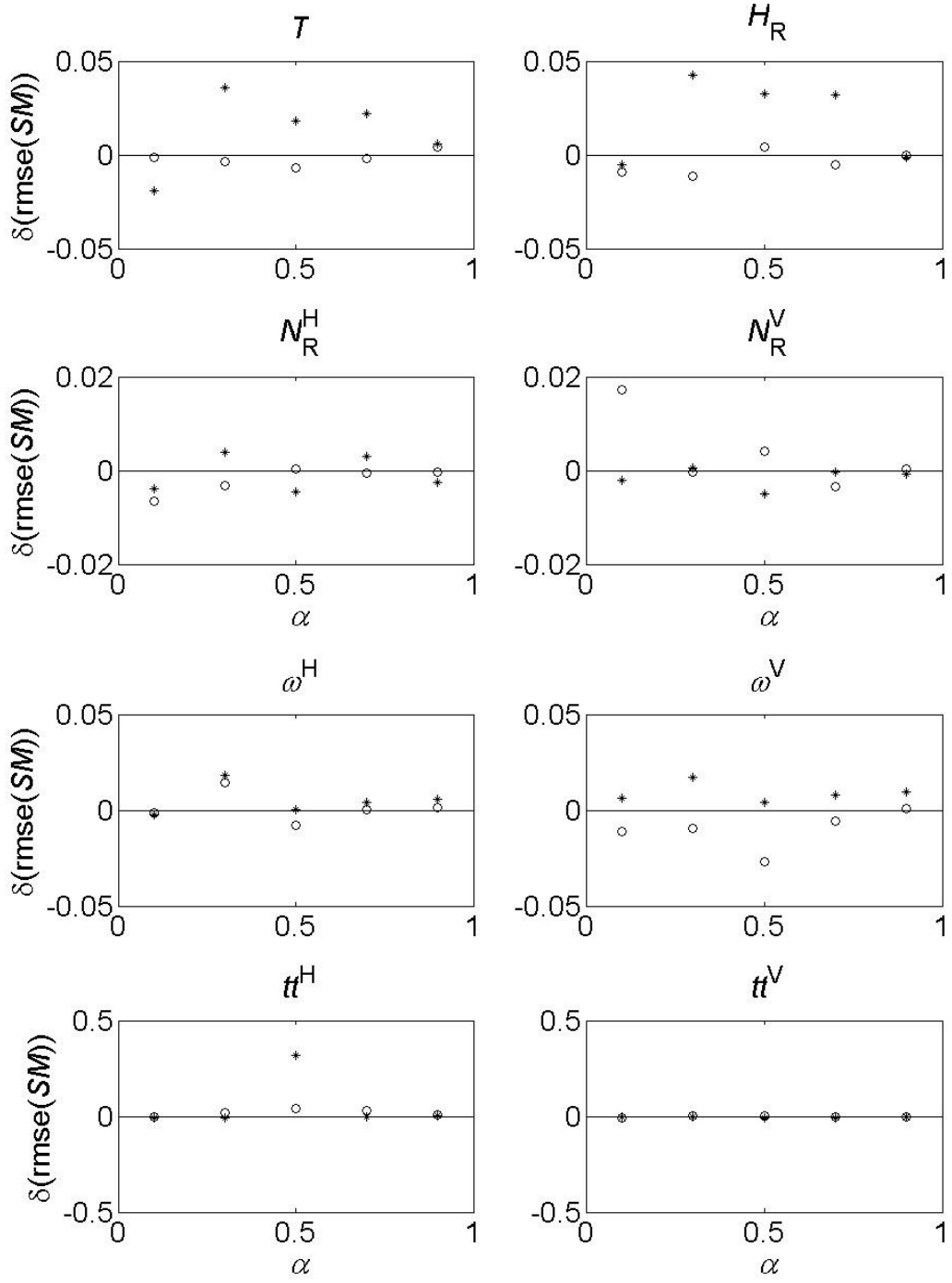

Figure 5-6: As for figure 5-5, but for 22/11 (dry conditions).

5.4.3 Effects of errors in L-MEB parameter values

In order to determine the effect of each fixed model parameter on RMSE(*SM*), a sensitivity analysis was performed. Simultaneous retrievals of SM_{swath} and $\tau_{NAD,swath}$ were performed for heterogeneous swaths ($0.01 \leq \alpha \leq 0.99$), each time with errors superimposed on one of the fixed L-MEB parameters, for 1st November (wet) and 22nd November (dry).

The resulting difference δ(RMSE(SM_{swath})) between the mean RMSE(SM_{swath}) values found for the 'error' and the 'default' situations is plotted *vs*. α for each parameter in figures 5-5 (wet) and 5-6 (dry), with values of RMSE(SM_{swath}) averaged per 0.2 increment in α. Note that the scales on the y-axis can differ per parameter. The specific values of each superimposed error are shown in the figure caption.
Figures 5-5 and 5-6 show that the effects of superimposed errors are much more obvious in wet conditions than in dry. In each plot, the difference between two markers indicates, for a given α, the sensitivity of the model to the parameter concerned. In wet conditions (figure 5-5), it can be seen that the effects of temperature T ($T = T_S = T_C$) and the roughness parameters H_R and $N_R^{H,V}$ are greatest in the case of the most highly mixed swaths (i.e. intermediate values of α). The parameters ω^V and tt^V also show the greatest effect on SM retrievals in the case of highly mixed swaths, whereas ω^H shows the most effect in more homogeneous grass or forest areas and tt^H shows no clear relationship with α. It is thus quite possible that the greater errors in retrieved SM_{swath} at intermediate α are caused by non-linear mixing effects of (most of) the model parameters. However, in dry conditions (figure 5-6) the effects of superimposed errors are less clearly concentrated at intermediate values of α. As said previously (§5.4.1.2), in dry conditions the difference between vegetation and soil emission is smaller, therefore it is not surprising that in this case the influence of α on the overall results is also smaller.
Besides the dependence on α, it is obvious that erroneous values of the default L-MEB parameters can lead to high errors in retrieved SM, especially in wet conditions. Given the difficulty of determining several of the L-MEB parameters (e.g. tt^P, H_R and N_R^P) independently, this issue will need attention from the very operational start of SMOS. Ideally, these parameters should be determined at the satellite scale by model inversion using actual SMOS data where possible.

5.5 Summary and Conclusions

The NAFE '05 experimental data set was used to investigate L-MEB soil moisture retrievals over mixed Eucalypt forest/grassland swaths. Airborne L-band observations were selected over swaths with varying fractions of forest cover (0-1), on five separate days with different moisture conditions. The data set was used to study the retrieval of soil moisture from heterogeneous swaths using two different approaches, both based on *a priori* knowledge of forest fraction (α). Model inputs for non-retrieved parameters were either default values taken from the literature or site- and time-specific values obtained from observations of nearby homogeneous swaths gathered during the same flight. Because of the experiment-specific configuration, the swath was used as the basic calculation unit.
In the first retrieval approach, swath-effective values of soil moisture (SM) and swath-effective vegetation optical depth (τ_{NAD}) were simultaneously retrieved using the L-MEB model. In the second approach, soil moisture and optical depth retrievals of the non-forested (i.e. grass) fraction of the swath were performed, while the forest contribution to swath emission was known from forward modelling. This is, to our knowledge, the first study to use experimental data rather than model simulations to specifically investigate the effect of forest cover fraction on soil moisture retrievals.

Because of the large spatial variation within the NAFE '05 experimental site, and the (375 m) resolution of the airborne swaths, a large amount of variation was present in

the observed brightness temperatures. Although the amount of ground measurements was limited and the data set showed a few systematic inconsistencies, some additional calibration steps were performed to limit the consequences of these issues, resulting in a consistent data set suitable for the anticipated study. Given the obvious and well known difficulties and limitations of airborne campaigns, the retrieval results were generally very reasonable.

Concerning the swath-effective retrievals, values of swath-effective soil moisture (SM_{swath}) were slightly overestimated compared to area-averaged *SM* values resulting from field measurements. Retrieved values of $\tau_{NAD,swath}$ showed a general increase with increasing forest fraction (α), as expected, but also an increasing overestimation with increasing forest fraction. Maximum retrieved values of SM_{swath}, and maximum errors in the retrieved values were found at intermediate values of forest fraction. These results are important for the SMOS mission as they indicate the difficulty in flagging upper limits of pixel forest fraction during soil moisture retrievals.

A subsequent sensitivity analysis for all L-MEB parameters showed that, especially in wet conditions, the errors superimposed on the parameter values often also had the greatest effect on retrieved SM_{swath} at intermediate values of forest fraction. Besides this, it was shown that erroneous values of the default L-MEB parameters can lead to high errors in retrieved *SM*, especially in wet conditions. At the SMOS scale, it will therefore be necessary to determine correct parameter values with actual SMOS data and model inversion.

Concerning the retrievals for the non-forested (in this case: grass) swath fractions, SM_G and $\tau_{NAD,G}$ were retrieved simultaneously, with a known forest emission derived from the homogeneous forest swaths in the area. Although these analyses were only valid for the range $0 \leq \alpha \leq 0.6$, retrieved values of SM_G and $\tau_{NAD,G}$ were generally reasonable and close to observed values. The procedure used in this study, which involves retrievals of canopy parameters over homogeneous swaths, followed by retrievals of *SM* and τ_{NAD} over heterogeneous swaths, can also be used when SMOS is operational.

Due to the use of experimental data focussed specifically on forests, the current study is the first to give a realistic idea of the errors and uncertainties involved in soil moisture retrievals from partly forested swaths. This is a relevant contribution to the analysis of heterogeneous pixels in future studies in general, and to studies concerning SMOS calibration and validation in particular.

Chapter 6

Summary and Conclusions

6.1 Background

This PhD research project was conducted as part of the background research for the Soil Moisture and Ocean Salinity (SMOS) mission of the European Space Agency (ESA), due for launch in 2009. The main goal of this study was to obtain an improved understanding of L-band (f = 1.4 GHz, λ = 21 cm) forest emission, in view of (SMOS) soil moisture retrievals from heterogeneous pixels containing fractional forest cover. Accurate soil moisture retrievals underneath homogeneous forest canopies are difficult to obtain due to high attenuation by the thick vegetation layer. However, modelling studies showed that in the case of heterogeneous pixels, under certain conditions it was still possible to retrieve an accurate soil moisture content for the non-forested part of the pixel, if forest emission was modelled correctly. Therefore, more detailed knowledge was needed of forest emission at L-band, including an understanding of the radiative transfer properties of the various forest layers and calibration of the forward model to be used in the SMOS soil moisture retrieval algorithm. Existing knowledge on these subjects was rather limited and almost wholly based on modelling studies. It was therefore especially important to obtain additional information from experimental observations. To this end, L-band radiometric data were obtained from tower measurements at the Bray experimental site in Les Landes forest, France in 2004, 2006 and 2007 (BRAY campaigns), and at the Jülich research site, Germany, in 2004 and 2005 (FOSMEX campaigns). The analyses based on these experimental data were used to better understand forest emission and radiative transfer properties. Airborne L-band data were obtained during the NAFE '05 campaign in South-East Australia in 2005. These data were used to investigate the results of soil moisture retrievals from heterogeneous forest pixels.

6.2 Summary and Conclusions

From July-December 2004 the experimental campaign 'Bray 2004' was conducted in the coniferous forest of Les Landes near Bordeaux, France, using a multi-angle L-band radiometer to observe the above-canopy forest emission at horizontal polarization. At the same time, ground measurements were done of soil and litter moisture content, while precipitation was also permanently monitored. This experiment was performed in order to improve the understanding of the L-band signal behaviour over forested areas for different wetness conditions and viewing angles. The greater part of the horizontally polarized L-band signal was found to be dominated by the influence of physical temperature. Variations in soil and/or litter moisture content were visible in the angular signal and in the above-canopy microwave emission, although the dynamic range of this last effect was very small. This, together with the fact that emissivity values were very high, was hypothesized to be due to the presence of a substantial litter layer. However, decoupling of soil and

litter effects was difficult because of the strong correlation found between soil and litter moisture.

In a calibration exercise of the L-band Microwave Emission of the Biosphere (L-MEB) model, which is the forward model in the SMOS Level 2 Soil Moisture algorithm, using L-band microwave observations over a coniferous (Pine) and a deciduous (mixed/Beech) forest, litter effects were taken into account by using an 'effective' soil roughness parameter resulting from empirical best-fits. The calibration resulted in working values of the main canopy parameters optical depth (τ_{NAD}), single scattering albedo (ω) and structure parameters tt^{H} and tt^{V}, besides the roughness parameters H_R and N_R^P. Using these calibrated values in the forward model resulted in a root mean square error (RMSE) in brightness temperature (T_B) of 2.8 to 3.8 K, depending on data set and polarization, which indicated a good model fit for various moisture conditions. The model parameters showed similar behaviour for both forest types, even though slightly different values were found for each site; notably, coniferous optical depth (0.67) was lower than that of the deciduous site (0.98). A sensitivity study was also conducted for the above parameters, and for temperature, soil moisture and precipitation, to indicate the change in RMSE(T_B) for errors in a given variable. The relationship between canopy optical depth and leaf area index (LAI) was investigated for the deciduous site. Not surprisingly, the correlation was very low, due to the fact that the main contribution to L-band forest emission comes from the branches rather than from the leaves/needles (Ferrazzoli *et al*., 2002). The results found in this study will be integrated in the operational SMOS Level 2 Soil Moisture retrieval algorithm.

Although the average canopy transmissivity in temperate coniferous and deciduous forests was found to be in the order of 0.4-0.5 (see also Guglielmetti *et al*. (2007, 2008)) and the canopy would therefore be expected to transmit a reasonable amount of ground emission, total emission observed above the canopy showed very little variation with varying soil moisture content, as said above. Moist litter present on the forest floor is known to obscure the soil emission and was hypothesized to be responsible for the small sensitivity in above-canopy emission found during Bray 2004. More knowledge on the L-band radiative properties of litter and understory layers was therefore needed to better understand the emission of the whole forest system.
In order to contribute toward this issue, an additional field experiment at the Bray site was conducted in 2007. Radiometric observations were done of the canopy and of different configurations of the forest floor, following sequential stripping of each forest floor layer. In combination with the long-term data set of above-canopy observations from 2004, this resulted in emissivity values of bare soil, soil-litter, soil-litter-grass and soil-litter-grass-canopy configurations for a range of soil and litter moisture values. Calculations involved the use of the Wilheit and L-MEB models, and a modified version of the approach presented by Schwank *et al*. (2008). The sensitivity to soil moisture was found to be substantially suppressed by the presence of a grass understory and litter. This corroborated the low correlation between soil moisture and above-canopy L-band emission. A detailed sensitivity analysis showed the effects of moisture content and litter layer thickness on the thermal sampling depth and emission of a soil-litter forest floor configuration. Several results of recent modelling and laboratory studies were confirmed by this study, which was to our knowledge the first to use *in situ* experimental data in this context.

Finally, airborne L-band data from the Australian National Airborne Field Experiment 2005 (NAFE '05) field campaign were used to investigate the influence of fractional forest cover on soil moisture retrievals from heterogeneous (grass/forest) pixels. This study was, to our knowledge, the first to use experimental data on this subject and was done in view of the upcoming SMOS mission, in order to contribute to calibration/validation studies and the analysis of heterogeneous land surfaces. Because the multi-angle observations were 'contained' in swaths, swaths were used instead of pixels as the basic surface unit in this study. Simultaneous retrievals of soil moisture (*SM*) and vegetation optical depth were done by inversion of the L-MEB zero-order radiative transfer model. This was done for two different retrieval configurations, the first consisting of swath-effective values of *SM* and τ_{NAD} and the second consisting of values of *SM* and τ_{NAD} for the non-forested (i.e. grass) fraction of the swath, with forest emission known from forward modelling. Model inputs for non-retrieved parameters were either default values taken from the literature or site- and time-specific values obtained from observations of nearby homogeneous swaths gathered during the same flight. The main focus of this study was on retrieval behaviour for various soil moisture conditions and forest fractions. Area-averaged retrieval results were generally very reasonable for both retrieval configurations. When retrieving swath-effective values of *SM* and τ_{NAD}, τ_{NAD} showed an increased overestimation with increased forest fraction. Highest retrieved values of *SM* were found at intermediate values of forest fraction. The results indicate the difficulty in flagging upper limits of pixel forest fraction during soil moisture retrievals, besides showing that erroneous parameter values can lead to high errors in retrieved *SM*, especially in wet conditions. This study is the first to give a realistic idea of the errors and uncertainties involved in soil moisture retrievals from partly forested swaths, and as such is expected to contribute to a better understanding of SMOS calibration/validation issues.

To summarize, this study has given some insight into the general applicability, uses and limitations of the L-MEB model in the case of forests. A model calibration has been performed over two general forest types, forest radiative transfer properties have been investigated and a better understanding has been obtained of the separate contributions of each forest layer to the total above-canopy forest emission. The high emissivity and low sensitivity to ground moisture found in above-canopy forest observations have been demonstrated and could be explained. An indication has been given regarding the feasibility of soil moisture retrievals underneath (partly) forested areas. In conclusion, a better understanding of forest L-band emission in view of soil moisture retrievals over partly forested pixels has been obtained. The fact that forest emission is relatively invariable over a range of moisture conditions may actually be an asset in soil moisture retrievals over heterogeneous pixels, as it facilitates correct emission modelling of the forested part of the pixel.

6.3 Recommendations for Future Research

This thesis only covers a very small part of the subject 'microwave forest emission' and many interesting aspects still remain open for future investigation, while the availability of global-scale SMOS observations will present a wealth of new research opportunities.

The L-MEB model was chosen for the SMOS mission as it is a simple model and thus particularly well suited to global-scale studies. Understandably, it is necessary to make certain assumptions concerning the model components and parameter values in order to deliver a global scale soil moisture product (i.e. a SMOS Level 2 end product). Where possible, default values of the L-MEB parameters should be determined at the satellite scale by model inversion using actual SMOS data. Furthermore, in the case of local or regional scale studies in which field measurements are available, a preferred approach for informed users might be to retrieve soil emission from the SMOS Level 1 brightness temperatures, rather than soil moisture, and then convert soil emission into soil moisture content using site-specific model inputs. Through the use of site-specific information, errors resulting from an imperfect choice of dielectric mixing model, soil texture properties and roughness values can be reduced. The availability of field measurements of soil properties thus allows for a more informed choice of model components and parameter values rather than mere defaults, and the former will in turn result in more correct values of soil moisture. A comparison of results from both approaches, i.e. direct retrieval of soil moisture and retrieval of soil emission followed by conversion into soil moisture, seems a very useful study in the context of SMOS. This also highlights the necessity of a comparison of the performance of various dielectric mixing models for different soil types and moisture conditions.

Besides studies based on the use of L-MEB, at a local scale it remains important to also use multiple-scattering models for the analysis of experimental forest observations, in order to obtain an optimal understanding of L-band forest emission characteristics. It has been shown (Mätzler *et al*., 2006) that if a truly detailed physical understanding of forest emission characteristics and radiative transfer properties is required, a multiple-scattering model will give the most physically correct results.

Once SMOS data become available, it will be extremely interesting to investigate the relationships between the L-MEB canopy parameters τ, ω and tt^P and forest characteristics such as vegetation species, structure and density. If such differentiation is possible, it could prove a very useful link between SMOS observations and ecological and/or allometric studies. Furthermore, changes in the above parameters with different conditions of internal and external water content should be investigated. At global and local scales, the relationship between optical depth and vegetation water content is an essential subject for further investigation, requiring both experimental and modelling studies. With the exception of a study by Ferrazzoli *et al*. (2002), existing analyses of this relationship mainly use the so-called '*b*-parameter' and almost exclusively concern grass and crops rather than woody biomass. Coupling of L-band forest observations with soil-vegetation-atmosphere transfer (SVAT) models is expected to aid global-scale monitoring of vegetation water content, and, ultimately, contribute to climate and drought forecasting.

It should be clear from the work presented in this thesis that, although the results are encouraging, modelling L-band forest emission remains a very challenging issue. There are still many gaps in our knowledge that need to be filled, and for this field experiments are essential, especially during the operational phase of SMOS. This thesis thus presents a strong argument to continue this line of research. Given the fact that forests constitute a major land cover type on a global scale, a continuation of this research will undoubtedly increase the potential of the SMOS mission to improve our understanding of the relationships between forest ecosystems and climate events.

Chapter 7

Samenvatting en Conclusies

7.1 Achtergrond

Dit promotie-onderzoek is uitgevoerd als deel van het achtergrondonderzoek voor de Soil Moisture and Ocean Salinity (SMOS) satellietmissie van de European Space Agency (ESA), welke in 2009 gelanceerd wordt. Het hoofddoel van dit onderzoek was om de L-band (f = 1.4 GHz, λ = 21 cm) straling van bossen beter te begrijpen, in verband met (SMOS) bodemvochtmetingen van heterogene pixels met gedeeltelijke bebossing. Boven een homogene bosbedekking zijn nauwkeurige bodemvochtmetingen moeilijk te realiseren omdat de straling van de bodem slechts gedeeltelijk door de dikke vegetatielaag wordt doorgelaten. Desondanks hebben modelstudies aangetoond dat het in het geval van heterogene pixels onder bepaalde omstandigheden nog steeds mogelijk is om een nauwkeurige bodemvochtmeting te verkrijgen voor het niet-beboste deel van de pixel, mits de straling van het beboste deel correct gemodelleerd wordt. Om deze reden is meer gedetailleerde kennis nodig van de L-band straling van bossen, waaronder een beter begrip van de stralingseigenschappen van de verschillende boslagen, en calibratie van het voorwaartse model dat gebruikt zal worden in het SMOS-algoritme voor bodemvochtoptimalisatie. Bestaande kennis van deze onderwerpen was bij aanvang van dit onderzoek erg beperkt en bijna geheel gebaseerd op modelstudies. Het was daarom bijzonder belangrijk om experimentele waarnemingen te gebruiken om de benodigde informatie te verkrijgen. Hiertoe zijn vanaf meettorens L-band radiometrische waarnemingen gedaan op het onderzoeksterrein Bray in het bos van Les Landes, Frankrijk in 2004, 2006 en 2007 (BRAY campagnes), en het onderzoeksterrein Jülich, Duitsland in 2004 en 2005 (FOSMEX campagnes). De analyses gebaseerd op deze experimentele data zijn gebruikt om de straling en de stralingseigenschappen van het bos beter te begrijpen. Verder zijn met behulp van vliegtuigen L-band data verkregen tijdens de NAFE ’05 campagne in zuidoost Australië in 2005. Deze zijn gebruikt om bodemvochtmetingen van heterogene pixels met een gedeeltelijke bebossing te onderzoeken.

7.2 Samenvatting en Conclusies

Van Juli-December 2004 had de veldwerkcampagne ‘Bray 2004’ plaats in het naaldbos van Les Landes, vlakbij Bordeaux, Frankrijk; met meervoudige hoekmetingen met een L-band radiometer werd de horizontaal gepolariseerde straling boven het bos gemeten. Tegelijkertijd werden op de grond metingen gedaan van bodemvocht en vocht in de strooisellaag terwijl tevens de neerslag permanent werd gemeten. Dit experiment werd uitgevoerd om het begrip te verbeteren van het L-band signaal boven bosgebieden bij verschillende vochtomstandigheden en observatiehoeken. Er werd gevonden dat het grootste gedeelte van het horizontaal gepolariseerde L-band signaal gedomineerd werd door de thermodynamische temperatuur. Variaties in bodemvocht en/of vocht in de strooisellaag waren wel

zichtbaar in het hoeksignaal en in de microgolfstraling boven het bos, hoewel het dynamisch bereik van dit laatste effect erg klein was. De hypothese werd gesteld dat dit verschijnsel, samen met het feit dat de straling erg hoog was, het gevolg was van de aanwezigheid van een behoorlijke strooisellaag. Het ontkoppelen van de effecten van de bodem en de strooisellaag was desondanks lastig vanwege een sterke correlatie tussen bodemvocht en strooiselvocht.

In een calibratie van het "L-band Microwave Emission of the Biosphere (L-MEB) model", het voorwaartse model in het algoritme van de "SMOS Niveau 2 Bodemvochtoptimalisatie", met behulp van L-band waarnemingen boven een naaldbos (Den) en een loofbos (gemengd/Beuk), werden strooisellaageffecten in aanmerking genomen door het gebruik van een effectieve bodemruwheidsparameter die het resultaat was van empirische 'best-fits'. De calibratie heeft geresulteerd in waarden van de belangrijkste parameters van de boslaag, te weten: optische diepte (τ_{NAD}), enkelvoudige verstrooiingsalbedo (ω), de structuurparameters tt^H en tt^V en de bodemruwheidsparameters H_R en N_R^P. Het gebruik van deze gecalibreerde waarden in het voorwaartse model resulteerde in een "root mean square error" (RMSE) in stralingstemperatuur (T_B) van 2.8 tot 3.8 K, afhankelijk van de dataset en de polarisatie, hetgeen duidt op een goede werking van het model voor verschillende vochtomstandigheden. De modelparameters vertoonden een vergelijkbaar gedrag voor beide typen bos, ook al werden iets verschillende waarden gevonden voor de twee locaties. Hierbij was het meest opvallende dat de optische diepte van het naaldbos (0.67) lager lag dan dat van het loofbos (0.98). Er is tevens een gevoeligheidsanalyse uitgevoerd voor de bovenstaande parameters, zowel voor temperatuur, bodemvocht als voor neerslag, om de verandering in RMSE(T_B) aan te geven bij het optreden van een fout in een bepaalde variabele. De relatie tussen optische diepte en leaf area index (LAI) is ook onderzocht voor het loofbos. Er werd een bijzonder lage correlatie gevonden, hetgeen niet onverwacht was aangezien de grootste bijdrage aan L-band straling van een bos van de takken afkomstig is en niet van de bladeren/naalden (Ferrazzoli *et al*., 2002). De resultaten van deze studie zullen worden geïntegreerd in het operationele algoritme van de "SMOS Niveau 2 Bodemvochtoptimalisatie".

Hoewel gevonden werd dat de gemiddelde doorlaatbaarheid van de bomenlaag in gematigde naald- en loofbossen rond de 0.4-0.5 ligt (zie ook Guglielmetti *et al*. (2007, 2008)), en dus verwacht mag worden dat de bomenlaag een redelijke hoeveelheid bodemstraling doorlaat, vertoonde de totale straling gemeten boven het bos erg weinig variatie met verschillen in bodemvocht, zoals hierboven vermeld. Het is bekend dat de aanwezigheid van een vochtige strooisellaag op de bosbodem de bodemstraling vermindert en de hypothese werd daarom gemaakt dat tijdens Bray 2004 de aanwezige strooisellaag verantwoordelijk was voor de lage gevoeligheid van de straling gemeten boven het bos. Meer kennis van de L-band stralingseigenschappen van de strooisel en kruidlagen was daarom nodig om de straling van het gehele bossysteem beter te begrijpen.
Om hieraan bij te dragen werd in 2007 een extra veldexperiment uitgevoerd op het terrein van Bray. Radiometrische waarnemingen werden gedaan van de bomenlaag en van verschillende configuraties van de bosbodem, nadat de verschillende lagen van de bosbodem opeenvolgend verwijderd waren. In combinatie met de lange-termijn dataset van L-band waarnemingen boven het bos uit 2004 resulteerde dit in stralingswaarden van de kale bodem, bodem-strooisel, bodem-strooisel-gras en bodem-strooisel-gras-bomen configuraties, voor een bepaald bereik van bodem- en

strooiselvochtwaarden. Bij de analyses werd gebruik gemaakt van de Wilheit en L-MEB modellen, samen met een aangepaste versie van de methode van Schwank *et al*. (2008). Er werd gevonden dat de gevoeligheid voor bodemvocht in grote mate onderdrukt wordt door de aanwezigheid van de gras- en strooisellagen. Dit resultaat bevestigde de lage correlatie tussen bodemvocht en de L-band straling boven het bos. Een gedetailleerde gevoeligheidsanalyse toonde de effecten aan van vochtgehalte en strooisellaagdikte op de thermische dempingsdiepte en op de straling van een bodem-strooisel configuratie van de bosbodem. Verschillende resultaten van recente modelleer- en laboratoriumstudies konden door deze studie worden bevestigd, die voor zover ons bekend de eerste is waarbij, in deze context, *in situ* experimentele data zijn gebruikt.

Tot slot werden L-band vliegtuigwaarnemingen van het "Australian National Airborne Field Experiment 2005" (NAFE '05) gebruikt om de invloed te onderzoeken van de beboste fractie in heterogene (gras/bos) pixels op de resulterende bodemvochtwaarden. Deze studie is uitgevoerd met het oog op de aankomende SMOS missie, om bij te dragen aan calibratie/validatie studies en aan de analyse van heterogene landoppervlakten. Voor zover bekend is dit de eerste studie die experimentele data gebruikt voor dit onderwerp. Omdat de meervoudige hoekwaarnemingen in loodrecht op de vliegrichting staande stroken werden gedaan, werd in deze studie een strook gebruikt als basiseenheid in plaats van een pixel. Gelijktijdige optimalisatie van bodemvocht (*SM*) en vegetatie optische diepte werden gedaan door inversie van het L-MEB model. Dit is uitgevoerd voor twee verschillende optimalisatieconfiguraties, waarvan de eerste bestond uit strook-effectieve waarden voor *SM* en τ_{NAD} en de tweede bestond uit waarden van *SM* en τ_{NAD} voor de niet-beboste (oftewel gras) fractie van de strook, waarbij de straling van het bos bekend was van voorwaarts modelleren. Modelinvoer voor de niet-geoptimaliseerde parameters waren ofwel standaardwaarden uit de literatuur ofwel locatie- en tijdspecifieke waarden verkregen van waarnemingen van nabijgelegen homogene stroken die gedaan waren tijdens dezelfde vlucht. Het voornaamste aandachtspunt van deze studie was het optimalisatiegedrag bij verschillende bodemvochtomstandigheden en bosfracties. Oppervlakte-gemiddelde resultaten waren over het algemeen redelijk voor beide optimalisatieconfiguraties. Wanneer strook-effectieve waarden van *SM* en τ_{NAD} geoptimaliseerd werden, vertoonde τ_{NAD} een oplopende overschatting met toenemende bosfractie. De hoogste geoptimaliseerde waarden van *SM* werden gevonden bij middelmatige bosfractiewaarden. De resultaten tonen de moeilijkheid aan van het identificeren van bovenlimieten van de pixel-bosfractie bij de bepaling van bodemvocht, naast het feit dat foutieve parameterwaarden kunnen leiden tot hoge fouten in het geoptimaliseerde *SM*, zeker in natte condities. Dit onderdeel van de studie geeft een realistisch beeld van de fouten en onzekerheden die optreden bij bodemvochtoptimalisatie van gedeeltelijk beboste stroken en draagt daarmee naar verwachting bij aan een beter begrip van SMOS calibratie/validatie kwesties.

Samenvattend heeft deze studie inzicht gegeven in de algemene toepasbaarheid, bruikbaarheid en beperkingen van het L-MEB model bij toepassing op bossen. Een modelcalibratie is uitgevoerd over twee algemene bostypen. De stralingseigenschappen van het bos zijn onderzocht en er is een beter begrip verkregen van de aparte bijdragen van elke boslaag aan de totale straling boven het bos. De hoge stralingswaarden en lage gevoeligheid voor bodemvocht die werden gevonden in de waarnemingen boven het bos zijn aangetoond en verklaard. Er is een indicatie

gegeven van de mogelijkheid om bodemvocht te meten van (gedeeltelijk) beboste oppervlakten. Om te concluderen is er een beter begrip van de L-band straling van bossen verkregen, met het oog op bodemvochtmetingen over gedeeltelijk beboste pixels. Het feit dat de straling van een bos relatief onveranderlijk is bij verschillende vochtomstandigheden gunstig voor de bepaling van bodemvocht van heterogene pixels, omdat het een correcte modellering van de straling van het beboste gedeelte van de pixel vereenvoudigt.

7.3 Aanbevelingen voor Toekomstig Onderzoek

Dit proefschrift behandelt slechts een klein gedeelte van het onderwerp 'microgolfstraling van bossen'. Veel interessante aspecten blijven nog open voor toekomstig onderzoek, terwijl de beschikbaarheid van globale SMOS waarnemingen nieuwe gelegenheden tot onderzoek zal bieden.
Het L-MEB model is voor de SMOS missie gekozen omdat het een relatief eenvoudig model is en daarom bijzonder geschikt is voor studies op globale schaal. De noodzaak aannames te doen wat betreft de modelcomponenten en parameterwaarden is begrijpelijk, aangezien de SMOS-missie is gericht op de levering van een bodemvochtproduct (oftewel een SMOS Niveau 2 eindproduct) op globale schaal. Zodra SMOS operationeel is, zouden, waar mogelijk, op satelliet-pixel schaal standaardwaarden van de L-MEB parameters vastgesteld moeten worden door modelinversie van echte SMOS data. Verder zou het, voor geïnformeerde gebruikers, in het geval van studies op locale of regionale schaal waarin veldmetingen beschikbaar zijn, de voorkeur hebben om bodemstralingswaarden uit de SMOS Niveau 1 stralingstemperaturen te optimaliseren in plaats van bodemvocht, en vervolgens de bodemstralingswaarden naar bodemvocht om te zetten met behulp van locatie-specifieke modelparameters. Door het gebruik van locatie-specifieke informatie kunnen fouten als gevolg van een niet geheel juiste keuze van het dielectrisch mengmodel van de bodem, en fouten in bodemtextuur en ruwheidseigenschappen van de bodem, worden gereduceerd. De beschikbaarheid van veldmetingen van de relevante bodemeigenschappen maakt een betere keuze van modelcomponenten en parameterwaarden mogelijk in plaats van standaardwaarden te gebruiken, wat zal resulteren in minder fouten in de uiteindelijke bodemvochtswaarde. Een vergelijking van de resultaten van beide aanpakken, oftewel directe optimalisatie vam bodemvocht en optimalisatie van bodemstraling gevolgd door conversie naar bodemvocht, lijkt een zinvolle studie in de context van SMOS. Dit toont tevens de noodzaak van een vergelijking van de prestaties van de verschillende dielectrische mengmodellen voor verschillende bodemtypen en vochtomstandigheden.
Naast studies gebaseerd op het gebruik van L-MEB, blijft het op locale schaal belangrijk om ook meervoudige verstrooiingsmodellen te gebruiken voor de analyse van experimentele boswaarnemingen, om een optimaal begrip te krijgen van de L-band stralingskarakteristieken van bossen. Eerder is aangetoond (Matzler *et al*., 2006) dat om een echt gedetailleerd fysisch begrip te verkrijgen van stralingskarakteristieken en stralingsgedrag, een meervoudig verstrooiingsmodel de meest fysisch correcte resultaten zal geven.
Wanneer SMOS data beschikbaar komen zal het bijzonder interessant zijn de relaties te onderzoeken tussen de L-MEB vegetatieparameters τ, ω en tt^P en boskarakteristieken zoals vegetatietype, -structuur en -dichtheid. Als het mogelijk is

hier patronen in te vinden zouden SMOS waarnemingen erg nuttig kunnen worden voor ecologische en/of allometrische studies. Verder zouden veranderingen in bovenstaande parameters bij verschillende gehaltes van intern en extern vegetatiewater onderzocht moeten worden. Op globale en locale schalen is de relatie tussen optische diepte en het watergehalte van de vegetatie een essentieel onderwerp voor verder onderzoek, en behoeft zowel experimentele als modelstudies. Met uitzondering van een studie door Ferrazzoli *et al*. (2002), gebruiken bestaande analyses van deze relatie voornamelijk de zogenaamde '*b*-parameter' en richten zich bijna exclusief op gras en gewassen, niet op houtige biomassa.
Het is te verwachten dat de koppeling van L-band boswaarnemingen en modellen van de uitwisselingsprocessen tussen bodem, vegetatie en atmosfeer (SVAT modellen) bij zal dragen aan monitoring van vegetatiewatergehalte op globale schaal en, uiteindelijk, aan betere klimaat- en droogtevoorspellingen.
Uit het werk dat in dit proefschrift is gepresenteerd moge duidelijk zijn dat het modelleren van de L-band straling van bossen een grote uitdaging blijft. Er zijn nog steeds vele leemtes in de beschikbare kennis, en voor dit onderzoeksveld zijn veldwerkexperimenten essentieel, met name tijdens de operationele fase van SMOS. Dit proefschrift vormt daarom een krachtig argument om deze lijn van onderzoek te vervolgen. Gezien het feit dat bossen op globale schaal een veel voorkomend landgebruikstype zijn, zal voortzetting van dit onderzoek ongetwijfeld bijdragen aan het belang van de SMOS missie voor het vergroten van het inzicht in de relatie tussen bosecosystemen en klimaat.

Appendix A

Microwave radiation modelling and Kirchhoff's law for three different observation configurations*

Equations A-1, A-2 and A-3 respectively describe total radiation measured by above-canopy, downward-looking observations (eq. A-1), below-canopy, upward-looking observations (eq. A-2) and below-canopy, downward-looking observations (eq. A-3). In these equations, $T_{B,sky}$, T_C and T_S are the sky brightness temperature, and the thermodynamic temperatures of the canopy and the soil, respectively. The variables t_C, e_C and r_C are the canopy transmissivity, emissivity and reflectivity, with the condition $t_C + e_C + r_C = 1$, and r_S is the soil reflectivity. In all cases Kirchhoff's law is fulfilled, i.e. the sum of the coefficients is 1.

$$T_B = T_{B,sky}\left[r_C + \frac{t_C^2 r_S}{1 - r_S r_C}\right] + T_C e_C\left[1 + \frac{t_C r_S}{1 - r_S r_C}\right] + T_S \frac{t_C (1 - r_S)}{1 - r_S r_C} \qquad \text{[A-1]}$$

$$T_B = T_{B,sky} \frac{t_C}{1 - r_S r_C} + T_C \frac{e_C}{1 - r_S r_C} + T_S \frac{r_C (1 - r_S)}{1 - r_S r_C} \qquad \text{[A-2]}$$

$$T_B = T_{B,sky} \frac{r_S t_C}{1 - r_S r_C} + T_C \frac{r_S e_C}{1 - r_S r_C} + T_S \frac{1 - r_S}{1 - r_S r_C} \qquad \text{[A-3]}$$

If it is assumed that multiple interactions between the canopy and the soil can be neglected, in which case $r_S \cdot r_C << 1$, the denominators in the above equations can be replaced by 1. This change does not affect Kirchhoff's law in equations A-2 and A-3, but it does in equation A-1, where the coefficient sum then becomes 1 - $t_C \cdot r_S \cdot r_C$. However, the resulting error is small and the derived equation A-4 can still be used as an approximation.

$$T_B = T_{B,sky}\left[r_C + t_C^2 r_S\right] + T_C e_C\left[1 + t_C r_S\right] + T_S t_C (1 - r_S) \qquad \text{[A-4]}$$

It should be noted that equation A-4 is slightly different from equation 4.1 on p. 228 of Mätzler *et al*. (2006). However, equation 4.1 and the appropriate terms in table 4.1 of Mätzler *et al*. (2006) can in fact be replaced by the expression A-4, except in the presence of significant reflectivities in which case the full expressions (e.g. A-1 to A-3) should be used.

The sky radiation term in equation 4.1 of Mätzler *et al*. (2006) was added in order to recover energy conservation by the use of a proper sky term fulfilling Kirchhoff's Law. It is derived as follows:

* This Appendix was based on notes and comments of C. Mätzler and A.A. van de Griend.

Accounting for multiple scattering leads to:

$$T_B{}^1 = T_{B,\,sky}\,.r_C + T_{B,\,sky}\,.t_C^2\,.r_S + T_{B,\,sky}\,.t_C^2\,.r_S^2\,r_C + T_{B,\,sky}\,.t_C^2\,.r_S^3\,r_C^2 + \ldots. + T_{B,\,sky}\,.t_C^n\,.r_S^{n+1}\,r_C^n \quad \text{[A-5]}$$

or

$$T_B{}^1 = T_{B,\,sky}\,.r_C + T_{B,\,sky}\,.t_C^2\,.r_S\,[1 + r_S\,r_C + r_S^2\,r_C^2 \ldots\ldots + r_S^n\,r_C^n] \quad \text{[A-6]}$$

For $r_S \cdot r_C < 1$ the following expression (geometric series) is valid:

$$\sum_{n=0}^{\infty}(r_S.r_C)^n = \frac{1}{(1-r_S.r_C)} \quad \text{[A-7]}$$

and therefore,

$$T_B{}^1 = T_{B,\,sky}\,.r_C + \frac{T_{B,\,sky}\,.t_C^2\,.r_S}{(1 - r_S\,.r_C)} \quad \text{[A-8]}$$

Under the assumption that multiple interactions can be neglected, i.e. $r_S \cdot r_C << 1$, the denominator in this equation is replaced by 1, which, however, affects Kirchhoff's law. A solution for this is to use an approximation of the geometric series (eq. A-5). In this approximation, only the first scattering term (soil-canopy-soil) is included and higher order terms are ignored because they become very small. Thus, the equation becomes:

$$T_B{}^1 = T_{B,\,sky}\,.r_C + T_{B,\,sky}\,.t_C^2\,.r_S + T_{B,\,sky}\,.t_C^2\,.r_S^2\,r_C \quad \text{[A-9]}$$

which can be written as:

$$T_B{}^1 = T_{B,\,sky}\,[t_C^2\,.r_S + r_C\,(1 + t_C^2\,.r_S^2)] \quad \text{[A-10]}$$

With $r_C = \omega(1\text{-}t_C)$, (see e.g. Van de Griend *et al.*, 1996) one finds:

$$T_B{}^1 = T_{B,\,sky}\,[t_C^2\,.r_S + \omega\,(1 - t_C)(1 + (t_C\,.r_S)^2] \quad \text{[A-11]}$$

Note that the power 2 coefficient in the last term of equation A-10 is missing in equation 4.1. of Mätzler *et al.* (2006).

References

Aubinet, M., Grelle, A., Ibrom, A., Rannik, U., Moncrieff, J., Foken, T., Kowalski, A.S.,
Martin, P.H., Berbigier, P., Bernhofer, C., Clement, R., Elbers, J., Granier, A., Grunwald, T., Morgenstern, K., Pilegaard, K., Rebmann, C., Snijders, W., Valentini, R. and Vesala, T. (2000). Estimates of the annual net carbon and water exchange of forests: The EUROFLUX methodology. *Advances in Ecological Research, 30*, 113-175.

Bartelink, H.H. (1997). Allometric relationships for biomass and leaf area of Beech (*Fagus sylvatica* L.). *Annals of Forest Science, 54(1)*, 39–50.

Berger, M., Kerr, Y., Font, J., Wigneron, J.-P., Calvet, J.-C., Saleh, K., Lopez-Baeza, E., Simmonds, L., Ferrazzoli, P., Van de Hurk, B., Waldteufel, P., Petitcolin, F., Van de Griend, A. A., Attema, E. and Rast, M., (2003). Measuring the Moisture in the Earth's Soil – Advancing the Science with ESA's SMOS Mission. *ESA Bulletin, 115*, 40-45.

Chauhan, N., Le Vine, D. and Lang, R. (1999). Passive and Active Microwave Remote Sensing of Soil Moisture under a Forest Canopy. *Proceedings of IGARSS 1999*, *4*, 1914-1916.

Crosson, W., Limaye, A.S. and Laymon, C.A. (2005). Parameter Sensitivity of Soil Moisture Retrievals From Airborne L-Band Radiometer Measurements in SMEX02. *IEEE Transactions on Geoscience and Remote Sensing, 43(7)*, 1517-1528.

Della Vecchia, A., Saleh, K., Ferrazzoli, P., Gurriero, L. and Wigneron, J.-P. (2006a). Simulating L-Band Emission of Coniferous Forests Using a Discrete Model and a Detailed Geometrical Representation. *IEEE Geoscience and Remote Sensing Letters, 3(3)*, 364-368.

Della Vecchia, A., Ferrazzoli, P., Giorgio, F. and Guerriero, L. (2006b). A large scale approach to estimate L band emission from forest covered surfaces. *Second Recent Advances in Quantitative Remote Sensing*, José A. Sobrino (Ed.), Servicio de Publicaciones, Universitat de Valencia, 925-930.

Della Vecchia, A., Ferrazzoli, P., Wigneron, J.-P. and Grant, J.P. (2007). Modeling forest emissivity at L-band and a comparison with multitemporal measurements. *IEEE Geoscience and Remote Sensing Letters, 4(4)*, 508-512.

Demontoux, F., Le Crom, B., Ruffié, G., Wigneron, J.-P., Grant, J.P., Mironov, V.L. and Lawrence, H. (2008). Electromagnetic characterization of soil-litter media – application to the simulation of the microwave emissivity of the ground surface in forests. *European Physical Journal - Applied Physics, 44*, 303-315.

Dobson, M.C., Ulaby, F.T., Hallikainen, M.T. and El-Rayes, M.A. (1985). Microwave Dielectric Behaviour of Wet Soil – Part II: Dielectric Mixing Models. *IEEE Transactions on Geoscience and Remote Sensing, 23*, 35-46.

Escorihuela, M.-J., Kerr, Y.H., de Rosnay, P., Wigneron, J.-P., Calvet, J.-C. and Lemaître, F. (2007). A simple model of the bare soil microwave emission at L-band," *IEEE Transactions on Geoscience and Remote Sensing, 45, 7*, 1978-1987.

Ferrazzoli, P. and Guerriero, L. (1996). Passive microwave remote sensing of forests: a model investigation. *IEEE Transactions on Geoscience and Remote Sensing, 34(2)*, 433-443.

Ferrazzoli, P., Guerriero, L. and Wigneron, J.-P. (2002). Simulating L-Band Emission of Forests in View of Future Satellite Applications. *IEEE Transactions on Geoscience and Remote Sensing, 40(12)*, 2700-2708.

Fung, A.K. (1994). *Microwave Scattering and Emission Models and Their Applications*. Artech House, Norwood (USA).

Grant, J.P., Wigneron, J.-P., Van de Griend, A.A., Kruszewski, A., Schmidl Søbjærg, S. and Skou, N. (2007). A field experiment on microwave forest radiometry: L-band signal behaviour for varying conditions of surface wetness," *Remote Sensing of Environment, 109(1)*, 10-19.

Grant, J.P., Saleh, K., Wigneron, J.-P., Guglielmetti, M., Kerr, Y., Schwank, M., Skou, N. and Van de Griend, A.A. (2008). Calibration of the L-MEB model over a coniferous and a deciduous forest. *IEEE Transactions on Geoscience and Remote Sensing, 46(3)*, 808-818.

Grant, J.P., Van de Griend, A.A., Schwank, M. and Wigneron, J.-P. (2009). Observations and Modelling of a Pine Forest Floor at L-Band. *IEEE Transactions on Geoscience and Remote Sensing,* in press.

Guglielmetti, M., Schwank, M., Mätzler, C., Oberdörster, C., Vanderborght, J. and Flühler, H. (2007). Measured microwave radiative transfer properties of a deciduous forest canopy. *Remote Sensing of Environment, 109(4)*, 523-532.

Guglielmetti, M., Schwank, M., Mätzler, C., Oberdörster, C., Vanderborght, J. and Flühler, H. (2008). FOSMEX: Forest Soil Moisture Experiments with Microwave Radiometry. *IEEE Transactions on Geoscienxe and Remote Sensing, 46(3)*, 727-735.

Hallikainen, M., Jääskeläinen, V.S., Pulliainen, J. and Koskinen, J. (2000). Transmissivity of Boreal Forest Canopies for Microwave Radiometry of Snow. *Proceedings of IGARSS 2000*, *IEEE International, 4*, 1564-1566.

Hornbuckle, B.K., England, A.W., De Roo, R.D., Fischman, M.A. and Boprie, D.L. (2003). Vegetation canopy anisotropy at 1.4 GHz. *IEEE Transactions on Geoscience and Remote Sensing, 41(10)*, 2211–2223.

Hornbuckle, B.K., England, A.W., Anderson, M.C. and Viner, B.J. (2006). The effect of free water in a maize canopy on microwave emission at 1.4 GHz. *Agricultural and Forest Meteorology, 138*, 180-191.

Institute for Applied Physics (Ed.). (1991). Handbook of the MORA 11.4 GHz radiometer. University of Bern, Switzerland.

Jackson, T.J. and O'Neill, P.E. (1990). Attenuation of soil microwave emissivity by corn and soybeans at 1.4 and 5 GHz. *IEEE Transactions on Geoscience and Remote Sensing, 28*, 978-980.

Jackson, T.J. and Schmugge, T.J. (1991). Vegetation Effects on the Microwave Emission of Soils. *Remote Sensing of Environment, 36*, 203-212.

Kavvadias, V.A., Alifragis, D., Tsiontsis, A., Brofas, G. and Stamatelos, G. (2001). Litterfall, litter accumulation and litter decomposition rates in four forest ecosystems in northern Greece. *Forest Ecology and Management, 144(1–3)*, 113–127.

Kerr, Y.H., Waldteufel, P., Wigneron, J.-P., Martinuzzi, J.-M., Font, J. and Berger, M. (2001). Soil Moisture Retrieval from Space: The Soil Moisture and Ocean Salinity (SMOS) Mission. *IEEE Transactions on Geoscience and Remote Sensing, 39(8)*, 1729-1735.

Kerr, Y.H., Waldteufel, P., Richaume, P., Davenport, I., Ferrazzoli, P. and Wigneron, J.-P. (2006). SMOS level 2 processor Soil Moisture Algorithm Theoretical Basis Document (ATBD). SM-ESL (CBSA), CESBIO, Toulouse, SO-TN-ESL-SM-GS-0001, V5.a, 15/03/2006.

Kerr, Y.H., Waldteufel, P., Richaume, P., Davenport, I., Ferrazzoli, P. and Wigneron, J.-P. (2007). SMOS Level 2 Processor for Soil Moisture, Algorithm Theoretical Based Document (ATBD). CESBIO, IPSL-Service d'Aéronomie, INRA-EPHYSE, Reading University, Tor Vergata University. SO-TN-ESL-SM-GS-0001 Issue 3.a, 05/12/2007.

Kirdyashev, K.P., Chukhlantsev, A.A. and Shutko, A.M. (1979). Microwave radiation of the earth's surface in the presence of vegetation cover. *Radiotekhnika, 24*, 256-264.

Kleshchenko, V.N., Komarov, S.A. and Mironov, V.L. (2002). Dielectric Properties of Needle Litter. *Journal of Communications Technology and Electronics, 47(11)*, 1202-1204.

Lang, R.H., Utku, C., De Matthaeis, P., Chauhan, N. and Le Vine, D.M. (2001). ESTAR and Model Brightness temperatures over forests: effects of soil moisture. *Proceedings of IGARSS 2001*, *IEEE International, 3*, 1300-1302.

Lang, R.H., Chauhan, N., Utku, C. and Le Vine, D.M. (2006). L-Band Active and Passive Sensing of Soil Moisture through Forests. *Proceedings of IEEE MicroRad 2006*, 193-196.

Loew, A. (2008). Impact of surface heterogeneity on surface soil moisture retrievals from passive microwave data at the regional scale: The Upper Danube case. *Remote Sensing of Environment*, *112*, 231-248.

Macelloni, G., Paloscia, S., Pampaloni, P. and Ruisi, R. (2001). Airborne multifrequency L- to Ka-band radiometric measurements over forests. *IEEE Transactions on Geoscience and Remote Sensing, 39(11)*, 2507-2513.

Masarovicova, E., Cicak, A. and Stefancik, I. (1996). Ecophysiological, biochemical, anatomical and productional characteristics of Beech (*Fagus sylvatica* L.) leaves from regions with different degree of immission impact. *Ecologia, 15(3)*, 337–351.

Mätzler, C. (1990). Seasonal Evolution of Microwave Radiation from an Oat Field. *Remote Sensing of Environment, 31*, 161-173.

Mätzler, C. (1994a). Microwave Transmissivity of a Forest Canopy: Experiments Made with a Beech. *Remote Sensing of Environment, 48*, 172-180.

Mätzler, C. (1994b). Passive Microwave Signatures of Landscapes in Winter. *Meteorology and Atmospheric Physics, 54*, 241-260.

Mätzler, C., Weber, D., Wüthrich, M., Schneeberger, K., Stamm, C. and Flühler, H. (2003). ELBARA, the ETH L-band radiometer for soil moisture research. *Proceedings of IGARSS 2003, IEEE International, 5*, 3058-3060.

Mätzler, C. (Ed.), Rosenkranz, P.W., Battaglia, A. and Wigneron, J.-P. (2006). *Thermal Microwave Radiation: Applications for Remote Sensing*. IET Electromagnetic Waves Series 52, London, UK.

Merlin, O., Walker, J.P., Panciera, R., Young, R., Kalma, J.D. and Kim, E.J. (2007). Calibration of a Soil Moisture Sensor in Heterogeneous Terrain with the National Airborne Field Experiment (NAFE) Data. *Proceedings of MODSIM 2007 International Congress on Modelling and Simulation*. Modelling and Simulation Society of Australia and New Zealand.

Mo, T., Choudhury, B.J., Schmugge, T.J., Wang, J.R. and Jackson, T.J. (1982). A model for microwave emission from vegetation-covered fields. *Journal of Geophysical Research, 87(C13)*, 11229-11237.

Ogée, J. and Brunet, Y. (2002). A forest floor model for heat and moisture including a litter layer. *Journal of Hydrology, 255*, 212-233.

Osono, T. and Takeda, H. (2006). Fungal decomposition of *Abies* needle and *Betula* leaf litter. *Mycologia, 98(2)*, 172–179.

Paloscia, S., Pampaloni, P., Santi, E., Pettinato, S., Della Vecchia, A., Ferrazzoli, P. and Guerriero, L. (2008). Soil moisture effect on microwave emission of forest canopies," *Proceedings of MICRORAD 2008*, *Microwave Radiometry and Remote Sensing of the Environment*, 1-4.

Pampaloni, P. (2004). Microwave radiometry of forests. *Waves in Random Media, 14*, S275-S298.

Panciera, R., Walker, .P., Kalma, J.D., Kim, E.J., Hacker, J., Merlin, O., Berger, M. and Skou, N. (2008). The NAFE'05/CoSMOS data set: Towards SMOS soil moisture retrieval, downscaling and assimilation. *IEEE Transactions on Geoscience and Remote Sensing*, *46(3)*, 736-745.

Pardé, M., Wigneron, J.-P., Chanzy, A., Kerr, Y.H., Calvet, J.-C., Waldteufel, P., Schmidl Søbjærg, S. and Skou, N. (2004). N-Parameter retrievals from L-band microwave measurements over a variety of agricultural crops. *IEEE Transactions on Geoscience and Remote Sensing, 42(6)*, 1168-1178.

Pellarin, T., Wigneron, J.-P., Calvet, J.-C., Berger, M., Douville, H., Ferrazzoli, P., Kerr, Y., Lopez-Baeza, E., Pulliainen, J., Simmonds, L. and Waldteufel, P. (2003a). Two-Year Global Simulation of L-Band Brightness Temperatures Over Land. *IEEE Transactions on Geoscience and Remote Sensing, 41(9)*, 2135-2139.

Pellarin, T., Calvet, J.-C., Wigneron, J.-P. (2003b). Surface Soil Moisture Retrieval From L-Band Radiometry: A Global Regression Study. *IEEE Transactions on Geoscience and Remote Sensing, 41(9)*, 2037-2051.

Pellarin, T., Kerr, Y.H. and Wigneron, J.-P. (2006). Global Simulation of Brightness Temperatures at 6.6 and 10.7 GHz Over Land Based on SMMR Data Set Analysis. *IEEE Transactions on Geoscience and Remote Sensing, 44(9)*, 2492-2505.

Porté, A., Bosc, A., Champion, I. and Loustau, D. (2000). Estimating the foliage area of Maritime pine (Pinus pinaster Aït) branches and crowns with application to modelling the foliage area distribution in the crown. *Annals of Forest Science, 57*, 73–86.

Porté, A., Trichet, P., Bert, D., and Loustau, D. (2002). Allometric relationships for branch and tree woody biomass of Maritime pine (Pinus pinaster Aït). *Forest Ecology and Management, 158*, 71-83.

Rüdiger, C., Hancock, G., Hemakumara, H.M., Jacobs, B., Kalma, J.D., Martinez, C., Thyer, M., Walker, J.-P., Wells, T. and Willgoose, G.R. (2007). Goulburn River experimental catchment data set. *Water Resources Research*, *43(10)*, W10403, doi:10.1029/2006WR005837.

Saleh, K., Wigneron, J.-P., Calvet, J.-C., Lopez-Baeza, E., Ferrazzoli, P., Berger, M., Wursteisen, P., Simmonds, L. and Miller, J. (2004a). The EuroSTARRS airborne campaign in support of the SMOS mission: first results over land surfaces. *International Journal of Remote Sensing, 25(1)*, 177-194.

Saleh, K., Guerriero, L., Della Vecchia, A., Ferrazzoli, P., Wigneron, J.-P., Porté, A., Guyon, D. and Champion, I. (2004b). A radiative model to simulate forest emission at L-band: Sensitivity of brightness temperature to forest components. *Proceedings of IGARSS 2004, IEEE International, 2*, 1025-1028.

Saleh, K., Porté, A., Guyon, D., Ferrazzoli, P. and Wigneron, J.-P. (2005). A forest geometric description of a Maritime Pine forest suitable for discrete microwave models. *IEEE Transactions on Geoscience and Remote Sensing, 43(9)*, 2024-2034.

Saleh, K., Wigneron, J.-P., de Rosnay, P., Calvet, J.-C., Escorihuela, M.J., Kerr, Y. and Waldteufel, P. (2006). Impact of rain interception by vegetation and mulch on the L-band emission of natural grass (SMOSREX Experiment). *Remote Sensing of Environment*, *101(1)*, 127-139.

Saleh, K., Wigneron, J.-P., Waldteufel, P., de Rosnay, P., Schwank, M., Calvet, J.-C. and Kerr, Y.H. (2007). Estimates of surface soil moisture over grass covers using L-band radiometry. *Remote Sensing of Environment, 109(1)*, 42-53.

Saleh, K., Kerr, Y., Richaume, P., Escorihuela, M., Panciera, R., Delwart, S., Wursteisen, P. and Wigneron, J.-P. (2009). Soil moisture retrievals at L-band following a two-parameter inversion approach. *Remote Sensing of Environment*, submitted.

Schmugge, T.J., Wang, J.R. and Asrar, G. (1988). Results from the Push Broom Microwave Radiometer Flights over the Konza Prairie in 1985. *IEEE Transactions on Geoscience and Remote Sensing, 26(5)*, 590-596.

Schmugge, T.J. and Jackson, T.J. (1998). Observations of coherent emissions from soils. *Radio Science, 33(2)*, 267-272.

Schwank, M., Mätzler, C., Guglielmetti, M. and Flühler, H. (2005). L-Band Radiometer Measurements of Soil Water Under Growing Clover Grass. *IEEE Transactions on Geoscience and Remote Sensing, 43(10)*, 2225-2237.

Schwank, M., Guglielmetti, M., Mätzler, C. and Flühler, H. (2008). Testing a New Model for the L-band Radiation of Moist Leaf Litter. *IEEE Transactions on Geoscience and Remote Sensing, 46(7)*, 1982-1994.

Søbjærg, S.S. (2002). Polarimetric Radiometers and their Applications, *PhD Thesis*, Technical University of Denmark, 144 pages.

Ulaby, F., Moore, R. and Fung, A. (1986). *Microwave Remote Sensing: Active and Passive, Vol. III: from Theory to Applications*. Artech House, Dedham, MA.

Van de Griend, A.A., Owe, M., De Ruiter, J. and Gouweleeuw, B.T. (1996). Measurement and Behavior of Dual-Polarization Vegetation Optical Depth and Single Scattering Albedo at 1.4- and 5-GHz Microwave Frequencies. *IEEE Transactions on Geoscience and Remote Sensing, 34(4),* 957-965.

Van de Griend, A.A., Wigneron, J.-P. and Waldteufel, P. (2003). Consequences of Surface Heterogeneity for Parameter Retrieval from 1.4 GHz Multi-Angle SMOS Observations. *IEEE Transactions on Geoscience and Remote Sensing, 41(4)*, 803-811.

Van de Griend, A.A., Wigneron, J.-P., and Waldteufel, P. (2004). Soil Moisture Retrieval from Heterogeneous Surfaces by 1.4 GHz Multi-Angle SMOS Observations using 'A Priori Knowledge' of Surface Cover Fractions. *Proceedings of IGARSS 2004, IEEE International, 7*, 4552-4555.

Van de Griend, A.A. and Wigneron, J-P. (2004a). On the Measurement of Microwave Vegetation Properties: Some Guidelines for a Protocol. *IEEE Transactions on Geoscience and Remote Sensing, 42 (10)*, 2277-2289.

Van de Griend, A.A. and Wigneron, J-P. (2004b). The b-factor as a function of frequency and canopy type at H-polarization. *IEEE Transactions on Geoscience and Remote Sensing, 42(4)*, 786–794.

Wang, J.R. and Choudhury, B.J. (1981). Remote sensing of soil moisture content over bare field at 1.4 GHz frequency. *Journal of Geophysical Research, 86*, 5277-5282.

Wigneron, J.-P., Chanzy, A., Calvet, J.-C., and Bruguier, N. (1995). A simple algorithm to retrieve soil moisture and vegetation biomass using passive microwave measurements over crop fields. *Remote Sensing of Environment, 51*, 331-341.

Wigneron, J.-P., Pardé, M., Waldteufel, P., Chanzy, A., Søbjærg, S. and Skou, N. (2004). Characterizing the dependence of vegetation model parameters on crop structure, view angle and polarization at L-band. *IEEE Transactions on Geoscience and Remote Sensing*, *42(2)*, 416-425.

Wigneron, J.-P., Kerr, Y.H., Waldteufel. P., Saleh, K., Escorihuela, M.-J., Richaume, P., Ferrazzoli, P., de Rosnay, P., Gurney, R., Calvet, J.-C., Grant, J.P., Guglielmetti, M., Hornbuckle, B., Mätzler, C., Pellarin, T. and Schwank, M. (2007). L-band Microwave Emission of the Biosphere (L-MEB) Model: description and calibration against experimental data sets over crop fields. *Remote Sensing of Environment, 107(4)*, 639-655.

Wilheit, T.T. (1978). Radiative Transfer in a Plane Stratified Dielectric. *IEEE Transactions on Geoscience and Remote Sensing, 16(2)*, 138-143.

Publications

Journals (peer-reviewed)

Grant, J.P., Van de Griend, A.A., Wigneron, J.-P., Saleh, K., Panciera, R. and Walker, J.P. (2009). On the Influence of Forest Cover Fraction on L-band Soil Moisture Retrievals from Heterogeneous Pixels using Multi-Angular Observations. *Remote Sensing of Environment*, submitted.

Grant, J.P., Van de Griend, A.A., Schwank, M. and Wigneron, J.-P. (2009). Observations and Modeling of a Pine Forest Floor at L-band. *IEEE Transactions on Geoscience and Remote Sensing*, in press.

Demontoux, F., Le Crom, B., Ruffié, G., Wigneron, J.-P., **Grant, J.P.**, Mironov, V.L. and Lawrence, H. (2008). Electromagnetic characterization of soil-litter media – application to the simulation of the microwave emissivity of the ground surface in forests. *European Physical Journal - Applied Physics, 44*, 303-315.

Grant, J.P., Saleh, K., Wigneron, J.-P., Guglielmetti, M., Kerr, Y., Schwank, M., Skou, N. and Van de Griend, A.A. (2008). Calibration of the L-MEB model over a coniferous and a deciduous forest. *IEEE Transactions on Geoscience and Remote Sensing, 46(3)*, 808-818.

Della Vecchia, A., Ferrazzoli, P., Wigneron, J.-P. and **Grant, J.P.** (2007). Modeling forest emissivity at L-band and a comparison with multitemporal measurements. *IEEE Geoscience and Remote Sensing Letters, 4(4)*, 508-512.

Grant, J.P., Wigneron, J.-P., Van de Griend, A.A., Kruszewski, A., Schmidl Søbjærg, S. and Skou, N. (2007). A field experiment on microwave forest radiometry: L-band signal behaviour for varying conditions of surface wetness. *Remote Sensing of Environment, 109(1)*, 10-19.

Wigneron, J.-P., Kerr, Y.H., Waldteufel, P., Saleh, K., Escorihuela, M.-J., Richaume, P., Ferrazzoli, P., de Rosnay, P., Gurney, R., Calvet, J.-C., **Grant, J.P.**, Guglielmetti, M., Hornbuckle, B., Mätzler, C., Pellarin, T. and Schwank, M. (2007). L-band Microwave Emission of the Biosphere (L-MEB) Model: description and calibration against experimental data sets over crop fields. *Remote Sensing of Environment, 107(4)*, 639-655.

Conference proceedings (peer-reviewed)

Walker J.P., E. Botha, G. Boulet, J. Balling, M. Bell, A. Berg, M. Berger, D. Biasoni, Y. Chen, E. Christen, R. de Jeu, P. de Rosnay, C. Dever, C. Draper, J. Fenollar, C. Gomez, **J.P. Grant**, J. Hacker, M. Hafeez, G. Hancock, D. Hansen, L. Holz, J. Hornbuckle, R. Hurkmans, T. Jackson, J. Johanson, P. Jones, S. Jones, J. Kalma, Y. Kerr, E. Kim, V. Kuzmin, V. Lakshmi, E. Lopez, V. Maggioni, P. Maisongrande, C. Martinez, L. McKee, O. Merlin, I. Mladenova, P. O'Neill, R. Panciera, V. Paruscio, R. Pipunic, W. Rawls, M. Rinaldi, C. Rudiger, P. Saco, K. Saleh, S. Savstrup-Kristensen, V. Shoemark, N. Skou, S. Søbjærg, G. Summerell, R. Teuling, H. Thompson, M. Thyer, J. Toyra, A. Tsang, T. Wells, P. Wursteisen and R. Young. (2007). The National Airborne Field Experiment Data Sets. *MODSIM 2007 International Congress on Modelling and Simulation. Modelling and Simulation Society of Australia and New Zealand*, CD-ROM.

Grant, J.P., Wigneron, J.-P., Van de Griend, A.A., Guglielmetti, M., Saleh, K. and Schwank, M. (2007). Calibration of L-MEB for soil moisture retrieval over forests. *IEEE International Geoscience and Remote Sensing Symposium (IGARSS)*, Barcelona, Spain, pp. 2248-2251.

Saleh, K., Floricioiu D., Kerr Y. H., Boulet G., Maisongrande P., de Rosnay P., Wigneron J.-P., Cano A., López-Baeza E., **Grant J.P.**, Balling J., Skou N., Berger M., Delwart S., Wursteisen P. and Walker J. P. (2007). The CoSMOS L-band Experiment in Southeast Australia. *IEEE International Geoscience and Remote Sensing Symposium (IGARSS)*, Barcelona, Spain, pp. 3948-3951.

Demontoux, F., Le Crom, B., Ruffié, G., Wigneron, J.-P., **Grant, J.P.** and Medina Hernandez, D. (2007). Inversion model validation of ground emissivity. Contribution to the development of SMOS algorithm. *IEEE International Geoscience and Remote Sensing Symposium (IGARSS)*, Barcelona, Spain, pp. 2570-2573.

Grant, J.P., Wigneron, J.-P., Van de Griend, A.A., Demontoux, F., Ruffié, G., Della Vecchia, A., Skou, N. and Le Crom, B. (2006). L-band radiometric behaviour of pine forests for a variety of surface moisture conditions. *Proceedings of the Second International Symposium on Recent Advances in Quantitative Remote Sensing (RAQRS-II)*, Valencia, Spain, pp. 931-936.

Wigneron, J.-P., Kerr, Y., Waldteufel, P., Ferrazzoli, P., Richaume, P., Saleh, K., Calvet, J.-C., Chanzy, A., Demontoux, F., de Rosnay, P., Escorihuela, M.-J., Cano, A., **Grant, J.P.**, Gurney, R., Hornbuckle, B., Kruszewski, A., López-Baeza, E., Mätzler, C., Pellarin, T., Ruffié, G., Schwank, M., Van de Griend, A.A., Mahmoodi, A. and Delwart, S. (2006). Recent Advances in modelling the land surface emission at L-band - Application to L-MEB in the operational SMOS algorithm. *Proceedings of the Second International Symposium on Recent Advances in Quantitative Remote Sensing (RAQRS-II)*, Valencia, Spain, pp. 860-865.

Grant, J.P., Van de Griend, A. A., Wigneron, J.-P., Søbjærg, S., Della Vecchia, A., Kruszewski, A., Debesa, S., Skou, N. and Balling, J. (2005). L-band multi-angle radiometric properties of pine forest; some preliminary results of Bray 2004. *Proceedings of SPIE, Remote Sensing for Agriculture, Ecosystems and Hydrology VII*, Vol. 5976, 59760A-1.